HELMHOLTZ
CENTRE FOR
ENVIRONMENTAL
RESEARCH – UFZ

PhD Dissertation 01/2013

Novel Colloidal Catalysts and Reagents for Oxidation of Organic Pollutants in Water

Klara Rusevova

Novel Colloidal Catalysts and Reagents for Oxidation of Organic Pollutants in Water

Von der Fakultät für Chemie und Mineralogie der Universität Leipzig

genehmigte

DISSERTATION

zur Erlangung des akademischen Grades

DOCTOR RERUM NATURALIUM

(Dr. rer. nat.)

von M. Sc. Klara Rusevova

geboren am 10. Oktober 1983 in Plovdiv, Bulgarien

Gutachter:

Prof. Dr. Frank-Dieter Kopinke

Prof. Dr. Francisco Medina Cabello

Tag der Verleihung: 17.12. 2012

Bibliographic description

Klara Rusevova

Novel Colloidal Catalysts and Reagents for Oxidation of Organic Pollutants in Water

University of Leipzig, Doctoral Thesis
163 Pages, 44 Figures, 12 Tables, 189 Citations

Abstract

Chemical oxidation processes, in particular *in situ* chemical oxidation (ISCO) with potassium permanganate (KMnO$_4$) and Fenton oxidation have emerged as efficient tools for treatment of organically contaminated water streams. Even though these techniques are considered as powerful regarding contaminant degradation, they face several practical limitations in a large scale. Thus, the aim of this study was to propose and test novel strategies in order to extend their applicability, whereby the integration of colloidal reagents and catalysts plays a key role.

A novel approach has been proposed for ISCO based on stabilized KMnO$_4$ particles, which can be introduced into the subsurface in order to form a reactive barrier for efficient plume remediation. Manganese dioxide (MnO$_2$) was tested as a suitable coating for KMnO$_4$ particles because of its insolubility in water, adsorptive and catalytic properties and environmental compatibility. The MnO$_2$-coated KMnO$_4$ particles (MCP) were synthesized by direct partial reduction of KMnO$_4$ microparticles in alcohol and their stability was tested in column experiments under flow-through conditions.

A significant contribution has been achieved in the field of advanced oxidation processes, where the conventional Fenton catalyst (dissolved Fe) was replaced by Fe-containing nanocatalysts in so-called heterogeneous Fenton-like reactions. Thus, typical problems of the homogeneous Fenton system, *i.e.* requirement of acidic pH conditions and removal of iron sludge, are avoided. For this purpose, nano-sized magnetic Fe(II,III) oxides and LaFeO$_3$ and BiFeO$_3$ perovskite minerals were synthesized and thoroughly tested as catalysts for oxidation of several model contaminants under environmentally relevant conditions.

Isotope fractionation studies were applied in order to obtain insight into the type of reactive species involved in the heterogeneous Fenton-like reaction using perovskite nanocatalysts. For this purpose fractionation factors (C and H) were compared with those of other chemical oxidation reactions (permanganate oxidation or homogeneous Fenton oxidation).

Klara Rusevova

Novel Colloidal Catalysts and Reagents for Oxidation of Organic Pollutants in Water

Kurzreferat

Die In-situ chemische Oxidation (ISCO) mit Kaliumpermanganat ($KMnO_4$) und die Fenton-Oxidation, sind als chemische Oxidationsprozesse ein effekives Instrument zur Behandlung von mit organischen Schadstoffen kontaminierten Wasserströmen. Obwohl diese Verfahren als wirksame Behandlungstechniken bezüglich des Abbaus organischer Schadstoffe betrachtet werden, weisen sie bei Anwendung im großen Maßstab verschiedene Nachteile auf. Daher ist das Hauptziel der vorliegenden Arbeit neue Strategien zur Verbesserung dieser Techniken vorzuschlagen und zu testen, wobei der Einsatz von kolloidalen Reagenzien und Katalysatoren eine Schlüsselrolle spielt.

Als ein neuer Ansatz für ISCO-Verfahren wurden stabilizierte $KMnO_4$-Partikel vogeschlagen, die in den Untergrund eingebracht werden und dort eine reaktive Barriere für die effiziente Sanierung von Schadstofffahnen bilden können. Mangandioxid (MnO_2) wurde aufgrund seiner Unlöslichkeit in Wasser, seiner adsorptiven und katalytischen Eigenschaften sowie Umweltverträglichkeit als Coating-Material getestet. Die mit MnO_2 beschichteten $KMnO_4$-Partikel (MCP) wurden in Alkohol synthetisiert und ihre Stabilität wurde in Säulen-Experimenten unter Durchflussbedingungen getestet.

Auf dem Gebiet der Advanced oxidation processes (AOPs) wurde ein wesentlicher Beitrag erreicht, indem der konventionelle Fenton-Katalysator (d.h. gelöstes Eisen) durch Fe-haltige Nanokatalysatoren in sogenannten heterogenen Fenton-artigen Reaktionen ersetzt wurde. Damit werden die typischen Probleme des homogenen Fenton-Systems, d.h. Notwendigkeit der Einstellung niedriger pH-Werte und Entfernung von Eisen-Schlamm, vermieden. Zu diesem Zweck wurden nanoskalige

Fe(II,III)-Oxide wie Magnetit (Fe_3O_4) sowie $LaFeO_3$ und $BiFeO_3$ als Perowskite synthetisiert und hinsichtlich ihrer katalytischen Aktivität für die Entfernung von mehreren Modell-Kontaminanten unter umweltrelevanten Bedingungen getestet. Um Hinweise zur Art der beteiligten reaktiven Spezies in der heterogenen Fenton-artigen Reaktion mit den Perowskit-Nanokatalysatoren zu erhalten, wurden Untersuchungen zur Isotopenfraktionierung durchgeführt. Die ermittelten Fraktionierungsfaktoren (C und H) wurden mit denen anderer Oxidationsreaktionen (homogene Fenton-Oxidation, Permanganatoxidation) verglichen.

Table of Contents

1. Introduction

In many parts of the world safe water supply and lack of sanitation remain a challenge [1]. During the last decades, expanded activity in agriculture and industrial processes has not only increased the demand of fresh water but has also contributed to the pollution of surface- and groundwater. Recent statistic numbers are alarming, 1.1 billion people in developing countries have inadequate access to water, and 2.6 billion lack basic sanitation [2]. Thus, more than ever, fresh water resources need to be protected and new water resources must be developed in order to meet the world's growing demand for fresh water.

Currently available water and wastewater treatment technologies such as physical, biological and chemical treatment are already at a technologically advanced level. However, the effectiveness of these processes becomes more and more limited due to new challenges [3]. Mainly the increasing number of discharged pollutants that have toxic and/or recalcitrant character (e.g., newly emerging problem pollutants, heavy metals, pharmaceuticals etc.) requires stricter prescriptive limits for pollutant concentrations. Thus, novel suitable approaches for their removal which meet cost, energy and environmental requirements are needed [3, 4]. In this respect the utilization of chemical processes is preferred due to their versatility and relatively fast destruction of contaminants. The common reaction mechanisms used for degradation of contaminants via chemical processes can be categorized as: hydrolysis, oxidation, reduction, and photolysis.

In case of organic pollutants, *chemical oxidation processes* are the most universal tool for treatment of contaminated groundwater, industrial effluents and wastewater. Oxidation processes possess several advantages that make them highly attractive: i) high reaction rates, ii) potential to reduce toxicity and possibly complete mineralization of treated contaminants iii) no concentration of waste for further treatment (e.g., as in case of membrane filtration or sorption on activated carbon) and iv) non-selective degradation allowing the treatment of pollutant mixtures at once.

For a long time, the predominant treatment technique for contaminated groundwater and soil in the industrial countries was the "pump and treat" approach [5]. However, due to the high costs (contaminated groundwater has to be pumped upwards and treated in technical facilities) and time demand (the average system operates for decades), this *ex*

situ approach started to be replaced by emerging *in situ* treatment techniques. In the last three decades treatment of the aquifer and soils by means of *in situ* chemical oxidation (ISCO) became a cost-effective and viable remediation technology [6]. As main advantages of ISCO are considered the applicability for a wide range of pollutants, *in situ* destruction of contaminants, transformation of aqueous, sorbed, and non-aqueous phases of contaminants, and comparable cost with other candidate technologies [7]. The most widely used oxidants in ISCO are permanganate salts (MnO_4^-), followed by Fenton reagent, persulfate and ozone [7].

In terms of wastewater treatment, advanced oxidation processes (AOPs) belong to the most powerful methods for the removal of recalcitrant organic constituents from industrial and municipal wastewater [8]. AOPs have also been suggested as a preliminary treatment step prior to biological treatment for contaminants hardly degradable by microorganisms [8, 9]. AOPs have a common chemical feature: the capability of generation of highly reactive oxygen species such as hydroxyl radicals (•OH) which can effectively attack a wide range of organic compounds. Ozone and hydrogen peroxide (H_2O_2) are the most often used oxidants in combination with a catalyst (e.g., transition metals) and with or without irradiation (e.g., ultraviolet, visible) [9]. When AOPs are applied in a right way, they give a great opportunity to reduce the contaminant concentration from several hundreds of ppm to less than 5 ppb. That is why they are called a "the treatment technique of the 21st century" [10].

Although these *chemical oxidation processes* have shown promising results, they face several practical limitations. The key of the improvement, of whether *in situ* remediation or wastewater treatment is needed, may consist in the implementation of the "nano-strategy". Nanomaterials as catalysts or reagents are highly attractive due to their unique size- and shape-dependent properties. Nanoparticles (NPs) made of metals, semiconductors, or oxides are of particular interest for their mechanical, electrical, magnetic, optical, chemical, and catalytic properties [11]. In the field of water purification, utilization of nano-sized catalysts and reagents has already gained a considerable attention.

The main objective of the present thesis is a contribution to the field of *chemical oxidation processes* based on the oxidizing agent potassium permanganate and heterogeneous Fenton-like catalysts. Existing approaches for oxidation of contaminants

in groundwater and wastewater should be improved by utilization of colloidal oxidation catalysts and reagents.

2. Background and principles

2.1. Nanoparticles in water treatment

Nanoparticles (NPs) are usually defined as particles having at least two external dimensions in the size range of 1-100 nm (*i.e.* nano-spheres and fibres, but not nano-sheets) [12]. Sometimes NPs have properties that are not found in the bulk sample of the same chemical composition. This, however, is not an essential criterion of NPs.

NPs have a great potential as water-purification catalysts and redox active reagents for several reasons. They may possess i) a high surface-to-volume ratio, ii) a significantly changed surface reactivity due to a high number of exposed active sites, and (lattice) defects, and iii) they allow reactions in suspension with little or no mass transfer restrictions [11, 13]. For water treatment in reactor systems, high reaction rates are desirable. While i) and ii) may lead to a high intrinsic reactivity of NPs, only the combination with iii) allows this high reactivity to be utilized efficiently.

The main advantage of employing NPs for field application (e.g., *in situ* remediation) is their mobility in porous matrices which allows *in situ* formation of reactive zones by injection of NP suspensions. There are several examples of catalyst and reagent NPs that have achieved promising results in bench or already in field scale. For example, TiO_2 NPs gained attention since they bear good prospects as photocatalysts (also for AOPs) for removal of the various classes of organic water pollutants [9, 11]. Palladium-containing colloids have shown a great potential as selective and extremely efficient catalyst for hydrodehalogenation of halogenated water contaminants such as trichloroethene (TCE), chlorobenzene or even fluorobenzene [14]. The most commonly utilized nanoparticulate reagent so far is zero-valent iron (nZVI), which has been applied at field scale worldwide for reductive dehalogenation of chlorinated aliphatic compounds in groundwater such as chlorinated ethenes [15]. A novel composite Carbo-Iron® consisting of activated carbon colloids and nZVI clusters combines the sorption properties of activated carbon and the reactivity of nano-scale iron metal [16] and is currently applied in its first field tests. Also, magnetic iron-oxide NPs such as magnetite (Fe_3O_4) and maghemite (γ-Fe_2O_3) have shown remarkable adsorption capacities in removal of toxic inorganic substances containing As(V), Cr(VI), Cd(II) or Pb(II) [17].

2.1.1. Size-dependent properties

More recently, researchers have emphasized that size-dependent properties should be the primary criterion rather than particle size when it comes to the definition of NPs [18].

In the studies dealing with metals and metal oxide NPs several interesting features have been found for particles in the size range below 20-30 nm [18, 19]. This size range is related to the exponential increase in the fraction of atoms localized at the surface as the size of the particle decreases. However, it is not only the relative number of atoms on the surface that markedly changes the properties of the solid. It was demonstrated that maghemite dramatically changes its adsorption capability when its size is reduced [20]. When normalized to the specific surface area (SSA), 11-nm maghemite NPs adsorb three times more arsenic compared to 20-nm maghemite NPs. This finding suggests a different adsorption mechanism, which is not resulting from the increase of the number of surface reactive sites, but is caused by the modification of the surface structure leading to the appearance of new types of surface adsorption sites and a significant decrease of the surface energy [20].

One of the most exciting examples is gold. Gold is known to be inert in the macroscopic scale. It has a fully filled d-orbital. But when the particle size is reduced to a few nanometres, gold NPs become extremely active oxidation catalysts [21]. Although the origin of this behaviour is still not fully understood, it seems that the catalytic activity arises from the size-dependent alteration of the electronic structure. Independent of the support and only for NPs smaller than 3 nm, decreasing particle size was associated with an increase in the 3d-electron density of the gold atoms and the onset of reactivity towards molecular oxygen.

NPs which are generated from ferro- or ferrimagnetic materials (e.g., iron oxides, ferrites) and which are below a certain size, in general 10-20 nm, can exhibit a unique form of magnetization called superparamagnetism [22]. Such NPs loose their magnetization in the absence of an external magnetic field due to additional relaxation mechanisms. Thus, superparamagnetic behavior can be described as a combination of paramagnetic and ferromagnetic behavior [23].

2.1.2. Nanoparticle synthesis

NPs can be synthesized by means of two approaches: i) "top-down" or ii) "bottom-up" [24]. The top-down approach involves the breaking down of the bulk material into nano-sized structures or particles using mechanical, chemical or other forms of energy with subsequent stabilization of the NPs. High-energy wet ball milling is a typical top-down approach for producing NPs. This is already a commercial process. However, the contamination of the material during comminution is a critical issue.

The approach, which has the potential of creating less waste and thus being more cost-efficient, is the bottom-up approach. This approach can provide access to extremely fine features and state-of-the-art structures [25]. It is based on building up a material from the bottom: atom-by-atom, molecule-by-molecule, or cluster-by-cluster. In crystal growth, growth species, such as atoms, ions and molecules, after impinging onto the growth surface, assemble into the crystal structure one after another. This results in less defects and more homogeneous chemical composition in comparison to attrition or milling. Synthesis of NPs in colloidal dispersion is a good example of the bottom-up approach in the synthesis of NPs.

As an interesting example, a bio-templating method used for the synthesis of inorganic NPs can be mentioned [26]. For instance *Shewanella oneidensis*, a bacterium with metal reducing capacity is capable to precipitate Pd NPs on its cell wall [27]. Magnetotactic bacteria can produce magnetite grains in their cells through biologically controlled mineralization [28].

Catalyst NPs tested in this study were fabricated by means of co-precipitation and sol-gel methods, which belong to the bottom-up approaches. These methods allow easy implementation, they are well controllable, and have moderate energy requirements.

2.1.3. Influence of mass-transfer on overall reaction rates

The reaction catalyzed by the solid catalyst occurs in the moment, when the substrate comes in contact with the active sites. These are usually located inside the catalyst pores (schematically depicted in Fig. 1a) or in case of the NP on its external surface (Fig. 1b).
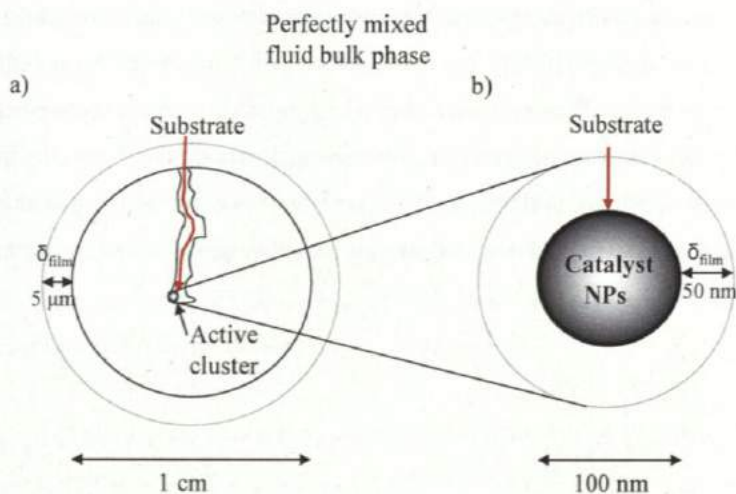
Fig. 1. A scheme of the substrate diffusion to active sites in systems with a) porous catalyst, b) NP catalysts (δ_{film} is the thickness of the diffusion boundary layer).

When reaction of a compound present in bulk solution occurs on a particle surface, the rate limiting step may be represented either by mass-transfer to the surface or reaction at the surface. Thus, due to the mass-transfer phenomena, the observed reaction rate is not necessarily the same as its intrinsic rate. The overall rate constant (k'; h^{-1}) is represented as the combination of a mass-transfer rate coefficient (k_L; $m\ h^{-1}$) and the intrinsic surface reaction rate constant (k_{surf}; h^{-1}):

$$\frac{1}{k'} = \frac{1}{k_L a} + \frac{1}{k_{surf}}$$

Eq. 1

where a ($m^2\ m^{-3}$) is the ratio of the geometric particle surface area to the volume of solution [29]. The relative values of $1/k_L a$ and $1/k_{surf}$ are comparable under conditions where mass-transfer limitations and surface reaction rates are both important. Under conditions where mass transfer is limiting, it holds $k_L a \ll k_{surf}$, and for surface-reaction limited conditions $k_L a \gg k_{surf}$ [29, 30].

For any type of suspended or fixed-bed particles the magnitude of $k_L a$ can be estimated by empirical correlations based on the dimensionless parameters Sherwood, Schmidt and Reynolds numbers [31].

Catalytic reactions utilizing porous catalysts usually face mass-transfer limitations (especially in the aqueous phase), i.e. the diffusion of the substrates through the external diffusion layer and more pronounced internal mass-transfer becomes rate-determining. This is eliminated in case of perfectly dispersed and mixed NPs. From the theory [32] for very small spherical particles ($d_p \ll 1$ μm) the thickness of the diffusion layer is approximated to $\delta_{film} = d_p/2$ and the mass-transfer coefficient can be obtained from Eq 2:

$$k_L = \frac{D_w}{\delta_{film}} = \frac{2D_w}{d_p}$$

Eq. 2

where D_w is the diffusion coefficient of the analyte in water (m^2 s^{-1}).

As an example two different particles will be compared: a nanoparticle with $d_p = 100$ nm and a microparticle with $d_p = 100$ μm. How the rate of mass-transfer varies when the two kinds of particles are employed, can be easily determined using Eq. 2. Since D_w remains constant in both cases, from Eq. 2 it can be deduced:

$$\frac{(k_L a)_{nano}}{(k_L a)_{micro}} = \frac{\delta_{film,micro}}{\delta_{film,nano}} \cdot \frac{a_{nano}}{a_{micro}}$$

Eq. 3

The external film thickness δ_{film} for the micro- and nanoparticle can be estimated to 5 μm and 0.05 μm respectively and a corresponds to ~ $1/d_p$. Using Eq. 3 for this example the ratio $(k_L a)_{nano}/(k_L a)_{micro}$ comes to 5 μm/0.05 μm · 100 μm/100 nm = 10^5. The difference of five orders of magnitude between both particle types fully justifies research on nanoparticulate catalysts and reagents.

Additional to the huge differences in external mass-transfer resistencies the pore diffusion into porous microparticles comes as a slow process. Usually, it retards the overall mass-transfer rates in such catalyst particles even more. This phenomenon is usually described by means of the Thiele-modulus, but shall not be further outlined here in detail.

2.2. Chemical oxidation processes for groundwater and wastewater treatment

2.2.1. ISCO with potassium permanganate

The most developed ISCO technique for the treatment of polluted subsurface areas is based on the oxidation with potassium permanganate ($KMnO_4$). $KMnO_4$ was recognized to be active under most environmental conditions (pH 3.5-12). It provides a rapid and cost-beneficial treatment especially for non-aqueous phase liquids (NAPL) such as TCE, tetrachloroethene (PCE) (Eqs. 4, 5), which in the past have been used in many industrial and commercial processes.

$$4\ KMnO_4 + 3\ C_2Cl_4 + 4\ H_2O \rightarrow 6\ CO_2 + 4\ MnO_2 + 4\ K^+ + 8\ H^+ + 12\ Cl^- \qquad \text{Eq. 4}$$

$$2\ KMnO_4 + C_2HCl_3 \rightarrow 2\ CO_2 + 2\ MnO_2 + 2\ K^+ + H^+ + 3\ Cl^- \qquad \text{Eq. 5}$$
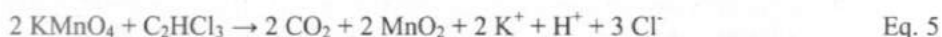
$KMnO_4$ is a strong chemical oxidant ($E^0 = 1.7$ V) and reacts primarily via direct electron transfer reactions rather then via radical intermediates as in case of Fenton reaction (described bellow). Permanganate is known to effectively attack the double bond of alkenes. The reaction mechanism that involves several reaction steps, including addition of permanganate ion across the carbon-carbon double bond to formation of cyclic ester, is described more detailed in [33, 34].

The effectiveness of ISCO with $KMnO_4$ depends on oxidant delivery to the contaminant which is controlled by subsurface transport processes including advection, dispersion, and diffusion [35] and on the persistence of the oxidant in the subsurface [7]. In practice $KMnO_4$ is injected in form of aqueous solution (2 to 4 wt.%), whereby it often moves along preferential pathways. The main drawbacks of ISCO associated with $KMnO_4$ are assigned to: i) high consumption of the oxidant by non-target compounds present in the subsurface and ii) non-uniform distribution of permanganate in the treatment zone, which can result in zones of incomplete contaminant degradation. Furthermore, when injected in solution, permanganate migrates with the flow of the groundwater. Thus, with respect to plume treatment, only a very limited zone of action is achieved, since a real mixing of reagent and contaminated groundwater cannot be achieved. With respect to source treatment, non-aqueous phase liquids (NAPLs) can hardly be contacted by the oxidant with sufficient amounts.

These problems can partly be overcome by designing a new delivery system based on a solid barrier for passive remediation, where the oxidant remains available and active for

a long period [36]. This concept is well known for the reductive treatment with ZVI [19]. However, for ISCO such an approach was not developed so far. One exception represents the so-called oxygen-releasing compound (ORC®) [37], which is a non-toxic and easy-to-handle powder (patented formulation of magnesium peroxide). ORC® is typically mixed with water to form a slurry and directly injected into contaminated soil and groundwater, where it provides a prolonged supply of oxygen (for a period up to about 12 months) and thus enhances in-situ bioremediation. However, ORC® delivers only molecular oxygen (O_2) which is a weak oxidant in chemical reactions.

2.2.2. ISCO with stabilized $KMnO_4$

A delivery system based on stabilized $KMnO_4$ particles would improve the ISCO performance with respect to the life time of the oxidant (over a period of months to years) without the need for continued injection of the oxidant. This would significantly reduce the operating costs and moreover it would make the material safer for working and handling. Fig. 2 illustrates the design of an ISCO technique with stabilized $KMnO_4$ particles. They could be injected as suspension into hydraulic fractures or used to fill trenches or boreholes in order to create *in situ* reactive barriers [38].

To obtain an oxidant with high mobility in porous matrices and to reach captured contaminants (NAPL phase), it is highly desirable to fabricate stabilized $KMnO_4$ particles in the lower micrometer to sub-micrometer range.
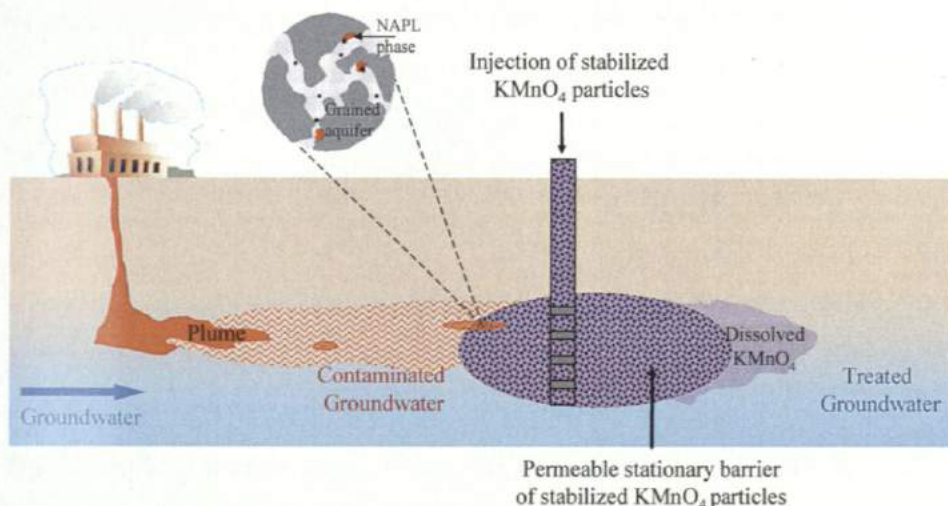
Fig. 2. Concept of application of stabilized KMnO₄ particles in a contaminated aquifer as a slow-release oxidant.
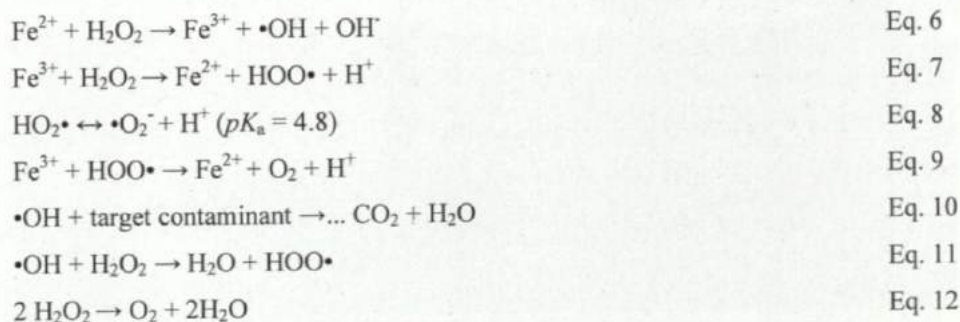
A controlled release of KMnO₄ may be achieved with a partial or complete encapsulation of permanganate grains in an inert shell. The shell can be made up of either inorganic material (e.g., cement) or organic material (e.g., various blends of waxy polymers) [38].

Previously, KMnO₄ particles encapsulated in paraffin wax [39] have been suggested as specifically-targeted oxidants for optimal *in situ* degradation of the NAPL phase. Paraffin wax is highly suitable for this approach, since it is insoluble in water but on the other hand is permeable for hydrophobic contaminants such as PCE [39]. The oxidation process is assumed to occur when the oxidant diffuses out through the shell and is released at the surface of the coating. Water also diffuses through the coating and can effect the release rate [38]. Although it was feasible to synthesize wax-coated microcapsules, the particle diameter was much too high (up to 5 mm) [39], which is by far not sufficient for the mobility of particles in the subsurface.

2.2.3. Oxidation with Fenton reagents

The hydroxyl radical (•OH) can be generated in aqueous solution by various AOPs. One of them is based on the reaction of dissolved Fe^{2+} and H_2O_2 (Eq. 6) which is called homogeneous Fenton reaction [40]. •OH, which is the second strongest oxidant ($E^\circ = 2.7$ V) next to fluorine, unselectively attacks the target contaminant to break it

down finally into CO_2 and water. Fenton reaction and related chemical reactions are presented in Eqs. 6-12:

$$Fe^{2+} + H_2O_2 \rightarrow Fe^{3+} + \bullet OH + OH^- \qquad \text{Eq. 6}$$

$$Fe^{3+} + H_2O_2 \rightarrow Fe^{2+} + HOO\bullet + H^+ \qquad \text{Eq. 7}$$

$$HO_2\bullet \leftrightarrow \bullet O_2^- + H^+ \ (pK_a = 4.8) \qquad \text{Eq. 8}$$

$$Fe^{3+} + HOO\bullet \rightarrow Fe^{2+} + O_2 + H^+ \qquad \text{Eq. 9}$$

$$\bullet OH + \text{target contaminant} \rightarrow ... CO_2 + H_2O \qquad \text{Eq. 10}$$

$$\bullet OH + H_2O_2 \rightarrow H_2O + HOO\bullet \qquad \text{Eq. 11}$$

$$2 H_2O_2 \rightarrow O_2 + 2H_2O \qquad \text{Eq. 12}$$

$\bullet OH$ is capable to destroy dissolved organic contaminants such as saturated and unsaturated halogenated hydrocarbons (e.g., trichloroethane, TCE), aromatic compounds (e.g., BTEX), pentachlorophenol (PCP), nitrophenols, detergents, pesticides, etc. [40]. Inorganic contaminants such as cyanide, sulphide, and nitrite undergo oxidation via $\bullet OH$ as well [7, 10]. The most common reactions of $\bullet OH$ with organic molecules are electrophilic substitution to aromatic compounds and addition to alkenes. Another class of $\bullet OH$ reactions is hydrogen abstraction from saturated compounds such as alkanes, a pathway that proceeds at a slower rate relative to electrophilic substitution and addition [41].

Iron can be applied as Fe^{2+} or Fe^{3+}. The role of the two species in the catalytic reaction cycle is different. If Fe^{2+} is applied in stoichiometric amounts to H_2O_2, one can call this 'stoichiometric Fenton reagent'. Fe is a reactant rather than a catalyst. In case of a large surplus of H_2O_2 one calls this 'catalytic Fenton reagent'. Fe plays the role of a catalyst. The main drawbacks of the homogeneous catalytic Fenton reagent for practical application are that the use of iron salts as catalyst requires its subsequent removal from the treated water, mostly as iron oxide sludge, and the necessity of working at low pH (about pH 3) to achieve acceptable conversion rates and to keep iron in a dissolved state. The operating problems related to homogeneous Fenton reaction can be prevented by replacement of dissolved iron ions by a solid catalyst (so-called heterogeneous Fenton-like reaction). The reaction pathways are considered to proceed likewise in homogeneous Fenton reaction according to the Haber and Weiss mechanism [42]. Fig. 3 illustrates the formation of $\bullet OH$ via catalytic activation of H_2O_2 on a particle surface.
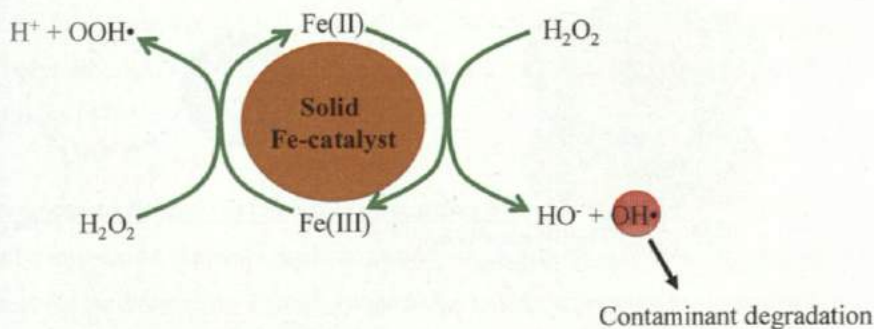
Fig. 3. Scheme of the catalytic activation of H_2O_2, including •OH formation and surface iron recycling in heterogeneous Fenton-like reaction.

In recent years there have been made strong efforts to develop catalysts suitable for practical application. An ideal catalyst possesses a high reactivity towards removal of various contaminants, efficient H_2O_2 utilization, stability over a broad range of working conditions (pH, temperature), and is environmentally benign. Commonly, porous materials with low environmental impact are used as a support for Fenton catalyst. Non-porous metal oxides, metal oxides composites or metals became attractive candidates as well [43, 44]. Although the research has made considerable progress in terms of heterogenization of the Fenton system, a catalyst which would fulfil all requirements was not found so far.

2.2.4. Nanostructured catalysts in heterogeneous Fenton systems
In heterogeneous catalysis materials with high SSA are needed. Two main types of nanocatalysts suggested for heterogeneous Fenton-like reaction are: i) catalyst supported on nanoporous materials including clays, silicas, zeolites or carbon materials and ii) nonsupported nanoparticulate catalysts based on metals or metal oxides. Fig. 4 schematically illustrates the H_2O_2 activation in a porous system (in this case a catalyst supported on a zeolite) and in a system using freely suspended catalyst NPs.
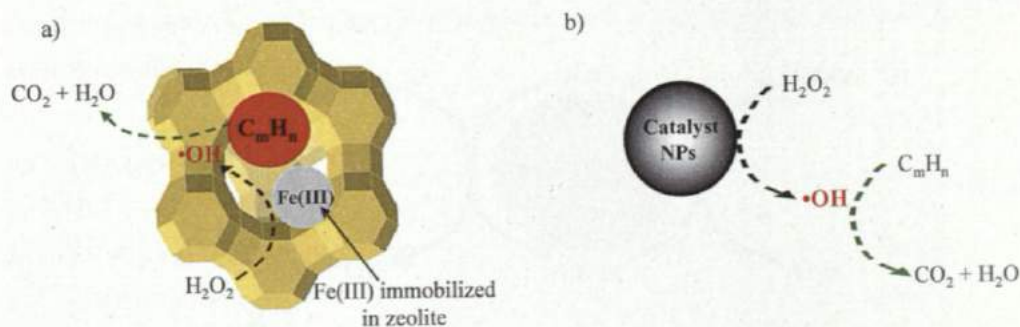
Fig. 4. A simplified scheme of the reaction pathways in heterogeneous Fenton-like reactions using a) nanoporous Fe-zeolite and b) nonsupported Fe-containing catalyst NPs.

Both of the systems have their advantages and shortcomings. The catalyst-on-support approach has the advantage that the support can be designed as an adsorbent so that the contaminants are enriched in the vicinity of the active sites. Furthermore, porous catalysts can be easily adapted to fixed-bed reactors in order to design continuous processes, which are often favored for high-throughput water treatment units. However, mass-transfer limitations or even size exclusion for large molecules (e.g., pharmaceuticals, dyes) can play a crucial role.

In comparison, in systems with catalyst NPs a minimum mass-transfer restriction is expected, since the reaction occurs on the external particle surface. However, separation and recycling of nanocatalysts at a technical scale still presents a challenge. The use of strong magnetic fields in combination with ferri- or ferromagnetic material properties offers an elegant solution for separation and recycling of NP catalysts.

Heterogeneous Fenton system based on nanoporous catalysts

For heterogeneous Fenton system using nanoporous materials several types of catalysts have been proposed. Isolated iron ions are immobilized on the porous support (e.g., Fe-zeolites and Fe-pillared clays) or clusters of iron oxides or mixed metal oxides are fixed on mesoporous alumosilicates or activated carbon (AC) [45, 46]. Among these catalysts zeolites (microporous, aluminosilicate minerals) doped with iron ions showed excellent adsorption properties and Fenton-like activity. It is important to stress that the adsorption of a contaminant depends on its hydrophilic or hydrophobic character and

the size of the molecule which has to be able to enter into the pores. Nevertheless, Fe-zeolites have been successfully applied for the removal of the fuel oxygenate methyl *tert*-butyl ether (MTBE) and, moreover, showed sufficient activity even at neutral pH conditions [47].

Heterogeneous Fenton system based on catalyst NPs

Mainly iron-oxide minerals such as magnetite, hematite, goethite etc. are of a great interest for heterogeneous Fenton systems due to their environmental compatibility and low costs. Nevertheless, there are some other candidates that are worth a short discussion. Interestingly, nZVI which is widely used as reducing agent for *in situ* water remediation was tested as potential Fenton-like catalyst. Actually, Fe(0) can react with O_2 (if present in the groundwater) forming the dissolved Fenton reagents, Fe^{2+} and H_2O_2, near the particle surface. The homogeneous Fenton process is responsible for the overall oxidant production. While the extent of oxidation increases with increasing nZVI concentration, the overall yield of oxidation is unfortunately poor, possibly due to quenching of reactive species by heterogeneous reactions with iron surfaces [48]. Use of bimetallic Ni-Fe NPs has been suggested in order to enhance the oxidative capacity of nZVI [49], however their applicability for any water treatment process must be seencritical due to toxicological concerns with Ni.

Gold NPs, one of the rare examples where a "true" nanoeffect is considered to occur, have emerged as a promising Fenton-like catalyst. Recently it has been reported that gold clusters supported on diamond nanoparticles (Au/DNP) is a highly efficient catalyst to promote the generation of •OH from H_2O_2 [50]. The size of the deposited gold (at the resolution limit of electron microscopy of 2 nm) is considered as the predominant reason for the outstanding catalytic activity of this material for phenol degradation with H_2O_2 compared to other gold catalysts [51]. Based on the existing data it is difficult to conclude the intrinsic catalytic property of gold NPs. However, its further investigation is highly relevant.

Orthoferrites with perovskite structure which are mixed metal oxides with the formula ABO_3 (A is a rare earth metal, B is a transition metal) exhibit a variety of interesting physical properties for instance, ferroelectric, dielectric behavior and chemical properties including heterogeneous catalytic activity, which arise from the crystal symmetry adopted by these materials. Perovskite-based oxides have been applied as

environmentally-friendly catalysts in processes such as catalytic combustion for automobile emissions control [52], or catalytic degradation of chlorinated compounds [53]. More recently, Fe-based perovskites ($AFeO_3$) are regarded as potential (photo)catalysts in Fenton-like systems for removal of various organic pollutants including phenolic substrates or synthetic dyes [54].

Lastly, among the various iron oxides which have been tested as heterogeneous Fenton-like catalysts nano-magnetite has been assumed as one of the most promising candidates. Magnetite is environmentally friendly, inexpensive, easy to recover, and it offers the possibility of recycling via magnetoseparation [55]. Moreover, the specific structural peculiarity is that iron can be cycled between the +2 and +3 oxidation states in the same structure due to the octahedral sites in magnetite. Some studies have emphasized magnetite as efficient catalyst for H_2O_2 activation and contaminant oxidation [56, 57]. This is the case under rather acidic reaction conditions (pH < 5) [56], which can enhance iron dissolution, thus leading to contribution of homogeneous Fenton reactions or when significant adsorption of the model contaminant onto the particle surface occurs [57, 58].

2.3. Isotope fractionation studies

Compound specific isotope analysis (CSIA) is an innovative tool for a qualitative and/or quantitative assessment of organic contaminant transformation in the environment [59]. Usually, the transformation process, which can be a chemical reaction or a microbiological conversion, changes the isotopic composition of the target compound in a characteristic manner. During chemical transformations (e.g., the cleavage or the formation of chemical bonds) a shift in the isotope ratios of the substrate and the product may occur. This effect is known as kinetic isotope fractionation and is due to the fact that bonds involving the lighter isotopes are usually weaker then bonds with the heavy isotopes and thus react faster. This leads to a progressive enrichment of the molecules containing heavy isotopes at the reacting bond in the remaining fraction of the substrate, while the degradation product is depleted in the heavy isotopes.

The bulk isotope composition of a given compound is commonly reported as difference in per mil with respect to an international standard, and as is denoted as $\delta^h E$ [59]:

$$\delta^h E = \left(\frac{R_{sample}}{R_{reference}} - 1 \right) \cdot 1000 \ [\permil]$$

Eq. 13

where R_{sample} and $R_{reference}$ are the ratios of the heavy isotope to light isotope in the sample and the international standard, respectively.

Stable isotope ratios (e.g., $^{13}C/^{12}C$, $^{2}H/^{1}H$) of individual organic contaminants can be analyzed with gas chromatography-isotope ratio mass spectrometry (GC-IRMS). They may be used as fingerprints to infer contamination sources, and may demonstrate, and even quantify, the occurrence of natural contaminant transformation by the enrichment of heavy isotopes that arises from degradation-induced isotope fractionation.

For biotic and abiotic processes, this fractionation is usually quantified by the "Rayleigh Equation" (Eq. 14):

$$\ln\left(\frac{\delta^{13}C_t + 1000}{\delta^{13}C_0 + 1000} \right) = \frac{\varepsilon}{1000} \cdot \ln f$$

Eq. 14

where f is the residual fraction of the substrate. The slope of the Rayleigh plot gives the bulk enrichment factor ε for the considered process. Fig. 5 shows an example of Rayleigh plot evaluation.
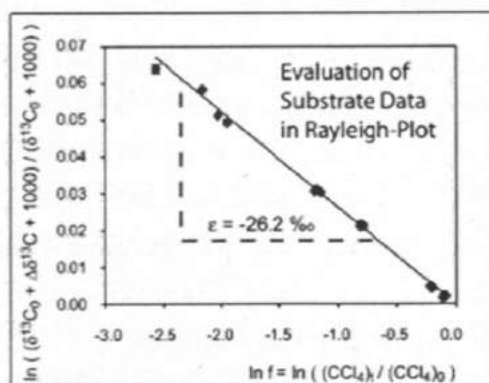

Fig. 5. Rayleigh plot obtained from the carbon-isotope fractionation measured during reductive dehalogenation of carbon tetrachloride (CCl_4) by a reduced iron porphyrine [59].

In the last decade great efforts were undertaken to determine enrichment factors ε for various biological and chemical processes under well defined laboratory conditions in order to provide basis for evaluation of contaminant transformation in the field.

2.4. Aims and scope of the present thesis

The main aim of this thesis was to introduce novel approaches in order to improve two well known remediation techniques, in particular *in situ* permanganate oxidation and oxidation with Fenton reagents. Due to the previously discussed specific features of NPs, elucidation of the potential improvements which can be achieved by application of colloidal reagents and catalysts in these processes is highly relevant.

The first part of this thesis (Manuscript 1) aims to invent a novel approach for stabilization of $KMnO_4$ particles, which can be introduced into the subsurface as reactive barrier for efficient plume remediation. According to our hypothesis, implementation of MnO_2 coating onto the permanganate particle would significantly decrease the solubility of $KMnO_4$ in aqueous media. Moreover, MnO_2 coating can act as an additional oxidant and adsorbent, and is considered as environmentally harmless. Success in this approach would mean a breakthrough for ISCO but also can be applied in other heterogeneous systems, where oxidant in solid phase is needed.

The second part of this thesis (Manuscripts 2 + 3) deals with the implementation of nanoparticulate catalysts in a heterogeneous Fenton-like system, which reduces the drawbacks of the homogeneous Fenton reaction, mainly the requirement of low reaction pH and formation of iron sludge. For this purpose catalysts with low-environmental impact were tested, in particular magnetic iron oxides and orthoferrites with perovskite structure. These catalysts were synthesized in the laboratory and characterized via different techniques. Their catalytic properties were evaluated based on batch experiments using several environmentally relevant contaminants. Furthermore, the mechanistic understanding and applicability evaluation for a relevant environmental catalysis process was thoroughly studied and discussed.

Finally, this thesis aims to better understand the reaction mechanisms that occur during the oxidation reactions with homogeneous and heterogeneous Fenton reagents (Manuscript 3 + 4). For this purpose, isotope fractionation studies based on CSIA were introduced.

References

[1] Progress on Sanitation and Drinking-Water, World Health Organization (WHO)/United Nations International Children's Fund (UNICEF) Joint Monitoring Programme for Water Supply and Monitoring, 2010.

[2] Human Development Reports, United Nations Development Programme (UNDP), (2006).

[3] H. Zhou, D.W. Smith, Advanced technologies in water and wastewater treatment, *Can. J. Civil. Eng.* 28 (2001) 49-66.

[4] A. Bhatnagar, A.K. Minocha, Conventional and non-conventional adsorbents for removal of pollutants from water - A review, *Indian J. Chem. Techn.* 13 (2006) 203-217.

[5] D.C. McKinney, M.D. Lin, Pump and treat groundwater remediation system optimization, *J. Water Res. Pl.-Asce* 122 (1996) 128-136.

[6] R.L. Siegrist, M.A. Urynowicz, O.R. West, M.L. Crimi, K.S. Lowe, Principles and Practices of In Situ Chemical Oxidation Using Permanganate, Battelle Press, Columbus, Ohio, 2001.

[7] S.G. Huling, B.E. Pivetz, In-Situ Chemical Oxidation, Engineering Issue 2006, avaliable on: http://www.epa.gov/ada/gw/isco.html.

[8] A.N. Soon, B.H. Hameed, Heterogeneous catalytic treatment of synthetic dyes in aqueous media using Fenton and photo-assisted Fenton process, *Desalination* 269 (2011) 1-16.

[9] M. Pera-Titus, V. Garcia-Molina, M.A. Banos, J. Gimenez, S. Esplugas, Degradation of chlorophenols by means of advanced oxidation processes: A general review, *Appl. Catal. B-Environ.* 47 (2004) 219-256.

[10] R. Munter, Advanced oxidation processes–current status and prospects, *Proc. Estonian Acad. Sci. Chem.* 50 (2001) 59-80.

[11] N. Savage, M.S. Diallo, Nanomaterials and water purification: Opportunities and challenges, *J. Nanopart. Res.* 7 (2005) 331-342.

[12] European Commission, Nanomaterials, avaliable on: http://ec.europa.eu/environment/chemicals/nanotech/index.htm.

[13] J.T. Nurmi, P.G. Tratnyek, V. Sarathy, D.R. Baer, J.E. Amonette, K. Pecher, C.M. Wang, J.C. Linehan, D.W. Matson, R.L. Penn, M.D. Driessen,

Characterization and properties of metallic iron nanoparticles: Spectroscopy, electrochemistry, and kinetics, *Environ. Sci. Technol.* 39 (2005) 1221-1230.

[14] H. Hildebrand, K. Mackenzie, F.D. Kopinke, Highly hctive Pd-on-magnetite nanocatalysts for aqueous phase hydrodechlorination reactions, *Environ. Sci. Technol.* 43 (2009) 3254-3259.

[15] W.X. Zhang, Nanoscale iron particles for environmental remediation: An overview, *J. Nanopart. Res.* 5 (2003) 323-332.

[16] K. Mackenzie, A. Schierz, A. Georgi, F.D. Kopinke, Colloidal activated carbon and carbo-iron - Novel materials for in-situ groundwater treatment, *Global Nest J.* 10 (2008) 54-61.

[17] A. Zach-Maor, R. Semiat, H. Shemer, Removal of heavy metals by immobilized magnetite nano-particles, *Desalin. Water Treat.* 31 (2011) 64-70.

[18] M. Auffan, J. Rose, J.Y. Bottero, G.V. Lowry, J.P. Jolivet, M.R. Wiesner, Towards a definition of inorganic nanoparticles from an environmental, health and safety perspective, *Nat. Nanotechnol.* 4 (2009) 634-641.

[19] P.G. Tratnyek, R.L. Johnson, Nanotechnologies for environmental cleanup, *Nano Today* 1 (2006) 44-48.

[20] M. Auffan, J. Rose, O. Proux, D. Borschneck, A. Masion, P. Chaurand, J.L. Hazemann, C. Chaneac, J.P. Jolivet, M.R. Wiesner, A. Van Geen, J.Y. Bottero, Enhanced adsorption of arsenic onto maghemites nanoparticles: As(III) as a probe of the surface structure and heterogeneity, *Langmuir* 24 (2008) 3215-3222.

[21] B. Hvolbaek, T.V.W. Janssens, B.S. Clausen, H. Falsig, C.H. Christensen, J.K. Norskov, Catalytic activity of Au nanoparticles, *Nano Today* 2 (2007) 14-18.

[22] C.T. Yavuz, J.T. Mayo, W.W. Yu, A. Prakash, J.C. Falkner, S. Yean, L.L. Cong, H.J. Shipley, A. Kan, M. Tomson, D. Natelson, V.L. Colvin, Low-field magnetic separation of monodisperse Fe_3O_4 nanocrystals, *Science* 314 (2006) 964-967.

[23] D. Horak, M. Babic, H. Mackova, M.J. Benes, Preparation and properties of magnetic nano- and microsized particles for biological and environmental separations, *J. Sep. Sci.* 30 (2007) 1751-1772.

[24] Y.L. Wang, Y.N. Xia, Bottom-up and top-down approaches to the synthesis of monodispersed spherical colloids of low melting-point metals, *Nano Letters* 4 (2004) 2047-2050.

[25] V.M. Rotello, Nanoparticles: Building Blocks for Nanotechnology, New York, 2004.

[26] K. Iwahori, I. Yamashita, Bio-template synthesis of nanoparticle by cage-shaped protein supramolecule, apoferritin, *J. Clust. Sci.* 18 (2007) 358-370.

[27] W. De Windt, P. Aelterman, W. Verstraete, Bioreductive deposition of palladium (0) nanoparticles on Shewanella oneidensis with catalytic activity towards reductive dechlorination of polychlorinated biphenyls, *Environ. Microbiol.* 7 (2005) 314-325.

[28] D.A. Bazylinski, R.B. Frankel, K.O. Konhauser, Modes of biomineralization of magnetite by microbes, *Geomicrobiol. J.* 24 (2007) 465-475.

[29] P.J. Vikesland, A.M. Heathcock, R.L. Rebodos, K.E. Makus, Particle size and aggregation effects on magnetite reactivity toward carbon tetrachloride, *Environ. Sci. Technol.* 41 (2007) 5277-5283.

[30] W.A. Arnold, W.P. Ball, A.L. Roberts, Polychlorinated ethane reaction with zero-valent zinc: pathways and rate control, *J. Contam. Hydrol.* 40 (1999) 183-200.

[31] P. Harriot, Mass transfer to particles: Part I. Suspended in agitated tanks, *AIChE J.* 8 (1962) 93-101.

[32] O. Levenspiel, Chemical Reaction Engineering. Chapter 14: Solid-catalyzed reactions, J. Wiley&Sons, New York, 1972.

[33] S. Dash, S. Patel, B.K. Mishra, Oxidation by permanganate: synthetic and mechanistic aspects, *Tetrahedron* 65 (2009) 707-739.

[34] K.C. Huang, G.E. Hoag, P. Chheda, B.A. Woody, G.M. Dobbs, Kinetic study of oxidation of trichloroethylene by potassium permanganate, *Environ. Eng. Sci.* 16 (1999) 265-274.

[35] J.L. Heiderscheidt, M. Crimi, R.L. Siegrist, M.A. Singletary, Optimization of full-scale permanganate ISCO system operation: Laboratory and numerical studies, *Ground Water Monit. R.* 28 (2008) 72-84.

[36] A.R. Gavaskar, Design and construction techniques for permeable reactive barriers, *J. Hazard. Mater.* 68 (1999) 41-71.

[37] Regenesis Bioremediation Products, Oxygen Release Compounds (ORC), (1996).

[38] C. Ross, L.C. Murdoch, D.L. Freedman, R.L. Siegrist, Characteristics of potassium permanganate encapsulated in polymer, *J. Environ. Eng.-Asce* 131 (2005) 1203-1211.

[39] N. Kang, I. Hua, P.S.C. Rao, Production and characterization of encapsulated potassium permanganate for sustained release as an in situ oxidant, *Ind. Eng. Chem. Res.* 43 (2004) 5187-5193.

[40] J.J. Pignatello, E. Oliveros, MacKay, Advanced oxidation processes for organic contaminant destruction based on the Fenton reaction and related chemistry, *Crit. Rev. Env. Sci. Technol.* 36 (2006) 1-84.

[41] G.V. Buxton, C.L. Greenstock, W.P. Helman, A.B. Ross, Critical review of rate constants for reactions of hydrated electrons, hydrogen-atoms and hydroxyl radicals (OH/O^-) in aqueous solution, *J. Phys. Chem. Ref. Data* 17 (1988) 513-886.

[42] F. Haber, J. Weiss, The catalytic decomposition of hydrogen peroxide by iron salts, *Proc. R. Soc. London, Ser. A.* 147, 332-351 (1934).

[43] E.G. Garrido-Ramirez, B.K.G. Theng, M.L. Mora, Clays and oxide minerals as catalysts and nanocatalysts in Fenton-like reactions - A review, *Appl. Clay Sci.* 47 (2010) 182-192.

[44] I. Magario, F.S.G. Einschlag, E.H. Rueda, J. Zygadlo, M.L. Ferreira, Mechanisms of radical generation in the removal of phenol derivatives and pigments using different Fe-based catalytic systems, *J. Mol. Catal. A-Chem.* 352 (2012) 1-20.

[45] A. Rey, M. Faraldos, J.A. Casas, J.A. Zazo, A. Bahamonde, J.J. Rodriguez, Catalytic wet peroxide oxidation of phenol over Fe/AC catalysts: Influence of iron precursor and activated carbon surface, *Appl. Catal. B-Environ.* 86 (2009) 69-77.

[46] A. Georgi, F.D. Kopinke, Interaction of adsorption and catalytic reactions in water decontamination processes Part I. Oxidation of organic contaminants with hydrogen peroxide catalyzed by activated carbon, *Appl. Catal. B-Environ.* 58 (2005) 9-18.

[47] A. Georgi, R. Gonzalez-Olmos, R. Kohler, F.D. Kopinke, Fe-Zeolites as Catalysts for Wet Peroxide Oxidation of Organic Groundwater Contaminants:

Mechanistic Studies and Applicability Tests, *Separ. Sci. Technol.* 45 (2010) 1579-1586.

[48]   S.E. Mylon, Q.A. Sun, T.D. Waite, Process optimization in use of zero valent iron nanoparticles for oxidative transformations, *Chemosphere* 81 (2010) 127-131.

[49]   C. Lee, D.L. Sedlak, Enhanced Formation of Oxidants from Bimetallic Nickel-Iron Nanoparticles in the Presence of Oxygen, *Environ. Sci. Technol.* 42 (2008) 8528-8533.

[50]   S. Navalon, R. Martin, M. Alvaro, H. Garcia, Gold on Diamond Nanoparticles as a Highly Efficient Fenton Catalyst, *Angew. Chem. Int. Edit.* 49 (2010) 8403-8407.

[51]   R. Martin, S. Navalon, M. Alvaro, H. Garcia, Optimized water treatment by combining catalytic Fenton reaction using diamond supported gold and biological degradation, *Appl. Catal. B-Environ.* 103 (2011) 246-252.

[52]   T. Seiyama, Total Oxidation of Hydrocarbons on Perovskite Oxides, *Catal. Rev.* 34 (1992) 281-300.

[53]   G. Sinquin, C. Petit, S. Libs, J.P. Hindermann, A. Kiennemann, Catalytic destruction of chlorinated C-2 compounds on a $LaMnO_{3+\delta}$ perovskite catalyst, *Appl. Catal. B-Environ.* 32 (2001) 37-47.

[54]   W. Luo, L.H. Zhu, N. Wang, H.Q. Tang, M.J. Cao, Y.B. She, Efficient removal of organic pollutants with magnetic nanoscaled $BiFeO_3$ as a reusable heterogeneous Fenton-like catalyst, *Environ. Sci. Technol.* 44 (2010) 1786-1791.

[55]   A. Dhakshinamoorthy, S. Navalon, M. Alvaro, H. Garcia, Metal nanoparticles as heterogeneous Fenton catalysts, *Chemsuschem* 5 (2012) 46-64.

[56]   H.Y. Niu, D. Zhang, S.X. Zhang, X.L. Zhang, Z.F. Meng, Y.Q. Cai, Humic acid coated Fe_3O_4 magnetic nanoparticles as highly efficient Fenton-like catalyst for complete mineralization of sulfathiazole, *J. Hazard. Mater.* 190 (2011) 559-565.

[57]   P. Baldrian, V. Merhautova, J. Gabriel, F. Nerud, P. Stopka, M. Hruby, M.J. Benes, Decolorization of synthetic dyes by hydrogen peroxide with heterogeneous catalysis by mixed iron oxides, *Appl. Catal. B-Environ.* 66 (2006) 258-264.

[58] X.F. Xue, K. Hanna, C. Despas, F. Wu, N.S. Deng, Effect of chelating agent on the oxidation rate of PCP in the magnetite/H_2O_2 system at neutral pH, *J. Mol. Catal. A-Chem.* 311 (2009) 29-35.

[59] M. Elsner, L. Zwank, D. Hunkeler, R.P. Schwarzenbach, A new concept linking observable stable isotope fractionation to transformation pathways of organic pollutants, *Environ. Sci. Technol.* 39 (2005) 6896-6916.

3. Overview of the following manuscripts

The objective of the study described in the first manuscript entitled as "Stabilization of potassium permanganate particles with manganese dioxide" was to develop stabilized permanganate particles with slow-release properties in order to obtain an oxidant applicable in reactive permeable barriers. Manganese dioxide (MnO_2) as suitable, in water insoluble coating was synthesized onto the $KMnO_4$ via direct partial reduction of $KMnO_4$ microparticles. The obtained MnO_2-coated $KMnO_4$ particles (MCP) were characterized via several techniques. The stability of MCP was tested in column experiments under flow-through conditions and compared with native $KMnO_4$. Moreover, to test the oxidation capacity of the MCP and thus enlarge the potential applications of permanganate oxidation processes for *in situ* remediation, reactions in non-aqueous media were carried out.

In the second manuscript entitled as "Nano-sized magnetic iron oxides as catalysts for heterogeneous Fenton-like reactions – influence of Fe(II)/Fe(III) ratio on catalytic performance", various Fe(II,III) oxides such as magnetite (Fe_3O_4) were tested for the catalytic oxidation of phenol with hydrogen peroxide (H_2O_2). The catalysts were prepared by a co-precipitation method or obtained commercially. The prepared samples were further characterized and tested in batch experiments under various reaction conditions. Furthermore, the chemical and physical stability of the nanocatalysts under Fenton conditions is thoroughly elucidated and discussed. Finally, batch experiments with various structurally distinct organic compounds were carried out in order to estimate the selectivity of the heterogeneous Fenton-like reaction catalyzed by Fe(II,III) oxide.

The third manuscript entitled as "$LaFeO_3$ and $BiFeO_3$ perovskites as nanocatalysts for contaminant degradation in heterogeneous Fenton-like reaction" deals with the applicability of two perovskite catalyst in the Fenton system under environmentally relevant conditions.
$LaFeO_3$ (LFO) and $BiFeO_3$ (BFO) were synthesized in the laboratory according to the sol-gel procedure and were characterized via different physicochemical techniques. Their catalytic properties were evaluated in batch experiments using phenol and methyl-

tert-butyl ether (MTBE) as model contaminants. Reaction conditions such as catalyst and H_2O_2 concentration, pH and temperature were varied, whereby the intrinsic catalytic activities of BFO and LFO were obtained. Furthermore, the reusability of the BFO perovskite was examined in several consecutive batch runs.

This manuscript also includes a detailed discussion of the results of compound specific isotope analysis (CSIA) for the perovskite-catalyzed Fenton-like reaction, in order to elucidate the type of reactive species involved. For this purpose, bulk enrichment factors for C and H during MTBE and ethyl-tert-butyl ether (ETBE) degradation (as determined in the fourth manuscript) were converted into kinetic isotope effects (*KIEs*) and compared with literature data for oxidation reactions involving •OH.

In the fourth manuscript entitled as "Critical evaluation of the 2D-CSIA scheme for distinguishing fuel oxygenate degradation reaction mechanisms" bulk enrichment factors for C and H (ε_C and ε_H) as well as their ratios (λ) were determined for MTBE and ETBE degradation in several biotic and abiotic systems. These data were used as basis for elucidating the relevance of the 2D-CSIA approach for a simple distinguishing of oxygenate biotransformation mechanisms and interpretation of groundwater plumes at field sites. The obtained isotope fractionation results for the perovskite-catalyzed reaction have been compared to other chemical oxidation systems such as permanganate oxidation, homogeneous Fenton- and Fenton-like ($Fe^{3+} + H_2O_2$) oxidation.

4. Stabilization of potassium permanganate particles with manganese dioxide

Klara Rusevova, Frank-Dieter Kopinke, Anett Georgi

Abstract

A new potassium permanganate reagent with slow-release properties was designed and tested for possible application in *in situ* chemical oxidation. For this purpose, MnO_2-coated $KMnO_4$ particles (MCP) were prepared by partial reduction of solid $KMnO_4$ using the acid-catalyzed reaction with n-propanol or the comproportionation of Mn(VII) and Mn(II) in n-propanol as reaction medium. Column tests showed that, for MCP with a residual $KMnO_4$ fraction of 70 wt%, the duration of permanganate release under flow-through conditions was prolonged by a factor of 10 compared to untreated $KMnO_4$. While $KMnO_4$ is too soluble to be used in reactive barriers, MCP could be introduced into the aquifer by filling of trenches or boreholes; this would allow a prolonged passive dosing of permanganate into the flowing groundwater. In addition, experiments were conducted in order to determine the oxidation capability of native $KMnO_4$ particles and MCP in CH_2Cl_2, a representative non-polar non-aqueous phase liquid (NAPL). It may be possible to utilize the significantly higher reactivity of MCP under these conditions for the design of slow-release permanganate particles for NAPL source treatment.

1. Introduction

Potassium permanganate ($KMnO_4$) has been widely used for the treatment of pollutants in drinking water and wastewater for over 50 yr. At the end of the last century, $KMnO_4$ also became widely used as an oxidant for *in situ* chemical oxidation (ISCO) (Siegrist et al., 2001), providing a rapid and cost-effective treatment technique for non-aqueous phase liquid (NAPL) source zones, or zones of high residual contamination.

$KMnO_4$, which is usually injected into the contaminated zone as an aqueous solution, is in many cases able to transform the contaminants into products that are harmless to the environment. The half-life or longevity of $KMnO_4$ depends on site-specific conditions (Huling and Pivetz, 2006). There are several problems associated with ISCO by permanganate. The first problem is non-target permanganate consumption – called Natural Oxidant Demand (NOD), in which permanganate, as a non-specific oxidant, reacts with natural organic matter and other naturally occurring species that can be oxidized (Urynowicz, 2008). Therefore, only a small fraction of the applied oxidant actually reaches and attacks the contaminant. The second problem is associated with the difficulty of controlling the distribution of permanganate in the subsurface. Non-uniform distribution of the oxidant can cause incomplete contaminant degradation. In many cases, source-zone treatment is not adequate for reaching remediation goals (regulatory limits), and treatment of the contaminated groundwater plume must also be implemented. A third problem is the formation of MnO_2 coatings on the surface of the NAPL phase during ISCO with dissolved $KMnO_4$, inhibiting further access to the oxidant (Crimi and Siegrist, 2004).

Permeable reactive barriers (PRBs) have gained significant attention as a remedial technology due to their favorable cost/benefit ratio and the potential of PRBs for reducing the spread of contaminants. PRBs are constructed in the subsurface such that they intercept a contaminant plume, provide a flow path through the reactive media, and transform the contaminant(s) into environmentally acceptable forms in order to attain remediation concentration goals down-gradient of the barrier (Gavaskar, 1999). The most widely known solid barrier for passive remediation is zero-valent iron, which is used in reactive barriers for the reduction of halogenated hydrocarbons (for instance, to convert trichloroethene (TCE) into ethene and ethane). To the best of our knowledge, no solid barrier is being used for passive *oxidative* remediation at the moment, with the

exception of oxygen-releasing compounds (ORCs) (Koenigsberg and Sandefur, 1999) which are used for *in situ* bioremediation. $KMnO_4$ is unsuitable for this technique due to its high solubility in water and subsequent mobility in groundwater, but a delivery system with a slow release of permanganate might overcome these obstacles. Two types of approaches for slow-release of permanganate have been proposed: (I) a delivery system consisting of $KMnO_4$ granules dispersed in an inert organic crystalline matrix for placement in wells (Lee and Schwartz, 2007; Lee et al., 2008) and (II) the preparation of single $KMnO_4$ particles stabilised by organic coatings (Kang et al., 2004; Ross et al., 2005). $KMnO_4$ encapsulated by paraffin wax has been proposed as a specifically-targeted oxidant for optimal *in situ* destruction of the contaminant with decreased NOD (Kang et al., 2004). Based on the finding that the paraffin wax dissolves rapidly in a perchloroethylene phase, the encapsulation approach was suggested for treatment of NAPL contaminations. Another work focused on the encapsulation of permanganate in various waxy polymers and studied the oxidant release properties of the respective microcapsules together with the degradation of TCE in water (Ross et al., 2005). The authors suggested that degradation of TCE is based not only on diffusion of permanganate into the water phase, but possibly also on the diffusion of TCE into the microcapsules, where it reacts with permanganate (Ross et al., 2005).
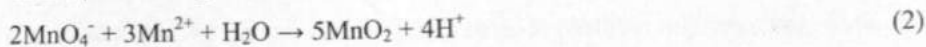
Permanganate particles with increased life time might be able to enter into NAPL phases. Thus the reaction medium would change from water (as in traditional applications of dissolved permanganate) towards a non-aqueous medium. The reactivity of aqueous permanganate towards many substrates is widely documented (Waldemer and Tratnyek, 2006), whereas its reactivity in more or less non-polar phases has not been so thoroughly investigated.

The objective of our study was to develop stabilized permanganate particles with slow-release properties, and possibly improved oxidation efficiencies in media other than water, which could enlarges the potential applications of permanganate oxidation processes for *in situ* remediation. In the first part of our paper, the reactivity of $KMnO_4$ in a non-polar solvent as a model situation for NAPLs is studied. $KMnO_4$ is known to be highly reactive in water. However, in organic synthesis, special procedures are applied in order to conduct oxidation reactions with permanganate in non-aqueous media. This includes application of organic-soluble permanganate salts, such as tetraethylammonium permanganate (Dash et al., 2009), or application of $KMnO_4$ on

solid supports. Immobilization of $KMnO_4$ on the surface of solid supports such as aluminum silicate, hydrated alumina or active MnO_2 can lead to modifications in its chemical reactivity and selectivity (Shaabani and Lee, 2001; Shaabani et al., 2004; Dash et al., 2009).

The second part of our paper focuses on a novel way of encapsulating $KMnO_4$ particles. A promising coating material for $KMnO_4$ particles with controlled-release properties could be manganese dioxide (MnO_2). Manganese dioxide is insoluble in water and organic solvents, and can act as adsorbent and catalyst (Hammel et al., 2002). MnO_2 also has further desirable properties: it can be prepared by low-cost procedures and is considered as environmentally harmless (Greenwood and Earnshaw, 1997). In the literature, the combination of $KMnO_4$ and active MnO_2 has been described as an effective oxidant for a variety of organic compounds under solvent-free and heterogeneous conditions (Shaabani et al., 2004).

In our experiments, we tried to synthesize MnO_2-coated $KMnO_4$ particles (MCP) directly by partial reduction of $KMnO_4$ microparticles. Two different reaction pathways were tested: (I) reduction of $KMnO_4$ by primary alcohols, and (II) redox reaction between Mn^{2+} and MnO_4^-.

$$4MnO_4^- + 3R\text{-}CH_2\text{-}OH \rightarrow 3R\text{-}COOH + 4MnO_2 + 4OH^- + H_2O \qquad (1)$$
$$2MnO_4^- + 3Mn^{2+} + H_2O \rightarrow 5MnO_2 + 4H^+ \qquad (2)$$

It is the basic idea of our approach, that the permanganate reduction takes place as heterogeneous reaction and that the formed MnO_2 adheres directly at the surface of the $KMnO_4$ particles. Primary alcohols, which cause only minor dissolution of $KMnO_4$, were used as reaction medium for both reactions and as reducing agent in reaction I.

2. Experimental part

2.1. Materials

All of the chemicals used in the following experiments: potassium permanganate, n-propanol, manganese(II) nitrate tetrahydrate, benzene, dichloromethane, benzaldehyde and H_2SO_4 (98%), were purchased from Merck (Germany) or Sigma-Aldrich

(Germany) and had a purity of $\geq 99\%$. $KMnO_4$ was sieved to a size fraction of 63 - 250 μm.

2.2. Experimental Methods

2.2.1. Solvent effect on oxidation with $KMnO_4$

Benzaldehyde was chosen as a model reactant for evaluating the influence of the reaction medium on the oxidation with potassium permanganate. Batch experiments were performed at ambient conditions ($23 \pm 2\ °C$) using glass vials with screw caps and Teflon-coated septa. Vials were shaken during the experiment on a horizontal shaker. The oxidation of benzaldehyde (10 mg) with $KMnO_4$ (0.5 g) was tested in three different systems: I) in 10 mL dichloromethane without the presence of water, II) in 10 mL dichloromethane which contained 0.5% v/v dissolved H_2O, and III) in a two-liquid-phase system consisting of 1 mL of water and 9 mL of dichloromethane. Benzene, (10 mg) which has a very low reactivity with permanganate (Waldemer and Tratnyek, 2006), was used as an inert internal standard in all three systems. Benzene, benzaldehyde and the product of oxidation, benzoic acid, were analyzed in aliquots of the dichloromethane phase by means of GC-MS (Agilent) in the selected ion monitoring mode. Samples were analyzed after 3 h reaction time and then after every 24 h for 4 d.

2.2.2. Preparation of MnO_2-coated $KMnO_4$ particles

The coating of $KMnO_4$ with MnO_2 was performed in batch experiments, carried out in 50 mL glass flasks placed on a heating plate with magnetic stirring. During the reaction the temperature was kept at 90 °C. $KMnO_4$ was treated according to the following procedures (R_0, R_1 or R_2), all with n-propanol as reaction medium. For reactions R_0 and R_1, 0.5 g $KMnO_4$ was suspended in 15 mL n-propanol. In the case of reaction R_1, additionally 100 μL H_2SO_4 (50 %) was added as catalyst. For reaction R_2, 0.1 g $Mn(NO_3)_2 \cdot 4H_2O$ was dissolved in 15 mL n-propanol, to which 0.5 g $KMnO_4$ particles were then added. Reaction times of 0.5, 1, 2 and 3 h were applied for each of the three procedures. The coated permanganate particles obtained were filtered, air dried and further investigated.

2.2.3. KMnO₄ release and recovery tests

The dissolution of $KMnO_4$ from MCP and the amount of residual $KMnO_4$ after the treatment were determined in a column experiment. A glass column (ID = 0.3 cm, l = 10 cm) was filled with a homogenous mixture of 0.3 g quartz sand (grain size $\leq$ 250 μm) and 0.1 g MCP or native $KMnO_4$ particles, for comparison under dry conditions. The filled column (bed height = 4.5 cm, bed volume = 0.32 cm³, porosity = 0.35) was flushed with CO_2 in order to accelerate the saturation of the column packing after starting the water flow. The water used for experiments was de-gassed by purging with helium. In the column experiment, water was pumped through the column in the upwards direction using a piston pump. The water flow rate was 0.7 mL min⁻¹. The kinetics of dissolution of the MCP was measured and compared with the kinetics of dissolution of the native $KMnO_4$.

In order to determine the recovery of $KMnO_4$, the effluent (dissolved $KMnO_4$) leaving the column was collected in a graduated vessel and the $KMnO_4$ concentration was determined spectrophotometrically at λ = 545 nm (using a UVmini-1240, Shimadzu). The total amount of $KMnO_4$ recovered in the effluent was related to the initially applied amount of $KMnO_4$.

2.2.4. Coating characterization

Images of $KMnO_4$ or MCP were obtained by means of scanning electron microscopy (SEM). SEM was accomplished using a Zeiss Ultra 55 with Gemini column and an acceleration voltage of 1-3 kV.

The specific surface area of MCP was determined by the BET method using the N_2 adsorption-desorption isotherms as measured by means of a Belsorp-miniII instrument. All samples were pre-treated at 150 °C; afterwards, N_2 adsorption was measured at 77 K.

X-ray powder diffraction (XRD) using a Bruker D8 Diffractometer at 20 °C with Cu $K\alpha$ radiation was used in order to determine the crystalline phases present in MCP.

2.2.5. Oxidation tests with MCP under anhydrous conditions

One g of MCP or native $KMnO_4$ was added to 10 mL dichloromethane containing 20 ppm benzaldehyde as reactant and 20 ppm benzene as inert internal standard. The flasks were placed on a shaker for 96 h at ambient temperature (23 ± 2 °C). Every 24 h, aliquots of the liquid phase were analyzed by means of GC-MS as described above.

3. Results and discussion

3.1. Solvent effect on oxidation with $KMnO_4$

The objective of the first experiment was to measure the reactivity of $KMnO_4$ in three different reaction media. No change in the color of the liquid was observed in the 1-phase systems (CH_2Cl_2 and CH_2Cl_2 with 0.5% v/v dissolved water), indicating that the $KMnO_4$ dissolution was insignificant. After addition of $KMnO_4$ to the 2-phase system (volume ratio CH_2Cl_2/water = 1/9) and shaking, $KMnO_4$ was immediately dissolved in the water phase. During a reaction time of 96 h, no significant change in benzaldehyde concentration was observed in dry CH_2Cl_2, in contrast to the other two systems. Figure 1 shows the rate of the benzaldehyde oxidation by $KMnO_4$ in the two water-containing media. Benzoic acid was detected as oxidation product in the water-containing systems but not in dry CH_2Cl_2 (detection limit is 10 μg L^{-1}, corresponding to a benzaldehyde conversion degree of 10^{-3} %).

The results obtained show that benzaldehyde oxidation nearly follows a pseudo-first-order kinetics.
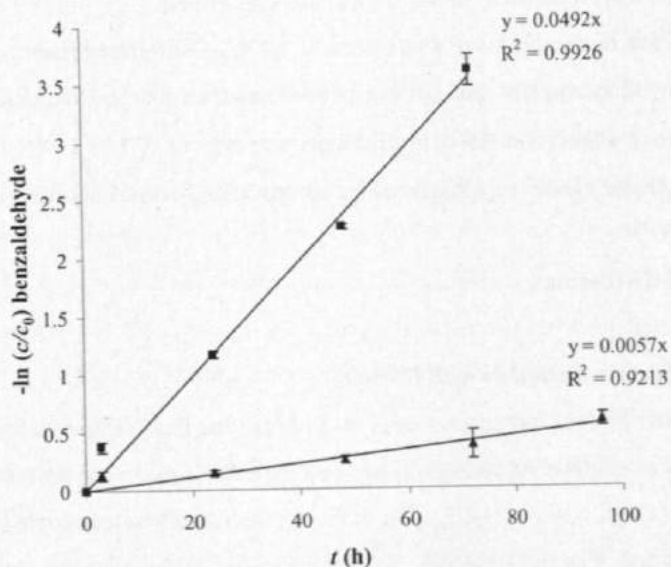
Fig. 1. Pseudo-first order plot of benzaldehyde degradation with KMnO₄ in two different media (■ 2-phase system, ▲ CH₂Cl₂ with dissolved water (0.5 % v/v)). Results shown are mean values of at least two experiments and the error represents the deviation of the single values from the mean value.

The rate constant for oxidation of benzaldehyde was almost 10 times higher in the 2-phase system than in CH_2Cl_2 with dissolved water (Fig. 1). In the 2-phase system, the permanganate was dissolved in water, whereas the benzaldehyde, due to its hydrophobicity, was predominantly present in the CH_2Cl_2 phase. Nevertheless, there is a significant degradation of benzaldehyde, either via its small dissolved fraction in the aqueous phase or due to a reaction of permanganate and benzaldehyde at the interface of the two phases. Also in the wet CH_2Cl_2 solvent phase there was a slow degradation of benzaldehyde which approximately followed a pseudo-first-order kinetics. In contrast, in the dry CH_2Cl_2 solvent phase containing KMnO₄, neither significant depletion of benzaldehyde nor production of benzoic acid were observed during the 4–d experimental period. Based on the detection limit determined for benzoic acid, we can conclude that the rate constant for benzaldehyde oxidation in this system is $< 10^{-7}$ h^{-1}, i.e. at least four orders of magnitude lower than in the presence of traces of water.

We are aware of the fact that the measured kinetics also reflects mass transfer processes, not just the pure chemical reaction kinetics. The results obtained in our experiments indicate that heterogeneous reactions of solid KMnO₄ in non-polar solvents in the

absence of water are extremely slow. This finding is relevant for the applicability of the concept of encapsulation of KMnO$_4$ by organic coatings which are intended to be dissolved in NAPL phases. In this case, the reactivity of the KMnO$_4$ particles will depend on the water content in the NAPL phase. NAPL phases consisting of chlorinated olefins, such as TCE, are expected to have higher water contents than those consisting of mineral oil hydrocarbons. One should keep in mind that dissolution of larger amounts of a non-polar wax in the NAPL phase will decrease the solubility of water.

3.2. Stabilization of KMnO$_4$ with MnO$_2$

In the first experiments, we investigated the dissolution and reduction of KMnO$_4$ by n-propanol. A color change of the alcohol phase from light violet via red to brown (formation of MnO$_2$ colloids) was observed within less than a minute after addition of the KMnO$_4$ particles to n-propanol. However, the weight loss of the KMnO$_4$ particles was insignificant, indicating that the solubility of KMnO$_4$ in n-propanol is sufficiently low for our purpose.

The scheme below (Fig. 2) shows the three procedures (R$_0$, R$_1$ and R$_2$) applied in our experiments in order to reduce the KMnO$_4$ surface to MnO$_2$. In all cases the reaction medium was n-propanol; in R$_1$, sulfuric acid was added in order to accelerate the reaction between KMnO$_4$ and n-propanol, whereas in R$_2$, Mn^{2+} was added as additional reducing agent. In all cases, the surface of the particles obtained after the treatment had the typical brown color of MnO$_2$.
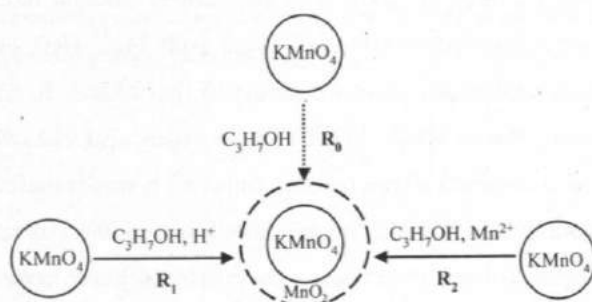

Fig. 2. Coating of KMnO$_4$ with MnO$_2$ (procedures R$_0$, R$_1$ and R$_2$).

3.3. Release and recovery tests

Dissolution rates and residual amounts of KMnO$_4$ for the MCP obtained by the various treatments were studied in column experiments. Column experiments were preferred to batch experiments because they are closer to aquifer conditions and because the mechanical stress on the particles due to shaking or stirring is avoided. The results are presented in Table 1. The factor of prolongation of KMnO$_4$ release (f_R) from the various MCP in relation to the native KMnO$_4$ particles was determined by the following equation:

$$f_R = \frac{t_{R,MCP}}{t_{R,native\ KMnO4}} \tag{3}$$

where t_R is the time period between the start of the water flow and the time after which the concentration of permanganate in the effluent was below an arbitrarily selected limit of 5 mg L^{-1}. The content of available KMnO$_4$ in MCP was determined by dividing the total amount of KMnO$_4$ detected in the column effluent within t_R by the applied mass of MCP.

The results presented in Table 1 show that the reaction between KMnO$_4$ and n-propanol is not efficient to gain a sufficient amount of MnO$_2$ coating. In contrast, significant changes of the composition and the dissolution properties were observed after treatment of KMnO$_4$ particles according to procedures R$_1$ and R$_2$. The percentages of reduction of the KMnO$_4$ particles to MnO$_2$, observed after the various reaction times, were similar for the reactions with acidified propanol (R$_1$) and with Mn^{2+} (R$_2$). After 30 min of reaction time, almost no changes could be observed, but after 1 h, about 25-30% of KMnO$_4$ had been converted to MnO$_2$. In the column experiment, the release of KMnO$_4$ from the MCP samples obtained after a reaction time of 1 h was completed within about 100 min, corresponding to elution of about 800 pore volumes of water. Very low amounts of permanganate were observed in the column effluent collected over more then 2 h for MCP obtained after 3 h of reaction (R$_1$ and R$_2$). Obviously, there is only a small amount of permanganate remaining in the MCP samples obtained after 3 h of reaction. This was also confirmed by ultrasound treatment of suspensions of these MCP, which did not release significant amounts of permanganate. MCP obtained after 1 h of treatment by procedures R$_1$ and R$_2$ can be considered as the optimum with respect to a

considerable release prolongation at an acceptable degree of $KMnO_4$ consumption for the formation of the MnO_2 coating. These products were used in the following studies and are denoted as MCP (R_1-1h) and MCP (R_2-1h), respectively.

Table 1 Results of column experiments on the release of permanganate from MCP obtained by means of reactions R_0, R_1 or R_2 after various reaction times: $KMnO_4$ release prolongation factor and content of available $KMnO_4$ in MCP in wt%.

Reaction	Reaction time (h)	$KMnO_4$ release prolongation factor (f_R) [1]	Available $KMnO_4$ in MCP in wt% [2]
R_0	0.5	0	100
	3	1.5	98
R_1	0.5	3	93
	1	12.5	75
	2	23	41
	3	not measurable [3]	2 [4]
R_2	0.5	2.8	96
	1	10	70
	2	20	48
	3	not measurable [3]	8 [4]

[1] f_R values determined for each type of MCP in at least 3 independent measurements differed by less than 10%.

[2] mean value of 3 independent experiments ± maximum deviation of the single values from the mean value

[3] not measurable due to insufficient release of $KMnO_4$

[4] determined from $KMnO_4$ detected in the effluent after elution of 100 mL of water

3.4. Coating characterization

SEM images of native $KMnO_4$ particles (A) and MCP (B, C, D) are depicted in Fig. 3. SEM analyses showed that the particle size was not dramatically influenced by the coating process. However they clearly show that there are significant changes in the surface structure after the treatment by reactions R_1 and R_2. Figure 3b and 3c present images of MCP (R_1-1h) containing a residual $KMnO_4$ fraction of 75 wt% and Fig. 3d shows MCP (R_2-1h) with 70 wt% $KMnO_4$. It is obvious that the MnO_2 shell is not

compact and has relatively wide cracks. These cracks are certainly very important for the permanganate release rate of MCP.
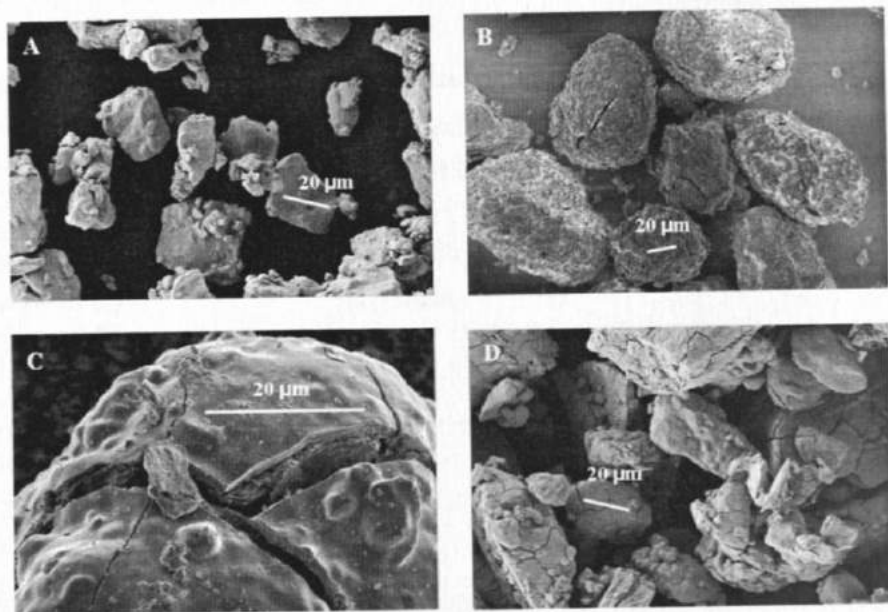

Fig. 3. SEM images of (A): native $KMnO_4$ particles, (B) and (C): MCP (R_1-1h), and (D): MCP (R_2-1h).

BET analysis shows significant changes in surface area and porosity of the samples after treatment by R_1 and R_2. The original $KMnO_4$ has a very low specific surface area ($0.04 \ m^2 \ g^{-1}$) without good adsorption properties. On the other hand, the MCP samples (R_1-1h) and (R_2-1h) appear to have a relatively high specific surface area (32 and 45 m^2 g^{-1}, respectively). Both samples show a broad pore size distribution, covering the micro- and mesopore range.

XRD analysis revealed that the prepared MCP coatings are X-ray amorphous materials. That means, aside from the signals from traces of potassium salts (K_2SO_4 or KNO_3), no other crystalline phases were detected. This is not surprising since it has been described in the literature that synthetic MnO_2 materials, similar to natural MnO_2 minerals, are rather poorly crystallized. Synthetic MnO_2 generally has numerous extended defects and a non-stoichiometric composition (Godart et al., 1992). Oxides of manganese are known to exhibit several identifiable crystal structures, which result from different assembly combinations of their basic molecular structural units, i.e. MnO_6 octahedra.

The octahedra may be joined together along their edges and/or corners to form "chain" patterns with void spaces ("tunnels"). MnO_2 structures are classifiable into one or more of the six fundamental crystal structures, which are α, β, γ, δ, ε, and ramsdellite.

3.5. Evaluation of the permanganate release properties of MCP

The optimal structure of the MCP coating depends on the intended application. For an application as injectable colloidal reagent, MCP with a particle size in the lower μm-range and a high stability in water are needed, in order to allow the preparation and handling of suspensions as well as to ensure transport over a sufficiently long distance in the subsurface. In this case, the synthesis of a closed MnO_2 coating with a low degree of micro- and mesoporosity would be ideal in order to provide the desired stability and facilitate a continuous very slow release of permanganate. The formation of cracks in the MnO_2 coating is undesirable for this application, but could not be prevented in the tested preparation procedures for MCP.

Nevertheless, the permanganate release properties of MCP might be interesting for the formation of reactive barriers by filling of trenches or boreholes. While $KMnO_4$ is too soluble to be used in reactive barriers, the prepared MCP can persist for a substantial duration and thus allow a prolonged passive dosing of permanganate into the flowing groundwater, similar to ORC (Regenesis, 2010).

3.6. MnO₂-coated permanganate in oxidation tests under anhydrous conditions

The presence of the MnO_2 coating on the $KMnO_4$ particles significantly increased the oxidation rate of benzaldehyde in CH_2Cl_2, which was used as a model for a DNAPL phase (Fig. 4). Decrease of benzaldehyde was $\leq 15\%$ and no benzoic acid was detected within 96 h for native $KMnO_4$ particles in dry CH_2Cl_2. The fastest oxidation of benzaldehyde occurred in the system with MCP obtained by procedure R_2, containing 70 wt% available $KMnO_4$, and about 10 wt% of surface and structural water in total. After 1 d, almost 75% of the benzaldehyde was oxidized. After a faster initial period, the degradation of benzaldehyde nearly follows a pseudo-first-order kinetics. Benzaldehyde conversion after 4 d was 95 and 68% for the reaction of MCP (R_2-1h) and MCP (R_1-1h), respectively.
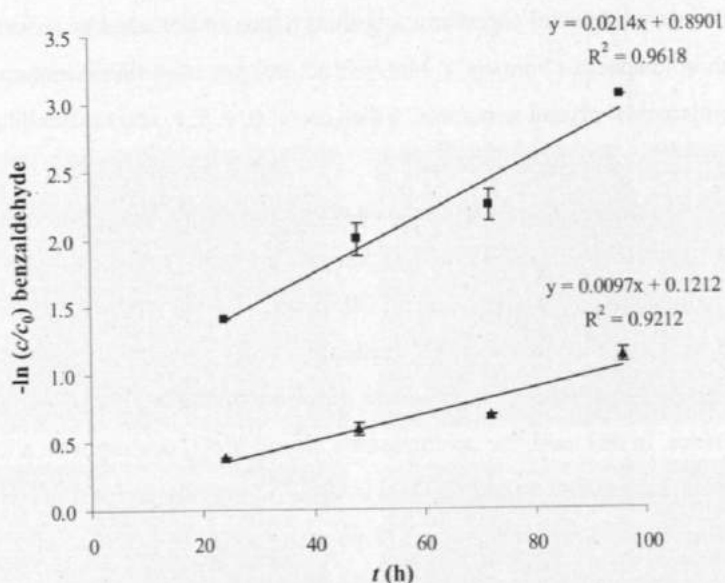
Fig. 4. Pseudo-first order plot for benzaldehyde oxidation with MCP in CH_2Cl_2, ($\blacksquare$ MCP (R_2-1h), $\blacktriangle$ MCP, (R_1-1h)). Results shown are mean values of at least two experiments and the error represents the deviation of the single values from the mean value.

From the experimental data and the literature cited at the beginning of this paper it is deduced that MnO_2 plays a significant role in the oxidation process. In synthetic organic chemistry, heterogeneous and solvent-free reactions play an increasing role and it has been observed that $KMnO_4$ must be activated using a solid support in many of these reactions. Synthetic (so-called activated) MnO_2 as support has been shown to catalyze various types of reactions under heterogeneous (i.e. non-aqueous) conditions (Shaabani and Lee, 2001). A general mechanism for this catalytic effect has not yet been identified. Both the supply of a hydrated surface for reactions which require proton-accepting species and the activation of permanganate ions by adsorption on the MnO_2 surface have been discussed as possible mechanisms (Dash et al., 2009). Both mechanisms are also conceivable in our reaction system. The MnO_2 coatings formed by reduction of $KMnO_4$ offer a hydrated surface which, due to its porosity, allows diffusion and adsorption of the reactants.

The use of MCP as core material might offer an improvement for the concept of wax- or polymer-coated $KMnO_4$ particles as described e.g. in (Ross et al., 2005).

This type of coating was developed in order to retard dissolution and unwanted consumption of $KMnO_4$ in the aqueous phase, and to induce a fast release after dissolution of the organic coating when in contact with a NAPL phase (Kang et al., 2004; Ross et al., 2005). Unlike pure $KMnO_4$, the composite of $KMnO_4$ *and* MnO_2 in MCP would be more reactive even in essentially water-free NAPL phases. Furthermore, an outer organic polymer shell on MCP would extend their life time. Thus, the two approaches might complement each other.

4. Conclusion

The oxidation capability of potassium permanganate was tested in different media. It shows very low activity in organic solvents without the presence of water.

A modified potassium permanganate reagent (MCP) with slow-release properties was designed and tested. For this purpose, micro-sized $KMnO_4$ particles were coated with MnO_2 by means of two different procedures: acid-catalyzed reduction with n-propanol and reaction with Mn^{2+} in n-propanol. The MnO_2 content of the MCP was controlled via the reaction time. Column tests showed that, for MCP with a residual $KMnO_4$ fraction of 70 wt%, the duration of permanganate release under flow-through conditions was prolonged by a factor of 10 compared to untreated $KMnO_4$. Thus MCPs have potential applications as slow-release oxidants in groundwater remediation. However, the release prolongation is considered to be only moderate, due to the inherent morphological properties of MnO_2. In addition, experiments on the oxidation of benzaldehyde as model compound in dry dichloromethane as solvent revealed that this reaction does not take place with native $KMnO_4$, but only with MCP. Obviously, the presence of MnO_2 in close contact with $KMnO_4$ can have a positive effect on oxidation reactions under heterogeneous conditions, i.e. in non-aqueous liquids. This property of MCP can possibly be utilized for the treatment of NAPL source zones, especially in combination with polymer coatings which guide the transport and release of the particles into the NAPL phase.

References

Crimi, M.L., Siegrist, R.L., 2004. Impact of reaction conditions on MnO_2 genesis during permanganate oxidation. *J. Environ. Eng.* 130, 562-572.

Dash, S., Patel, S., Mishra, B.K., 2009. Oxidation by permanganate: Synthetic and mechanistic aspects. *Tetrahedron* 65, 707-739.

Gavaskar, A.R., 1999. Design and construction techniques for permeable reactive barriers. *J. Hazard. Mater.* 68, 41-71.

Godart, C., Latroche, M., Fretigny, C., Levyclement, C., 1992. Exafs studies of synthetic gamma-MnO_2 and related pryolusite and ramsdellite minerals. *Phys. Status Solidi A* 132, 253-268.

Greenwood, N.N., Earnshaw, A. (Eds.), 1997. Chemistry Of The Elements. Butterworth Heinemann.

Hammel, C.F., Tuzinski, P.A., Boren, R.M., 2002. Pretreatment And Regeneration Of Oxides Of Manganese United States Patent 7041270.

Huling, S.G., Pivetz, B.E., 2006. In-Situ Chemical Oxidation - Engineering Issue. http://www.epa.gov/nrmrl/pubs/600r06072/600r06072.pdf.

Kang, N., Hua, I., Rao, P.S.C., 2004. Production and characterization of encapsulated potassium permanganate for sustained release as an in situ oxidant. *Ind. Eng. Chem. Res.* 43, 5187-5193.

Koenigsberg, S.S., Sandefur, C.A., 1999. The use of oxygen release compound for the accelerated bioremediation of aerobically degradable contaminants: The advent of time-release electron acceptors. *Remediation Journal* 10, 3-29.

Lee, E.S., Schwartz, F.W., 2007. Characteristics and applications of controlled-release kmno4 for groundwater remediation. *Chemosphere* 66, 2058-2066.

Lee, E.S., Woo, N.C., Schwartz, F.W., Lee, B.S., Lee, K.C., Woo, M.H., Kim, J.H., Kim, H.K., 2008. Characterization of controlled-release kmno4 (crp) barrier system for groundwater remediation: A pilot-scale flow-tank study. *Chemosphere* 71, 902-910.

Ma, S.B., Lee, Y.H., Ahn, K.Y., Kim, C.M., Oh, K.H., Kim, K.B., 2006. Spontaneously deposited manganese oxide on acetylene black in an aqueous potassium permanganate solution. *J. Electrochem. Soc.* 153, C27-C32.

Regenesis, 2010. http://www.regenesis.com/.

Ross, C., Murdoch, L.C., Freedman, D.L., Siegrist, R.L., 2005. Characteristics of potassium permanganate encapsulated in polymer. *J. Environ. Eng.* 131, 1203-1211.

Shaabani, A., Lee, D.G., 2001. Solvent free permanganate oxidations. *Tetrahedron Lett.* 42, 5833-5836.

Shaabani, A., Mirzaei, P., Naderi, S., Lee, D.G., 2004. Green oxidations. The use of potassium permanganate supported on manganese dioxide. *Tetrahedron* 60, 11415-11420.

Siegrist, R.L., Urynowicz, M.A., West, O.R., Crimi, M.L., Lowe, K.S. (Eds.), 2001. Principles And Practises Of In Situ Chemical Oxidation Using Permanganate. Battelle Press, Columbus, Ohio.

Urynowicz, M.A., 2008. In situ chemical oxidation with permanganate: Assessing the competitive interactions between target and nontarget compounds. *Soil sediment contam.* 17, 53-62.

Waldemer, R.H., Tratnyek, P.G., 2006. Kinetics of contaminant degradation by permanganate. *Environ. Sci. Technol.* 40, 1055-1061.

5. Nano-sized magnetic iron oxides as catalysts for heterogeneous Fenton- like reactions: Influence of Fe(II)/Fe(III) ratio on catalytic performance

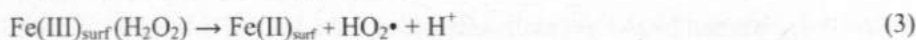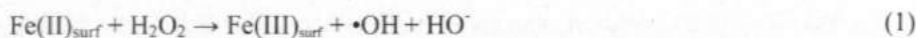Klara Rusevova, Frank-Dieter Kopinke, Anett Georgi

Abstract

Nano-sized Fe(II,III) oxides with various Fe(II)/Fe(III) ratios were characterized and tested as catalysts for the oxidative degradation of phenol via Fenton-like reactions at neutral pH. Under conditions typically applied for wet peroxide oxidation, Fe(II) in magnetite is oxidized to Fe(III), successively converting the mineral into maghemite. The residual Fe(II) content in the catalyst core is of only minor benefit for the catalytic activity in phenol oxidation, *i.e.* magnetite is not superior to maghemite. Achievable reaction rates for phenol degradation appeared to be rather low, e.g., phenol half-life of about 12 h when 3 g L^{-1} magnetite and 5 g L^{-1} H_2O_2 were applied. Preceding surface-reduction of maghemite by $NaBH_4$, leading to an over-stoichiometric Fe(II) content compared to magnetite, only enhanced the non-productive decomposition of H_2O_2 rather than the rate of phenol degradation. Reaction rates were shown to be relatively insensitive to catalyst concentration in the range of 1-10 g L^{-1}, probably resulting from a scavenging of reactive species by the catalyst surface, whereby particle agglomeration seems to play a key role. Degradation experiments with various structurally distinct compounds were carried out, indicating a similar selectivity of the heterogeneous Fenton-like system to that known for oxidation with •OH.

1. Introduction

Advanced oxidation processes (AOPs) involving the production of highly reactive hydroxyl radicals (•OH) have shown great potential for the treatment of organic pollutants in water and soil at large scales. The •OH for AOPs can be produced in a system with dissolved iron and hydrogen peroxide (homogenous Fenton reaction) according to the Haber-Weiss mechanism [1]. They are strong, relatively non-selective oxidants which are able to destroy a wide range of organic substrates [2]. The main shortcomings of the homogeneous Fenton process are the necessity of working at low pH (~3) and the formation of iron oxide sludge. To overcome these drawbacks, research has focused on the idea of replacing dissolved iron with solid catalysts in so-called heterogeneous Fenton-like reactions. The general requirements for heterogeneous catalysts in wet oxidation are: high efficiency related to contaminant removal rates and H_2O_2 utilization, minimum leaching, stability over long periods of application, and effectiveness at extended ranges of pH and temperature.

A large number of studies dealing with heterogeneous catalysts suitable for the Fenton system have been previously reported. Garrido-Ramirez et al. reviewed several solid materials indicating good efficiency for Fenton-like reactions [3]. Promising results were achieved for metal-supported catalysts such as transition-metal-exchanged zeolites [4] or mesoporous materials [5], pillared interlayered clays containing Fe or Cu [3], as well as non-porous solids such as iron oxide minerals (e.g., magnetite, maghemite, hematite, goethite) [6-9]. Novel modified S-doped α-Fe_2O_3 [10], and mixed iron oxides containing metals such as Co, Cu, Mn, Ni, V, Zn, have also been used with some successes [11-13]. However, the introduction of heavy metals as catalyst constituents must be scrutinized with respect to its environmental compatibility. The mechanism of mineral-catalysed H_2O_2 activation is still poorly understood. In analogy to the Haber-Weiss mechanism, Voelker and Kwan suggested that the activation of H_2O_2 via iron-surface species is achieved via the followings steps (Eqs. 1-3) [14].

$$Fe(II)_{surf} + H_2O_2 \rightarrow Fe(III)_{surf} + •OH + HO^- \tag{1}$$

$$Fe(III)_{surf} + H_2O_2 \rightarrow Fe(III)_{surf}(H_2O_2) \tag{2}$$

$$Fe(III)_{surf}(H_2O_2) \rightarrow Fe(II)_{surf} + HO_2• + H^+ \tag{3}$$

Recently, utilization of nano-range (1-100 nm) catalysts in water purification has become more popular [15]. In terms of catalysts or reagents for water purification, the nanoparticles offer a high specific surface area (SSA), and in some cases (e.g., for nZVI [16]) different properties in comparison to their bulk phase might positively influence the reaction efficiency. For water treatment in reactor systems, high reaction rates are desirable, whereby nanoparticles can be beneficial since few or no mass-transfer limitations are expected. This can be an advantage for the treatment of large contaminant molecules such as dyes and pharmaceuticals, which are considerably limited in diffusion through microporous catalysts. On the other hand, the separation and recycling of nanocatalysts at a technical scale still presents a challenge.

Among the various iron oxide minerals, magnetite (Fe_3O_4), containing both Fe(II) and Fe(III) in molar ratio 1:2, is a promising catalyst for oxidative processes using H_2O_2 [6, 12, 17]. Furthermore, the magnetic properties of magnetite allow easy and complete separation from the treated medium by means of magnetic separation [18]. Its catalytic properties are often assigned to its Fe(II) content, which is considered to be the key parameter in Fenton-like reactions [6, 8, 19]. Moreover, the octahedral site in the magnetite structure, containing both Fe(II) and Fe(III) ions, allows the Fe species to be reversibly oxidized and reduced while keeping the same structure [12]. However, magnetite is known to be instable under oxidizing conditions (H_2O_2, O_2) where it is slowly oxidized to maghemite (γ-Fe_2O_3) [20-23], which has the same spinel-type structure but contains only Fe(III). Although several models have been proposed to describe the magnetite oxidation kinetics, the most common model suggests that the diffusion of Fe(II) to the particle surface is the rate-determining step [24, 25]. Other models are based on changes in magnetite redox potential upon oxidation, which induce changes in the reactivity of the material [21].

While for larger particles the formation of a passivating shell can prevent complete oxidation of magnetite, nanomagnetite could be more sensitive towards this process. However, in most previous studies dealing with magnetite as Fenton-like catalyst, the potential change in Fe(II)/Fe(III) ratio during the oxidation reaction was not explicitly considered. Xue et al. [19] used two commercial Fe(II,III) oxides with different particle size and determined their Fe(II)/Fe(III) ratio before application as catalyst for Rhodamine B degradation by H_2O_2. They concluded that the Fe(II,III) oxide with larger particle size (<5 μm) and higher Fe(II)/Fe(III) ratio (0.43) exhibited better oxidation

efficiency for dye removal than the nanosized material (<50 nm, original Fe(II)/Fe(III) ratio of 0.24) on the basis of both, mass and surface area normalization. Differences in mineral structural properties (crystallography, Fe(II) content) were considered to be potential reasons for the different oxidation efficiencies of the two samples [19]. The difference in particle size and agglomeration tendency of the studied Fe(II,III) oxides leading to different conditions for consumption of reactive species by the catalyst surface, might have played an additional role.

Thus, the aim of this study was to elucidate the effects of Fe(II)/Fe(III) ratio in magnetic nano-sized iron oxides on phenol removal and H_2O_2 decomposition at neutral pH. For this purpose: (i) commercial Fe(II,III) oxide, (ii) freshly synthesized 'stoichiometric' magnetite, and (iii) iron oxides with over-stoichiometric Fe(II) content derived from magnetite were examined. Moreover, the stability and reusability of the catalyst, which are key parameters for practical applications, were investigated.

2. Experimental

2.1. Chemicals

Nano-sized Fe(II,III) oxide (≥98% trace metal basis, particle size <50 nm) was obtained from Sigma Aldrich, Germany. Iron(III) chloride hexahydrate (99%), iron(II) chloride tetrahydrate (99%), hydrogen peroxide (30 wt%), phenol (>98.8%), p-cresol (>98%), MTBE, cis-1,2- dichloroethene (cis-DCE), 1,2-dichloroethane (1,2-DCA), chlorobenzene (MCB), ammonia solution (25 wt%) and n-hexane were obtained from Merck, Germany and used as received. Titanium(IV) oxysulphate solution (1.9-2.1%) for determination of H_2O_2 was obtained from Fluka, Germany.

2.2 Synthesis and reductive pre-treatment of Fe(II,III) oxide

2.2.1 Magnetite synthesis

Magnetite was prepared in the laboratory by the well known procedure of co-precipitation of Fe^{2+} and Fe^{3+} (molar ratio 1:2) in basic solution (NH_4OH). 0.043 mol $FeCl_3 * 6H_2O$ and 0.0216 mol $FeCl_2 * 4H_2O$ were dissolved in 400 mL deionized water (deaerated with Ar) under vigorous stirring in inert atmosphere. 15 mL of NH_4OH was quickly added to the solution and black precipitates of magnetite were obtained.

Afterwards, the magnetite was washed several times with deionized water (using magnetoseparation), dried in vacuum, and stored in a dark glass bottle.

2.2.2. Reductive pre-treatment of commercial Fe(II,III) oxide

Activation of Fe(II,III) oxide was based on reduction of the surface in order to obtain a higher Fe(II)/Fe(III) ratio. The treatment was carried out *in-situ* by adding 1.5 M NaBH$_4$ to the batch reactor containing 3 g L^{-1} of the catalyst in deionized water. After 24 h of shaking, the catalyst was removed by magnetoseparation, washed three times with deionized water and used directly in oxidation experiments.

2.3. Catalyst characterization

X-ray powder diffraction data of all three samples were collected at room temperature on a D8 diffractometer (Bruker) with Cu-K$_\alpha$ radiation and a step size of 2Theta = 0.01° (LynX Eye detector). In the cases of freshly prepared samples, a drying step under inert atmosphere was performed and the samples were subjected directly to analysis. Primary particle size distribution was determined via transmission electron spectroscopy (TEM). For TEM imaging (Philips-CM), the dry particles were embedded into glue (M-Bond 610) to form a bulk sample. The SSA of magnetite was determined by the BET method using N$_2$ adsorption-desorption isotherms measured at 77 K with a Belsorp-miniII instrument (Bel, Japan). The sample was degassed at 373 K before the analysis was conducted. The zeta potential of the catalysts studied was determined with a Zetasizer Nano ZS (Malvern Instruments, UK, $c_{particle}$ = 10 mg L^{-1} suspended in 3 mM NaNO$_3$).

2.4. Procedure of oxidation experiments

Batch experiments were carried out at ambient conditions (T = 22 ± 2 °C) using cylindrical glass vessels (60 mL) with screw caps having a PTFE-lined septum. The reaction medium was prepared by adding 3 g L^{-1} catalyst to a solution containing phenol as model contaminant with an initial concentration of 25 mg L^{-1}. The suspension was placed for 5 min in a sonication bath, and then the reaction was started by adding 5 g L^{-1} H$_2$O$_2$. The reactions were carried out at neutral pH in order to minimize any contribution of homogeneous Fenton reaction (due to leached Fe). The pH was set to 7.0 by adding 0.01 M NaOH and kept neutral during the reaction (7.0 ± 0.3). The recycling experiment was started in the same way. After each reaction cycle, the catalyst was magnetically separated from the reaction medium and washed three times

with deionized water, after which phenol solution and H_2O_2 were freshly added. Three cycles were conducted in total.

Batch reactors were shaken throughout the duration of experiments. At given time intervals, samples for phenol and H_2O_2 determination were taken from the reactor after the magnetoseparation of the catalyst; the reaction suspensions were then sonicated for 5 min in order to re-disperse the catalyst and placed again on the shaker. In control batches, where the reaction (in presence of phenol, catalyst and H_2O_2) was carried out with and without sonication treatment for 30 min, no difference in phenol degradation was observed. That means the 5 min ultrasound treatment, which was applied in order to facilitate an optimal re-dispersion of the solid catalysts after each sampling by magnetoseparation, did not interfere with the chemical reaction.

Data shown in the figures are mean values of at least two experiments; the error represents the deviation of the single values from the mean value.

2.5. Chemical analysis

Phenol concentration was determined by means of GC-MS (Shimadzu) after liquid-liquid extraction of 1 mL sample with 1 mL n-hexane containing p-cresol as an internal standard. H_2O_2 concentration was measured spectrophotometrically at $\lambda = 405$ nm with a UVmini-1240 (Shimadzu) after adding titanyl sulphate to the sample to form a yellow complex [26]. Possible leaching of iron (Fe(II) and Fe(III)) was determined using ICP-MS analysis. The molar ratio of Fe(II)/Fe(III) in the iron-oxide catalyst was determined spectrophotometrically using a modified 1,10-phenanthroline method after complete dissolution of the solid sample in 6 M HCl [27].

3. Results and discussion

3.1 Catalyst characterization

Determination of Fe(II) and Fe(III) content revealed that the reductive pre-treatment of commercial Fe(II,III) oxide was successful and that a high Fe(II)/Fe(III) ratio of 1.44 ± 0.02 was obtained. The commercial Fe(II,III) oxide exhibited a low ratio of 0.11 ± 0.01 possibly because of its longer storage under oxidizing conditions. The Fe(II)/Fe(III) ratio of the freshly synthesized magnetite, 0.52 ± 0.02, corresponded to the expected stoichiometry of magnetite.

Diffractograms of commercial Fe(II,III) oxide, freshly synthesized magnetite and pre-treated Fe(II,III) oxide are depicted in Fig. 1. For all samples, the obtained XRD results correspond to the pattern expected for a crystalline magnetite or maghemite (γ-Fe$_2$O$_3$) phase. Both magnetite and maghemite possess a spinel-type structure and thus cannot be easily differentiated from each other by XRD analysis [18, 28]. However, by combining the results of XRD analysis and determination of the Fe(II)/Fe(III) ratio, we can conclude that the freshly synthesized sample indeed consists predominantly of magnetite, whereas the commercial nano-sized Fe(II,III) oxide appears to consist mainly of maghemite with a small residual content of Fe(II) most likely in the particle core.
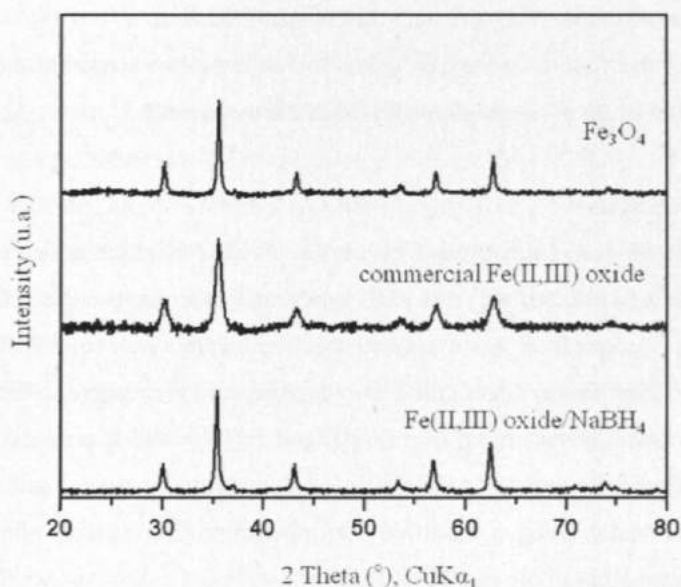

Fig. 1. Diffractograms of commercial Fe(II,III) oxide, magnetite and reduced Fe(II,III) oxide.

Reductive pre-treatment of the commercial Fe(II,III) oxide with NaBH$_4$ did not modify its crystalline structure. Lago et al., when performing reduction of magnetite with H$_2$ at 300 °C (starting with the presence of small amounts of oxidized phases), did not detect any new crystalline phase in XRD. On the other hand, an increase in the lattice parameter and magnetization clearly showed the reduction of oxidized phases to form magnetite [29].

TEM imaging showed crystallite sizes in the nanometre range for commercial Fe(II,III) oxide and freshly synthesized magnetite, as in Fig. 2. The main particle size is assigned to a range of 20-30 nm. Particles appeared to have a uniform crystalline phase, with no indication for the presence of a hematite phase or any amorphous structure.
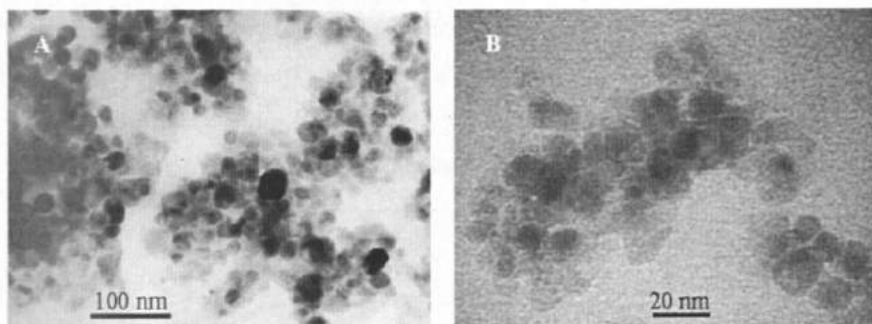

Fig. 2. TEM images of (A) commercial Fe(II,III) and (B) magnetite.

Further physicochemical properties of commercial Fe(II,III) oxide and magnetite are summarized in Table 1. Zeta potential is often used as a parameter to predict the stability of colloidal dispersions [30]. An empirical rule states that values $\leq |\pm 30|$ mV imply incipient instability. Measurement results (Table 1) indicate that suspensions of the commercial Fe(II,III) oxide and the freshly magnetite are instable in aqueous medium. At pH = 7 the agglomeration is particularly strong, since the repulsion forces between the particles are negligible (PZC ~ 7-8). Furthermore, in the case of magnetic particles, the agglomeration is enhanced by magnetic-dipole interactions [21]. Therefore, one can assume that the catalyst suspension consists mainly of agglomerates rather than of (primary) nanoparticles.

Table 1 Physicochemical characterization of the commercial Fe(II,III) oxide and freshly synthesized magnetite.

Catalyst	SSA ($m^2 g^{-1}$)	Point of zero charge (pH)	Zeta potential at pH = 7.0 (mV)
commercial Fe(II,III) oxide	46	7.02	-13.4
magnetite	95	7.90	-15.6

3.2. Phenol oxidation at neutral pH with various Fe(II,III) oxides

In the first set of batch experiments, the catalytic activity of the three iron oxide catalysts with various Fe(II)/Fe(III) ratios was tested. Before the reaction was started, adsorption of phenol on the catalyst was determined. After 24 h of equilibration, no significant depletion of phenol was observed in any of the catalyst suspensions (<5% phenol depletion in the aqueous phase at a catalyst concentration of 3 g L^{-1}). In control batches where only H_2O_2 and phenol were present, no significant oxidation of phenol was determined in 24 h of reaction (<10%). Fig. 3 shows the catalytic performance of the tested iron oxides for phenol oxidation over a 24 h period.
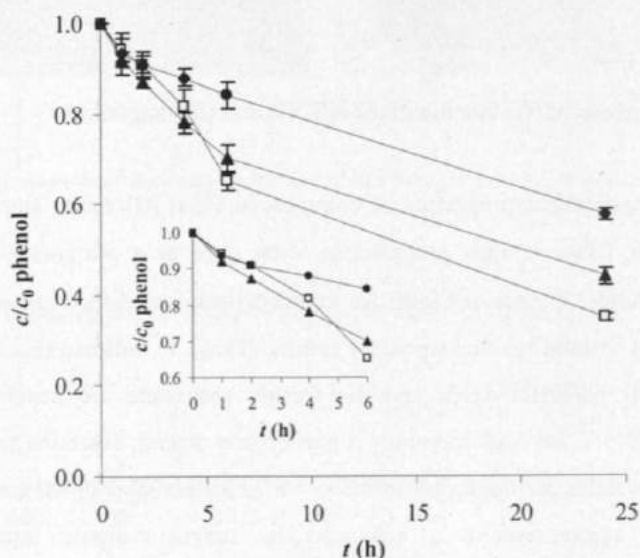

Fig. 3. Kinetics of phenol oxidation in a heterogeneous Fenton-like system with various iron oxide catalysts at neutral pH (the first six hours of phenol oxidation presented in detail in the inset): □ commercial Fe(II,III) oxide, ▲ magnetite, ● reduced Fe(II,III) oxide ($c_{cat} = 3$ g L^{-1}, $c_{0,H2O2} = 5$ g L^{-1}, $c_{0,phenol} = 25$ mg L^{-1}, pH = 7.0 ± 0.3).

The obtained results show similar catalytic behaviour for all tested catalysts (42 to 65% phenol removal in 24 h). In catalytic homogeneous Fenton reactions initiated by Fe(II), a faster initial period of reaction is often observed, since production of •OH can start immediately by the fast reaction of Fe(II) with H_2O_2 [31]. After its consumption, the recycling of Fe(III) to Fe(II) is expected to become the rate-determining step, so that

contaminant oxidation continues at a lower rate. However, this type of kinetics was not observed for the heterogeneous Fenton reaction, even with the catalysts containing considerable amounts of Fe(II), *i.e.* reduced Fe(II,III) oxide and freshly prepared magnetite. On the other hand, significant differences in the rates of H_2O_2 decomposition during phenol degradation were observed (Fig. 4).
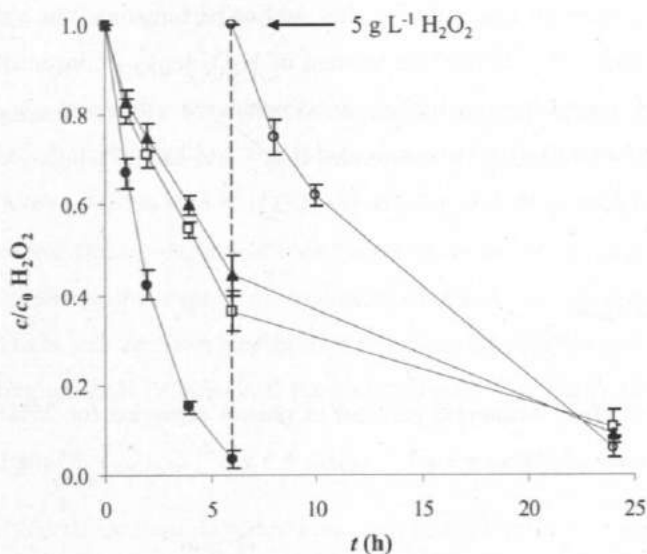

Fig. 4. Kinetics of H_2O_2 decomposition during batch experiments with various iron oxide catalysts: □ commercial Fe(II,III) oxide, ▲ magnetite, ● reduced Fe(II,III) oxide, ○ new dosage of 5 g L^{-1} H_2O_2 in reaction with reduced Fe(II,III) oxide (c_{cat} = 3 g L^{-1}, $c_{0,H2O2}$ = 5 g L^{-1}, $c_{0,phenol}$ = 25 mg L^{-1}, pH = 7.0 ± 0.3).

H_2O_2 decomposition followed pseudo-first-order kinetics, at least during the first 6 h of reaction, whereas in the period between 6 and 24 h the reaction slowed down slightly (Supplementary Information, SI, Fig. S1). The observed pseudo-first-order rate constant (k') for H_2O_2 decomposition in the first 6 h was approximately 4 times higher with reduced Fe(II,III) oxide (k' = (0.52 ± 0.07) h^{-1}) than in the reaction with commercial Fe(II,III) oxide (k' = (0.16 ± 0.02) h^{-1}) and magnetite (k' = (0.13 ± 0.02) h^{-1}). In the case of phenol oxidation, the situation was reversed, i.e. the lowest catalytic activity was for reduced Fe(II,III) oxide. Furthermore, a second dosage of 5 g L^{-1} H_2O_2 into the system with reduced Fe(II,III) oxide (dashed line in Fig. 4) was still not sufficient for complete

phenol removal. The high consumption of H_2O_2 in case of the reduced Fe(II,III) oxide could be due to changes in the surface structure, including formation of different iron phases with low crystallinity (hardly detectable by XRD), structural defects or even incorporation of boron species in the structure. Irrespective of the mechanistic interpretation, it can be concluded that $NaBH_4$ treatment of magnetic Fe(II,III) oxide has an adverse effect on its catalytic activity for Fenton-like reactions.

As a further parameter for evaluation of the catalyst performance, the value R_{25} (mol mol^{-1}) was introduced. R_{25} defines the amount of H_2O_2 (n_{H2O2}) consumed per mol of phenol (n_{phenol}) degraded in the reaction period between t = 0 h and $t_{0.25,phenol}$, *i.e.* the time at which 25% of the phenol was degraded (Eq. 4 and Table 2).

$$R_{25} = \left(\frac{n_{H2O2}}{n_{phenol}} \right)_{t=0.25,phenol} \tag{4}$$

Table 2 Moles of H_2O_2 consumed per mol of phenol degraded for 25% reduction in phenol concentration (R_{25}) ($c_{cat} = 3$ g L^{-1}, $c_{0,H2O2} = 5$ g L^{-1}, $c_{0,phenol} = 25$ mg L^{-1}, pH = 7 ± 0.3).

Catalyst	t_{25} (h)	R_{25} (mol mol^{-1})
commercial Fe(II,III) oxide	5.0	1250
magnetite	5.2	1090
reduced Fe(II,III) oxide	12.5	3350

Compared to the stoichiometric amount of H_2O_2 (14 mol) needed to mineralize one mol of phenol (idealized homogeneous Fenton), the consumption of H_2O_2 in the various heterogeneous systems is extremely high. Slow phenol removal, accompanied by fast H_2O_2 decomposition, leads to the assumption that the heterogeneously catalysed H_2O_2 decomposition involves two reaction pathways occurring simultaneously. In addition to the 'productive' pathway involving •OH formation, there is a 'non-productive' ("parasitic") pathway which occurs due to the reaction of H_2O_2 with the catalyst surface leading to species with low reactivity (e.g., hydroperoxy/superoxide radicals, Eq. 3). Furthermore, strong competition for consumption of •OH by other non-target species

(H_2O_2, catalyst surface) can lead to inefficient utilization of H_2O_2 for contaminant degradation (Eqs. 5, 7, 8).

$$\cdot OH + HO_2\cdot/O_2^- \rightarrow O_2 + H_2O/HO^- \tag{5}$$

$$HO_2\cdot \leftrightarrow \cdot O_2^- + H^+ \ (pK_a = 4.8) \tag{6}$$

$$\cdot OH + H_2O_2 \rightarrow HO_2\cdot + H_2O \tag{7}$$

$$\cdot OH + Fe(II)_{surf} \rightarrow Fe(III)_{surf} + HO^- \tag{8}$$

In the literature, a possible non-radical mechanism via high-valent iron species (e.g., Fe(IV)) is frequently discussed [32]. In homogeneous phase, these species are less reactive and more selective than $\cdot OH$ [32, 33]. However, the reactivity of surface-bound Fe(IV) species is certain to depend on their coordination and is still largely unknown.

In order to evaluate the degree of oxidation of the Fe(II) in the catalysts, their Fe(II)/Fe(III) ratio was determined after 24 h of phenol degradation (without any drying step), indicating unstable behaviour of the catalysts with high Fe(II) content (see Table 3).

Table 3 Fe(II)/Fe(III) ratio of the tested iron oxide catalysts obtained before and after reaction ($c_{cat} = 3$ g L^{-1}, $c_{0,H2O2} = 5$ g L^{-1}, $c_{0,phenol} = 25$ mg L^{-1}, pH = 7 ± 0.3, $t = 24$ h).

Catalyst	Fe(II)/Fe(III) ratio before reaction	Fe(II)/Fe(III) ratio after reaction
commercial Fe(II,III) oxide	0.11 ± 0.01	0.10 ± 0.02
magnetite	0.52 ± 0.02	0.15 ± 0.01
reduced Fe(II,III) oxide	1.44 ± 0.02	1.07 ± 0.03

The Fe(II)/Fe(III) ratio which was obtained after use of the magnetite in the reaction is equivalent to a conversion of about 70% of the magnetite into maghemite. This illustrates the fast oxidation of magnetite nanoparticles in the presence of H_2O_2. The consumption of H_2O_2 for this oxidation reaction is not contradicting with the similar rates of H_2O_2 decomposition in the magnetite and commercial Fe(II,III) oxide, since according to stoichiometry, it consumes only about 10% of the applied H_2O_2 concentration. The remaining low Fe(II) content in the commercial Fe(II,III) oxide as

well as magnetite after oxidation is in line with observations reported in the literature, which describe a slow-down of further magnetite oxidation after partial conversion of magnetite into maghemite (*i.e.* a passivating effect) [21].

A reduction in the Fe(II) content during the oxidation reaction was also observed in the case of the reduced Fe(II,III) oxide, which might contribute to the deceleration of the H_2O_2 decomposition during the time course of the reaction. However, in the case of the commercial Fe(II,III) oxide (where the Fe(II)/Fe(III) ratio is unaffected) another factor must be responsible for the deviation of H_2O_2 decomposition from pseudo-first-order kinetics after long reaction times (SI, Fig. S1). A possible reason can be seen in the particle agglomeration which was visually observed when no ultrasonic treatment was carried out (as was the case in the night period, i.e. between 6 and 24 h of reaction time). Agglomerates in a size range of about 1 µm were determined using laser diffraction analysis. Agglomeration of catalyst particles can affect the available reactive surface area (site blockage) and/or the active sites can become less accessible for H_2O_2 (kinetic effect). Often, organic stabilizers (e.g. poly(ethylene) glycol acid, poly(vinyl alcohol) etc. [34]) are used in order to provide electrostatic and/or steric stabilization of nanoparticles. Unfortunately, all organic matter is an additional consumer of reactive species in heterogeneous Fenton reaction systems and can also increase the leaching of iron [8]. However, a deactivation of the catalyst surface during phenol degradation must be taken into account anyway, as will be discussed in the section dealing with stability and reusability of the catalyst.

Overall, the very similar behaviour of magnetite and the commercial Fe(II,III) oxide with respect to H_2O_2 decomposition and phenol degradation suggests that the catalytic effects are mainly related to the processes occurring at the outer surface of the nanoparticles. In the case of magnetite, this surface quickly becomes depleted in Fe(II) due to oxidation by H_2O_2, and the recycling between Fe(III) and Fe(II) at the particle surface becomes the rate-determining step. The iron redox state in the particle core plays only a minor role.

With respect to magnetization values magnetite and maghemite are very similar ($M_S(Fe_3O_4)$ = 90 emu g^{-1}, $M_S(\gamma$-$Fe_2O_3)$ = 83.5 emu g^{-1}) [28] and for various applications maghemite is even preferred over magnetite due to its relatively high chemical stability. Together with the results of our catalytic tests, we conclude that the

conversion of magnetite into maghemite has no negative effects on its applicability in heterogeneous Fenton reactions.

For the subsequent investigations (influence of H_2O_2 and catalyst concentration, reusability of the catalyst and chemical selectivity of degradation) commercial Fe(II,III) oxide was tested, since it can be expected to have reached a relatively stable redox-state under oxidation conditions.

3.4. Influence of initial H_2O_2 concentration and catalyst load

Within the range of 1-10 g L^{-1} H_2O_2, the rate of phenol degradation increased with increasing initial H_2O_2 concentration when the catalyst concentration was kept at 3 g L^{-1}, reaching a half-life for phenol degradation of about 7 h at 10 g L^{-1} H_2O_2 (SI, Fig. S2). This is in accordance with the assumption that H_2O_2 can reach the role of a dominant •OH consumer only at the highest H_2O_2 concentration as discussed in SI.

By increasing the catalyst concentration from 1 to 10 g L^{-1}, H_2O_2 decomposition was strongly enhanced. In the experiment with 10 g L^{-1} catalyst, the oxidant disappeared nearly 20 times faster than in the reaction with 1 g L^{-1} (Fig. 5).
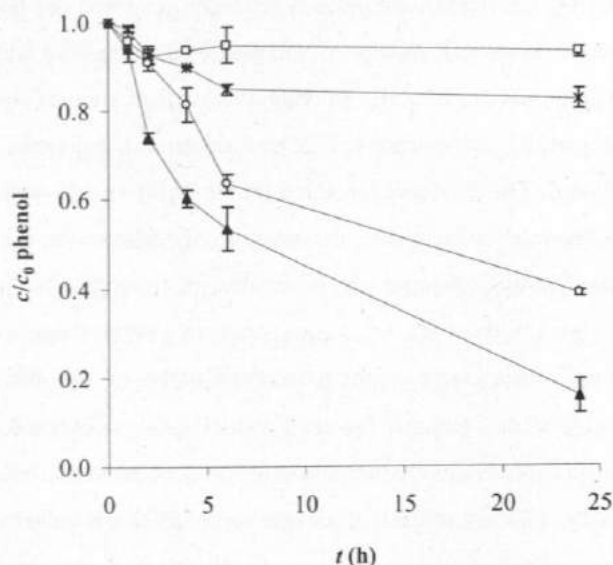

Fig. 5. H_2O_2 decomposition at various catalyst concentrations of commercial Fe(II,III) oxide: ▲ 10 g L^{-1}, ■ 5 g L^{-1}, ○ 1 g L^{-1} ($c_{0,H2O2}$ = 5 g L^{-1}, $c_{0,phenol}$ = 25 mg L^{-1}, pH = 7.0 ± 0.3).

In contrast, the rate of phenol degradation was much less affected by the increase in the catalyst concentration (SI, Fig. S3). In principle, the rate of •OH formation should be proportional to the available reactive surface area. However, in analogy to the case of H_2O_2 as source and consumer of •OH [14], one can anticipate that in a system where the catalyst surface is the dominant consumer of •OH, a further increase in catalyst surface area does not affect the steady-state concentration of •OH radicals. Thus, no increase in contaminant degradation would occur when the catalyst load is increased. This was exactly what we observed in our experiment. However, increased consumption of •OH due to increased concentration of individual catalyst particles requires that •OH radicals produced on the surface of one particle react with the surface of another particle. Since the lifetime of •OH radicals is extremely short, they are not able to diffuse over long distances into the bulk solution phase. Considering only H_2O_2 and phenol as •OH consumers, an average lifetime of 200 ns, corresponding to a diffusion distance of about 20 nm, can be predicted (see SI, Eq. S1 and S2). For particles with a diameter >1 µm, this distance would be clearly smaller than the typical diffusion layer thickness around the particle, meaning that •OH radicals would not reach the water bulk phase but would only be able to react with the surface of their origin. In this case, adverse effects of an increase in the catalyst concentration due to potentially increased consumption of •OH are not to be expected. However, in case of nanoparticles, additional factors can play a role: they tend to agglomerate, whereby fraction and conformation of the agglomerates formed depend on particle concentration. Due to formation of agglomerates, the active surface can be reduced. This is, however, not a major factor in our system, since H_2O_2 decomposition is enhanced by increasing the catalyst concentration in the expected way. Apparently, the particle agglomerates are loose enough to enable the access of H_2O_2 molecules to their inner surface but are tight enough to quench a large fraction of the •OH radicals formed. This effect might have contributed to the different oxidation efficiency observed for nano- and micro-sized Fe(II,III) oxides observed in [19]. Due to their strong agglomeration tendency, the possibility to accelerate the oxidation reaction by increasing the concentration of Fe(II,III) oxide nanoparticles is rather limited.

3.5. Stability and reusability of the catalyst

We tested the commercial Fe(II,III) oxide in three subsequent oxidation cycles under identical conditions. The main difference between the cycles was obtained with respect

to H_2O_2 decomposition rates, which dramatically decreased with reuse of the catalyst (Fig. 6b). When comparing the initial reaction rates (first 6 h) with the end of the oxidation test, in the third reuse of the catalyst the phenol oxidation stagnated (Fig. 6a). The degree of H_2O_2 utilization for phenol oxidation improved with the reuse of the Fe(II,III) oxide. This is illustrated by the R_{25} values of 1200, 500 and 230 mol mol^{-1} obtained for the 1st, 2nd and 3rd cycle respectively.
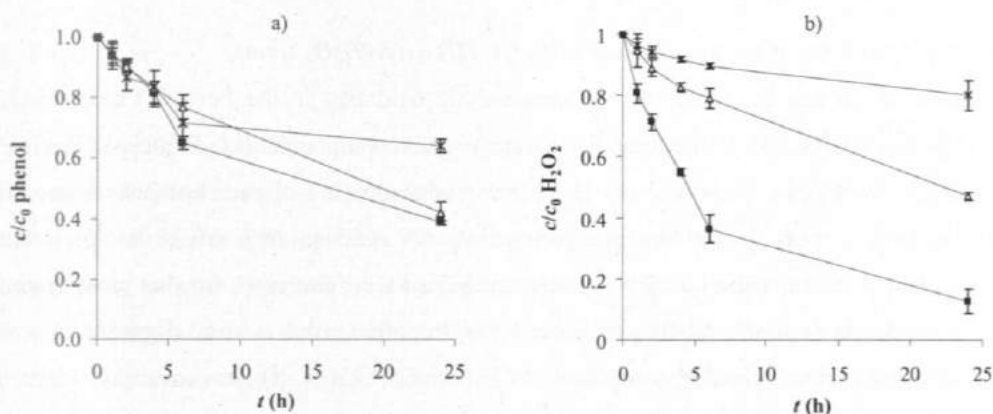

Fig. 6. a) Phenol degradation and b) H_2O_2 consumption in a 3-cycles oxidation test with commercial Fe(II,III) oxide: ■ cycle 1, Δ cycle 2, × cycle 3 (c_{cat} = 3 g L^{-1}, $c_{0,H2O2}$ = 5 g L^{-1}, $c_{0,phenol}$ = 25 mg L^{-1}, pH = 7.0 ± 0.3).

In the absence of phenol, the rate of H_2O_2 consumption remained constant throughout the three cycles (data not shown). The amount of leached iron was determined in the aqueous solution obtained at the end of each reaction after magnetoseparation and filtration through a 0.22 μm PTFE filter. After each cycle, an iron concentration lower than 0.01 mg L^{-1} was detected. The instability of the catalyst was primarily observed visually, since after the second and third cycle a slightly brown solution was obtained. This means that rather than dissolved iron, colloidal iron oxyhydroxide precipitates were formed, which were retained in the filtration step. This was not observed in phenol-free reactions, where the reaction suspensions remained colourless. The XRD pattern of the recovered catalyst did not reveal any changes in the crystalline structure.

To sum up, the results clearly show that the Fe(II,III) oxide catalyst is slowly deactivated with repeated application for phenol oxidation. The instability of the catalyst can be most likely attributed to the passivation of the surface due to the

interaction of surface iron with intermediates of phenol oxidation. Typical products of phenol oxidation in Fenton-like reactions are e.g. hydroquinone, catechol, succinic and other low-molecular weight organic acids [35]; many of them are able to complex iron ions. The complexation of iron by organic intermediates can either block the active centres of the catalyst (*i.e.* compete with H_2O_2 adsorption) or cause a destruction of active surface structures.

3.6. Selectivity of the degradation in Fe(II, III) oxide/H_2O_2 system

In order to test the selectivity of the catalytic oxidation in the Fe(II,III) oxide/H_2O_2 system, a cocktail of 5 structurally distinct organic compounds (MTBE, cis-DCE, 1,2-DCA, MCB, phenol) was used. The starting concentration of each compound was 10 mg L^{-1}. Extents of conversion, analysed after a reaction time of 24 h (X_{24h}), are summarized in Table 4. The fastest oxidation was observed for the unsaturated compounds cis-DCE, MCB and phenol. On the other hand, a slow degradation was detected for the saturated compounds MTBE and 1,2-DCA. These conversion degrees are compared with second-order rate constants of the various model compounds with •OH, taken from the literature [36, 37].

Table 4 Rate constants of reaction with •OH ($k_{n,•OH}$) for the various model compounds obtained from the literature and turnover within 24 h of reaction (X_{24h}) in the Fe(II,III) oxide/H_2O_2 system ($c_{cat} = 3$ g L^{-1}, $c_{0,H2O2} = 5$ g L^{-1} (+ 2nd addition of 2.5 g L^{-1} H_2O_2 after 6 h), $c_0 = 10$ mg L^{-1} each of MTBE, 1,2-DCA, cis-DCE, MCB and phenol, pH = 7.0 ± 0.3).

Compound	$k_{n,•OH}$ (x 10^9 M^{-1} s^{-1})[a]	Heterogeneous Fenton-like system
		X_{24h} (%)
1,2-DCA	0.79	10 ± 1
MTBE	1.6	12 ± 2
cis-DCE	5.4 ± 1.8	64 ± 4
MCB	5.1 ± 1.2	60 ± 4
Phenol	14	51 ± 3

[a] Rate constant for reaction of phenol with •OH obtained from [36], rest of the rate constants obtained from [37].

The selectivity of the reactive species formed in the heterogeneous Fenton-like system is similar to the selectivity known for •OH radicals. Unsaturated compounds are preferentially attacked by addition of radicals, whereas saturated compounds can only react via H-abstraction from C-H bonds. The apparent reaction selectivities, however, may be superimposed by sorptive substrate enrichment close to the reactive sites. This could explain the higher reaction rate of MCB compared to the more reactive phenol.

4. Conclusion

In summary, this study has shown that nano-sized magnetite is not stable and is converted to maghemite in the presence of H_2O_2, starting from the surface and continuing to the core of the particle. The presence of residual Fe(II) in the nanoparticle core appears to be unimportant for the catalytic activity in phenol degradation by H_2O_2. If the Fe(II) content is raised above the stoichiometric ratio of magnetite by treatment with $NaBH_4$, then only the non-productive decomposition of H_2O_2 is accelerated. The fact that contaminant degradation cannot be significantly accelerated by increasing the catalyst concentration above a few g L^{-1} indicates that the Fe(II,III) oxide surfaces of nanoparticle agglomerates play an important role as consumer of •OH radicals. Formation of reaction intermediates affects the reactivity and stability of the Fe(II,III) oxide surface. The selectivity of the heterogeneous Fenton-like system is similar to that of free •OH radicals, which implies that •OH radicals also play a major role in the heterogeneous systems.

References

[1]   J.J. Pignatello, E. Oliveros, A. MacKay, Advanced oxidation processes for organic contaminant destruction based on the Fenton reaction and related chemistry, Crit. Rev. Env. Sci. Technol. 36 (2006) 1-84.

[2]   G.V. Buxton, C.L. Greenstock, W.P. Helman, A.B. Ross, Critical review of rate constants for reactions of hydrated electrons, hydrogen atoms and hydroxyl radicals ($^{\bullet}$OH/O^{-}) in Aqueous-Solution, J. Phys. Chem. Ref. Data 17 (1988) 513-886.

[3]   E.G. Garrido-Ramirez, B.K.G. Theng, M.L. Mora, Clays and oxide minerals as catalysts and nanocatalysts in Fenton-like reactions - A review, Appl. Clay Sci. 47 (2010) 182-192.

[4]   R. Gonzalez-Olmos, A. Georgi, U. Roland, H. Toufar, F.D. Kopinke, Fe-zeolites as catalysts for chemical oxidation of MTBE in water with H_2O_2, Appl. Catal. B Environ. 89 (2009) 356-364.

[5]   M. Hartmann, S. Kullmann, H. Keller, Wastewater treatment with heterogeneous Fenton-type catalysts based on porous materials, J. Mater. Chem. 20 (2010) 9002-9017.

[6]   K. Hanna, T. Kone, G. Medjahdi, Synthesis of the mixed oxides of iron and quartz and their catalytic activities for the Fenton-like oxidation, Catal. Commun. 9 (2008) 955-959.

[7]   I.R. Guimaraes, L.C.A. Oliveira, P.F. Queiroz, T.C. Ramalho, M. Pereira, J.D. Fabris, J.D. Ardisson, Modified goethites as catalyst for oxidation of quinoline: Evidence of heterogeneous Fenton process, Appl. Catal. A Gen. 347 (2008) 89-93.

[8]   R. Matta, K. Hanna, T. Kone, S. Chiron, Oxidation of 2,4,6-trinitrotoluene in the presence of different iron-bearing minerals at neutral pH, Chem. Eng. J. 144 (2008) 453-458.

[9]   J.J. Wu, M. Muruganandham, J.S. Yang, S.S. Lin, Oxidation of DMSO on goethite catalyst in the presence of H_2O_2 at neutral pH, Catal. Commun. 7 (2006) 901-906.

[10]   L.Q. Guo, F. Chen, X.Q. Fan, W.D. Cai, J.L. Zhang, S-doped alpha-Fe_2O_3 as a highly active heterogeneous Fenton-like catalyst towards the degradation of acid orange 7 and phenol, Appl. Catal. B Environ. 96 (2010) 162-168.

[11]   T. Valdes-Solis, P. Valle-Vigon, S. Alvarez, G. Marban, A.B. Fuertes, Manganese ferrite nanoparticles synthesized through a nanocasting route as a highly active Fenton catalyst, Catal. Commun. 8 (2007) 2037-2042.

[12]   R.C.C. Costa, M.F.F. Lelis, L.C.A. Oliveira, J.D. Fabris, J.D. Ardisson, R.R.V.A. Rios, C.N. Silva, R.M. Lago, Novel active heterogeneous Fenton system based on $Fe_{3-x}M_xO_4$ (Fe, Co, Mn, Ni): The role of M^{2+} species on the reactivity towards H_2O_2 reactions, J. Hazard. Mater. 129 (2006) 171-178.

[13]   J.H. Deng, J.Y. Jiang, Y.Y. Zhang, X.P. Lin, C.M. Du, Y. Xiong, $FeVO_4$ as a highly active heterogeneous Fenton-like catalyst towards the degradation of Orange II, Appl. Catal. B Environ. 84 (2008) 468-473.

[14]   B.M. Voelker, W.P. Kwan, Rates of hydroxyl radical generation and organic compound oxidation in mineral-catalyzed Fenton-like systems, Environ. Sci. Technol. 37 (2003) 1150-1158.

[15]   D.K. Tiwari, J. Behari, P. Sen, Application of nanoparticles in waste water treatment, World Appl. Sci. J. 3 (2008) 417-433.

[16]   Y.A. Zhuang, S. Ahn, R.G. Luthy, Debromination of polybrominated diphenyl ethers by nanoscale zerovalent iron: Pathways, kinetics, and reactivity, Environ. Sci. Technol. 44 (2010) 8236-8242.

[17]   P. Baldrian, V. Merhautova, J. Gabriel, F. Nerud, P. Stopka, M. Hruby, M.J. Benes, Decolorization of synthetic dyes by hydrogen peroxide with heterogeneous catalysis by mixed iron oxides, Appl. Catal. B Environ. 66 (2006) 258-264.

[18]   Z.X. Sun, F.W. Su, W. Forsling, P.O. Samskog, Surface characteristics of magnetite in aqueous suspension, J. Colloid Interface Sci. 197 (1998) 151-159.

[19]   X.F. Xue, K. Hanna, N.S. Deng, Fenton-like oxidation of Rhodamine B in the presence of two types of iron (II, III) oxide, J. Hazard. Mater. 166 (2009) 407-414.

[20]   M.M. Scherer, C.A. Gorski, J.T. Nurmi, P.G. Tratnyek, T.B. Hofstetter, Redox behavior of magnetite: Implications for contaminant reduction, Environ. Sci. Technol. 44 (2010) 55-60.

[21] P.J. Vikesland, A.M. Heathcock, R.L. Rebodos, K.E. Makus, Particle size and aggregation effects on magnetite reactivity toward carbon tetrachloride, Environ. Sci. Technol. 41 (2007) 5277-5283.

[22] Y.K. Sun, M. Ma, Y. Zhang, N. Gu, Synthesis of nanometer-size maghemite particles from magnetite, Colloid Surface A 245 (2004) 15-19.

[23] J. Tang, M. Myers, K.A. Bosnick, L.E. Brus, Magnetite Fe_3O_4 nanocrystals: Spectroscopic observation of aqueous oxidation kinetics, J. Phys. Chem. A 107 (2003) 7501-7506.

[24] C.A. Gorski, J.T. Nurmi, P.G. Tratnyek, T.B. Hofstetter, M.M. Scherer, Redox behavior of magnetite: Implications for contaminant reduction, Environ. Sci. Technol. 44 (2010) 55-60.

[25] C.A. Gorski, M.M. Scherer, Influence of magnetite stoichiometry on Fe(II) uptake and nitrobenzene reduction, Environ. Sci. Technol. 43 (2009) 3675-3680.

[26] G. Eisenberg, Colorimetric determination of hydrogen peroxide, Ing. Eng. Chem. Anal. Ed. 15 (1943) 327-328.

[27] J.W. Stucki, W.L. Anderson, The quantitative assay of minerals for Fe^{2+} and Fe^{3+} using 1,10-phenanthroline: 1. Sources of variability, Soil. Sci. Soc. Am. J. 45 (1981) 633-637.

[28] A. Espinosa, A. Serrano, A. Llavona, J.J. de la Morena, M. Abuin, A. Figuerola, T. Pellegrino, J.F. Fernandez, M. Garcia-Hernandez, G.R. Castro, M.A. Garcia, On the discrimination between magnetite and maghemite by XANES measurements in fluorescence mode, Meas. Sci. Technol. 23 (2012).

[29] R.M. Lago, R.C.C. Costa, F.C.C. Moura, J.D. Ardisson, J.D. Fabris, Highly active heterogeneous Fenton-like systems based on Fe^0/Fe_3O_4 composites prepared by controlled reduction of iron oxides, Appl. Catal. B Environ. 83 (2008) 131-139.

[30] H. Hildebrand, D. Kuhnel, A. Potthoff, K. Mackenzie, A. Springer, K. Schirmer, Evaluating the cytotoxicity of palladium/magnetite nano-catalysts intended for wastewater treatment, Environ. Pollut. 158 (2010) 65-73.

[31] K.H. Chan, W. Chu, Modeling the reaction kinetics of Fenton's process on the removal of atrazine, Chemosphere 51 (2003) 305-311.

[32] A.L.T. Pham, C. Lee, F.M. Doyle, D.L. Sedlak, A silica supported iron oxide catalyst capable of activating hydrogen peroxide at neutral pH values, Environ. Sci. Technol. 43 (2009) 8930-8935.

[33] R. Gonzalez-Olmos, F. Holzer, F.D. Kopinke, A. Georgi, Indications of the reactive species in a heterogeneous Fenton-like reaction using Fe-containing zeolites, Appl. Catal. A Gen. 398 (2011) 44-53.

[34] D. Horak, M. Babic, H. Mackova, M.J. Benes, Preparation and properties of magnetic nano- and microsized particles for biological and environmental separations, J. Sep. Sci. 30 (2007) 1751-1772.

[35] J. Herney-Ramirez, M.A. Vicente, L.M. Madeira, Heterogeneous photo-Fenton oxidation with pillared clay-based catalysts for wastewater treatment: A review, Appl. Catal. B Environ. 98 (2010) 10-26.

[36] A.K. De, B. Chaudhuri, S. Bhattacharjee, B.K. Dutta, Estimation of OH radical reaction rate constants for phenol and chlorinated phenols using UV/H_2O_2 photo-oxidation, J. Hazard. Mater. 64 (1999) 91-104.

[37] NDRL/NIST Solution Kinetics Database on the WEB, http://kinetics.nist.gov/ kinetics/index.jsp

Supplementary Information

Fig. S1. Pseudo-first-order kinetics of H_2O_2 decomposition during phenol oxidation: □ commercial Fe(II,III) oxide, ▲ magnetite, • reduced Fe(II,III) oxide, ○ new dosage of 5 g L^{-1} in reaction with reduced Fe(II,III) oxide ($c_{cat} = 3$ g L^{-1}, $c_{0,H2O2} = 5$ g L^{-1}, $c_{0,phenol} = 25$ mg L^{-1}, pH = 7.0 ± 0.3).
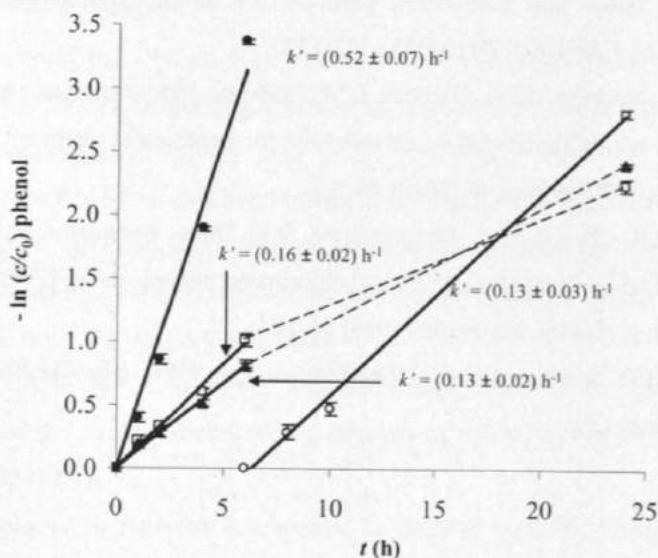
The observed decrease in reaction rates over longer time (*i.e.* 6 – 24 h) may be due to several factors: i) increasing agglomeration when no ultrasound treatment was carried out and/or ii) deactivation of the catalyst surface, which is discussed in more detail in connection with experiments on extended catalyst reuse in recycling experiments.

Fig. S2. Phenol degradation with commercial Fe(II,III) oxide at various initial H_2O_2 concentrations: ▲ 10 g L^{-1}, ○ 5 g L^{-1}, × 2.5 g L^{-1}, □ 1 g L^{-1} (c_{cat} = 3 g L^{-1}, $c_{0,phenol}$ = 25 mg L^{-1}, pH = 7.0 ± 0.3).
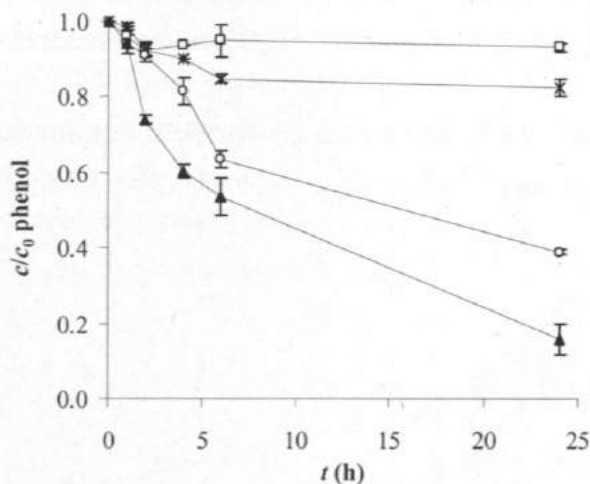

With respect to the influence of H_2O_2 concentration on the rate of contaminant degradation, the existence of an optimal concentration range has been reported in many studies; this can be explained by the fact that H_2O_2 acts not only as a source but also as a consumer of •OH. Under conditions where H_2O_2 is the dominant consumer of •OH in a Fenton system, it can be predicted that a further increase in H_2O_2 concentration will not enhance contaminant degradation rates, because the steady-state concentration of •OH remains unchanged [14]. The relative importance of the various •OH consumers can be estimated from the products of their second-order rate constants and concentrations in the reaction system. With $k_{OH,phenol}$ = 1.41 × 10^{10} M^{-1} s^{-1} [36] and $k_{OH,H2O2}$ = 2.7 × 10^7 M^{-1} s^{-1} [14], phenol and H_2O_2 are almost equally important as consumers of •OH in our reaction system, containing 25 mg L^{-1} phenol and 5 g L^{-1} H_2O_2 with $k_{OH,phenol}$ × c_{phenol} = 3.8 × 10^6 s^{-1} and $k_{OH,H2O2}$ × c_{H2O2} = 4.0 × 10^6 s^{-1}, respectively. It was only at the highest concentration of H_2O_2 applied (10 g L^{-1}) that phenol possibly became insignificant as consumer of •OH. Within the range of 1-10 g L^{-1} H_2O_2, the rate of phenol degradation increased with increasing initial H_2O_2 concentration (Fig. 5),

which is in accordance with the assumption that H_2O_2 can reach the role of a dominant •OH consumer only at the highest H_2O_2 concentration.

In systems with 1 and 2.5 g L^{-1}, 25% phenol reduction was not achieved. Therefore, the stoichiometric efficiency of H_2O_2 conversion was determined for the reaction period between $t = 0$-6 h, revealing a consumption of about 1000-1500 mol H_2O_2 per mol of phenol degraded for the whole range of initial H_2O_2 concentrations applied.

Fig. S3. Phenol conversion at various loads of commercial Fe(II,III) oxide: ▲ 10 g L^{-1}, ■ 5 g L^{-1}, ○ 1 g L^{-1} ($c_{0,H2O2} = 5$ g L^{-1}, $c_{0,phenol} = 25$ mg L^{-1}, pH = 7.0 ± 0.3).
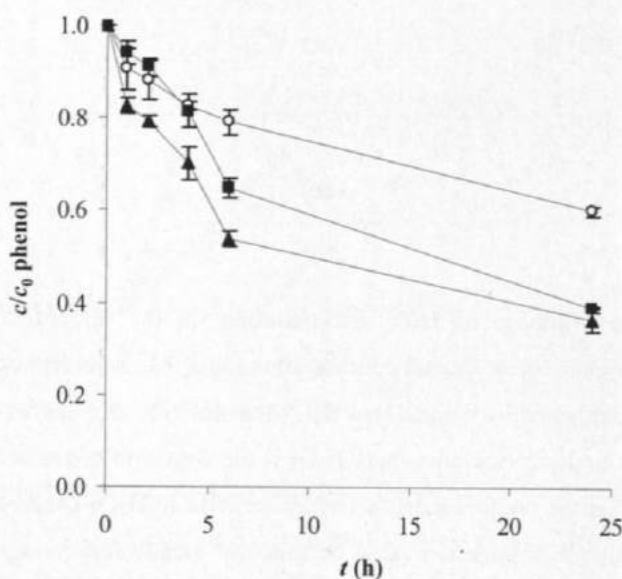
Eqs. S1 and S2

The average diffusion distance of hydroxyl radicals (L) can be estimated by Eqs. S1 and S2:

$$L = \sqrt{2 \cdot D \cdot \tau_{OH}} \quad [nm] \tag{S1}$$

$$\tau_{OH} = \frac{1}{\sum k_a \cdot [a]} [s] \tag{S2}$$

where D is the diffusion coefficient in water (approximately 10^{-5} cm^2 s^{-1}) and τ_{OH} is an average half-life of •OH. τ_{OH} is calculated based upon the concentrations of all •OH consumers [a] and their second-order rate constants (k_a) for reaction with •OH.

References

[S1] B.M. Voelker, W.P. Kwan, Rates of hydroxyl radical generation and organic compound oxidation in mineral-catalyzed Fenton-like systems, Environ. Sci. Technol. 37 (2003) 1150-1158.

[S2] NDRL/NIST Solution Kinetics Database on the WEB, http://kinetics.nist.gov/ kinetics/index.jsp

6. LaFeO$_3$ and BiFeO$_3$ perovskites as nanocatalysts for contaminant degradation in heterogeneous Fenton-like reaction

Klara Rusevova, Anett Georgi, Roberto Köferstein, Monica Rosell,
Frank-Dieter Kopinke
(*submitted*)

Abstract:

The present study examines the applicability of two iron-containing perovskites, particularly LaFeO$_3$ (LFO) and BiFeO$_3$ (BFO), as nanocatalysts for heterogeneous Fenton-like reactions. LFO and BFO synthesized according to a sol-gel method using citric acid as complexing agent have a crystallite size of about 60-70 nm with specific surface areas of 5.2 m^2 g^{-1} for LFO and 3.2 m^2 g^{-1} for BFO. In heterogeneous Fenton-like reactions, LFO and BFO showed similar pseudo-first order rate constants for phenol oxidation (k'_{LFO} = (0.13 ± 0.01) h^{-1} and k'_{BFO} = (0.15 ± 0.01) h^{-1}) at pH = 7 when 0.1 g L^{-1} catalyst and 3.0 g L^{-1} H$_2$O$_2$ were applied. Degradation efficiency was improved for both perovskites approximately by a factor of three when the pH value was slightly decreased to pH = 5. An increase of the reaction temperature from 20 °C to 60 °C during the BFO-catalyzed reaction lead to a significant acceleration of phenol removal of about one order of magnitude (k'_{BFO} = (1.9 ± 0.1) h^{-1}). High stability and reusability of the BFO particles with respect to MTBE degradation and H$_2$O$_2$ activation was confirmed in four successive oxidation batches. In addition, the mechanism of the perovskite-catalyzed Fenton-like system was studied by applying compound-specific stable isotope analysis (CSIA). The perovskite-catalyzed oxidation seems to follow a similar pathway as the homogeneous Fenton reaction, which means that •OH radicals play a dominant role as primary reactive species.

1. Introduction

Generation of hydroxyl radicals (•OH) by reaction of Fe^{2+} salts with hydrogen peroxide (H_2O_2) is well known as homogeneous Fenton reaction [1, 2]. This approach was suggested as an efficient treatment technique for recalcitrant pollutants. The main drawbacks of the homogeneous Fenton reaction are i) tight working pH (about pH = 3) in order to achieve acceptable reaction rates and ii) production of precipitated wastes, mostly in form of iron sludge, which requires their subsequent removal. [1]. In recent years, increasing attention has been paid to research on heterogeneous Fenton-like systems as alternatives in order to overcome these problems. An optimal solid catalyst for heterogeneous Fenton-like reactions should be able to form •OH from H_2O_2 over a wide pH range and show high efficiency with respect to contaminant degradation and H_2O_2 utilization, limited metal ion leaching and long-term stability. Operating costs and environmental compatibility have to be taken into account as well. In terms of heterogenization of the Fenton system, two main approaches are considered for catalytic activation of H_2O_2: i) immobilization of transition metal catalysts on porous materials such as silica, alumina, zeolite, clays or activated carbon [3-5] and ii) use of non-porous metals or metal oxides [6-8]. Although these types of catalysts were shown to have considerable activities for heterogeneous Fenton-like degradation of various contaminants, there is still room for substantial performance improvement with respect to the above mentioned criteria. Since the catalytic activity of pure iron oxides for Fenton-like oxidation is limited [9] research on the use of mixed metal oxides is receiving increasing interest. Orthoferrites with perovskite structure fabricated as nano-catalysts might be a promising option in this respect.

Perovskite-type oxides with the general formula ABO_3, where A is a rare earth metal and B a transition metal, have attracted many scientists due to their fascinating and well defined structure and intrinsic properties. They found applications such as solid oxide fuel cells, magnetic and electrode materials, chemical sensors and catalysts [10, 11]. The reason for the catalytic versatility of perovskites is seen in the high mobility of oxygen and the stabilization of unusual oxidation states in their structure, which leads to oxygen non-stoichiometry [11]. With the background of a potential application as catalyst in carbon-based electrodes, perovskites containing transition metals (e.g., A = La and B = Fe, Mn or Cr) were studied with respect to their ability to catalyze H_2O_2

decomposition [12-14]. These studies indicate that H_2O_2 decomposition depends not only on the metal composition but also on the concentration of highly oxidized transition metal sites (e.g., Ni^{III} and Fe^{IV}) [15] and oxygen non-stoichiometry [14].

So far only few studies have investigated the applicability of perovskite-type oxides in heterogeneous Fenton-like reactions [16-21]. Luo et al. [19] demonstrated high catalytic performance of $BiFeO_3$ nanoparticles for Rhodamine B (RhB) degradation at pH = 5 (e.g., half-live t_{50} = 20 min for c_{cat} = 0.5 g L^{-1}, $c_{0,RhB}$ = 10 µM and $c_{0,H2O2}$ = 10 mM). For RhB as large molecule which is negatively charged at pH = 5 electrostatic attraction and thus adsorption to the $BiFeO_3$ surface (showing a positive charge at this pH) might have positively affected the degradation. Degradation of phenol as a compound with low adsorption tendency was only studied at pH = 3, showing a lower degradation rate than RhB [19].

$LaFeO_3$ perovskites prepared by the "self-combustion" procedure were studied as heterogeneous Fenton-like catalysts for phenol degradation in the pH range of 2 to 4.5 [17]. Synthesis conditions appeared to strongly influence the structural characteristics as well as the catalytic activity of the $LaFeO_3$ samples prepared by this method. The sample with the lowest crystal domain size revealed the highest catalytic activity for phenol oxidation at pH = 3.7 and 40 °C (e.g., t_{50} = 15 min, c_{cat} = 1 g L^{-1}, $c_{0,phenol}$ = 0.5 mM, H_2O_2 dosage 2 mM h^{-1}) [17].

The aim of our study was to substantiate the applicability of perovskite catalysts for heterogeneous Fenton-like reaction. For this purpose $LaFeO_3$ (LFO) and $BiFeO_3$ (BFO) as iron-containing perovskite-type oxides with different crystal structures were synthesized by sol-gel procedures. Among the various wet chemistry methods for synthesis of nano-sized perovskite materials [22] (self-combustion, co-precipitation and sol-gel methods), sol-gel procedures are considered as most promising for up-scaled production based on evaluation of energy consumption, controllability and product properties. The obtained LFO and BFO perovskites were tested as nanocatalysts for heterogeneous Fenton-like reaction under conditions convenient for practical application, *i.e.* near ambient conditions and nearly neutral to slightly acidic pH range. The catalytic activity of the perovskites was evaluated with respect to achievable degradation rates for two model contaminants (phenol and methyl *tert*-butyl ether, MTBE) and H_2O_2 utilization. The influence of the employed reaction conditions, in particular H_2O_2 and catalyst concentrations, reaction pH and temperature on

contaminant degradation as well as the stability and reusability of the catalyst were studied. Additionally, isotope fractionation studies were carried out in order to assess the possible reaction pathways in the perovskite-catalyzed oxidation.

2. Experimental part

2.1. Chemicals and Materials

Lanthanum nitrate hexahydrate ($La(NO_3)_3 \cdot 6H_2O$), iron nitrate nonahydrate ($Fe(NO_3)_3 \cdot 9H_2O$), iron sulphate heptahydrate ($FeSO_4 \cdot 7H_2O$), citric acid monohydrate ($C_6H_8O_7 \cdot H_2O$), bismuth nitrate heptahydrate ($Bi(NO_3)_3 \cdot 5H_2O$), ethylene glycol, 2-methoxymethanol, nitric acid, n-hexane, d_5-phenol, phenol, MTBE, ethyl *tert*-butyl ether (ETBE) and H_2O_2 (30 wt.%) were obtained from Sigma Aldrich or Merck, Germany, with the highest purity and used as received. Titanium(IV) oxysulphate solution (1.9-2.1%) for determination of H_2O_2 was obtained from Fluka, Germany.

2.2 Synthesis of LFO

LFO was prepared by the sol-gel method following the procedure reported in [22]. In a 200 mL glass beaker 0.01 mol $La(NO_3)_3 \cdot 6H_2O$ and 0.01 mol $Fe(NO_3)_3 \cdot 9H_2O$ were dissolved in 100 mL deionized water and placed on a magnetic stirrer. 0.01 mol of citric acid was added as complexant. The resulting yellowish-brown sol was heated to 80 °C for 12 h in order to induce gel formation. Afterwards, the sample was placed in a muffle furnace and calcined at 600 °C for 2 h and after that the temperature was raised to 800 °C at 5 K min^{-1} and kept at this temperature again for 2 h.

2.3. Synthesis of BFO

BFO was synthesized according to a modified sol-gel method as described in [19]. In a 50 mL glass beaker 0.01 mol $Fe(NO_3)_3 \cdot 9H_2O$ and 0.01 mol $Bi(NO_3)_3 \cdot 5H_2O$ were dissolved in 25 mL 2-methoxymethanol, followed by adding 20 μL HNO$_3$. The mixture was placed on a magnetic stirrer and 0.01 mol citric acid (as complexant) and 15 mL ethylene glycol (as dispersant) were added. The resulting mixture was heated to 100 °C for 10 h to obtain a dark viscous resin. Afterwards, the sample was placed in a muffle furnace heated to 550 °C (5 K min^{-1}) and calcined for 2 h at this temperature.

2.4. Characterization of the catalyst

XRD analysis was used in order to identify the crystal structure of the prepared solid catalysts. XRD patterns were recorded on a Bruker D8 Diffractometer at room temperature using Cu K_α radiation. TEM images were obtained with a Jeol 1011 (Jeol instruments, Japan). The specific surface area (SSA) was determined by the BET method with a Belsorp-miniII instrument (Bel, Japan). The samples were pre-treated at 423 K and N_2 adsorption-desorption isotherms were measured at 77 K. The particle size distribution and zeta potential of the catalysts were measured with Mastersizer 2000 and Zetasizer Nano ZS, respectively, both from Malvern instruments. For these measurements the particle suspensions ($c = 25$ mg L^{-1}) were stabilized by addition of sodium hexametaphosphate (SHMP, $c = 1$ g L^{-1}).

2.5. Procedure of oxidation experiments

The reactions were carried out in 100 mL cylindrical glass vessels with Teflon-coated screw caps, which were thoroughly washed with concentrated HCl and deionized water before use. 0.1 g L^{-1} of catalyst were suspended in an aqueous solution containing the model compound (25 mg L^{-1} phenol or 50 mg L^{-1} MTBE). The suspension was adjusted to pH = 7 and treated in an ultrasonic bath for 10 min for homogenization. Afterwards the reaction was started by adding 3 g L^{-1} H_2O_2 as oxidant. The pH of the reaction medium was kept constant (pH = 7.0 ± 0.2) by adding 0.1 M NaOH. Batch reactors were continuously stirred on magnetic stirrer with 500 rpm throughout the duration of experiments and at given time intervals, samples for phenol or MTBE and H_2O_2 analysis were taken. Experiments at a reaction temperature of 40 °C and 60 °C were conducted in thermostated water bath.

In case of the recycling experiment, the reactions were carried out with MTBE as a model contaminant at (40 ± 2) °C and pH = 7. After each cycle the starting concentrations were adjusted to 50 mg L^{-1} and 5 g L^{-1} for MTBE and H_2O_2 respectively. Data shown in the figures are mean values of at least two experiments and the error represents the deviation of the single values from the mean value.

The procedures applied for isotope fractionation studies are described in [23] and are briefly summarized in the Supporting Information (SI).

2.7. Analytical methods

Concentration of phenol was determined by GC-MS analysis (QP2010, Shimadzu) after liquid-liquid extraction of 1 mL aliquots of the reaction suspension with 1 mL n-hexane containing d_5-phenol as an internal standard. The concentration of MTBE was monitored by means of headspace sampling with gas tight syringes and GC-MS analysis (QP2010, Shimadzu). H_2O_2 concentration was measured at $\lambda = 405$ nm with a UV-VIS spectrophotometer (UVmini-1240, Shimadzu) after adding titanyl sulfate solution (a yellow complex is formed). In addition, possible cation leaching (La, Bi, Fe) was determined using ICP-MS (Sciex ELAN 5000, Perkin Elmer).

3. Results and Discussion

3.1. Characterization of the catalyst

The XRD pattern of LFO is in agreement with phase-pure orthorhombic $LaFeO_3$, whereas BFO showed reflections of rhombohedral $BiFeO_3$ and traces of monoclinic Bi_2O_3 (Fig. 1). The mean crystallite size was estimated from the obtained XRD data according to Scherrer equation [24] as 60-70 nm for both perovskites. The equivalent particle diameters calculated according to $d_{p,equiv} = 6 / (SSA \times \rho)$ with ρ as the bulk densities of the two perovskites ($\rho_{BiFeO3} = 8.3$ g cm^{-3}, $\rho_{LaFeO3} = 6.3$ g cm^{-3}) are 210 nm and 180 nm for BFO and LFO, respectively. This indicates aggregation of the particles which was also confirmed by the TEM images (Fig. 2). Aggregation phenomena during synthesis due to the high temperature calcination necessary for formation of the perovskite phase have been described also by others [25]. Zeta potentials determined for the two perovskites at pH = 7 revealed values around $|\pm 30|$ mV (see Table 1), which indicates incipient instability of their aqueous suspension due to low electrostatic repulsion. Table 1 summarizes the physicochemical properties of the investigated LFO and BFO catalysts.

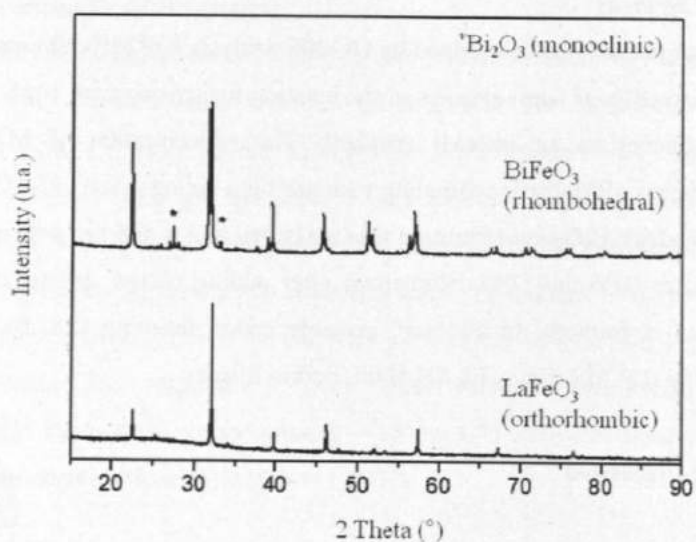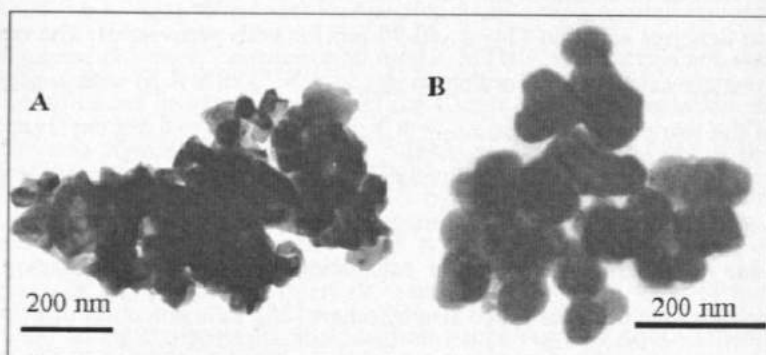**Fig. 1.** XRD patterns of synthesized LFO and BFO
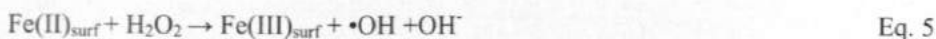

Fig. 2. TEM images of LFO (A) and BFO (B)
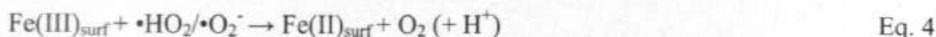
Table 1 Physicochemical properties determined for LFO and BFO catalyst samples.

Catalyst	BET ($m^2 g^{-1}$)	Point of zero charge (PZC)	Zetapotential (mV) at pH = 7
LFO	5.2	8.9	25
BFO	3.2	5.6	-31

3.2. Oxidation experiments

At first, preliminary oxidation tests were carried out in order to estimate the catalytic activity of the prepared LFO and BFO samples and assess the kinetics of phenol degradation. Fig. 3 demonstrates the removal of phenol with a half-life of about 5 h at a catalyst concentration of 100 mg L^{-1} at neutral pH conditions ($c_{0,H2O2} = 3$ g L^{-1}, $c_{0,phenol} = 25$ mg L^{-1}). In comparison, pure magnetic Fe(II,III) oxides showed much lower catalytic activities when applied under similar conditions. In a previous study we observed only 40% removal of phenol at a catalyst concentration of 1 g L^{-1} within 24 h when commercial nanosized Fe(II,III) oxide (SSA = 45 m^2 g^{-1}) was applied ($c_{0,H2O2} = 5$ g L^{-1}, $c_{0,phenol} = 25$ mg L^{-1}, pH = 7) [9].

The depletion of H_2O_2 within a reaction period of 24 h was < 20%. In a control batch containing H_2O_2 without the presence of catalyst, the depletion of phenol (< 10%) and MTBE (< 5%) was negligible within 24 h. The adsorption of the model contaminants, i.e. phenol and MTBE, onto the perovskite catalysts was tested in batch experiments using a suspension with 1 g L^{-1} catalyst and 25 mg L^{-1} phenol (or 50 mg L^{-1} MTBE). After 24 h of equilibration, no significant depletion of phenol or MTBE was observed (< 5%). Thus, the observed contaminant degradation in the presence of the synthesized BFO and LFO nanoparticles at pH = 7 can be ascribed to a heterogeneous Fenton-like process. The formation of hydroxyl radicals on solid iron-containing catalysts has been suggested to proceed via the following mechanism (Eqs. 1-6):

$$Fe(III)_{surf} + H_2O_2 \rightarrow Fe(III)_{surf}(H_2O_2) \qquad \text{Eq. 1}$$

$$Fe(III)_{surf}(H_2O_2) \rightarrow Fe(II)_{surf} + \bullet HO_2 + H^+ \qquad \text{Eq. 2}$$

$$HO_2\bullet \leftrightarrow \bullet O_2^- + H^+ \ (pK_a = 4.8) \qquad \text{Eq. 3}$$

$$Fe(III)_{surf} + \bullet HO_2/\bullet O_2^- \rightarrow Fe(II)_{surf} + O_2 \ (+ H^+) \qquad \text{Eq. 4}$$

$$Fe(II)_{surf} + H_2O_2 \rightarrow Fe(III)_{surf} + \bullet OH + OH^- \qquad \text{Eq. 5}$$

$$contaminant + \bullet OH \rightarrow ... CO_2 + H_2O \qquad \text{Eq. 6}$$

where H_2O_2 firstly forms a complex with Fe(III) sites at the catalyst surface (Eq. 1), which subsequently is converted to Fe(II) (Eq. 2). Surface Fe(II) reacts with H_2O_2 under formation of •OH and Fe(III) (Eq. 5).

Phenol degradation could be well fitted to pseudo-first order kinetics over the whole reaction period of 24 h in case of the BFO catalyst (Fig. 4).

In case of LFO, pseudo-first order fit was reasonable within the first 6 h of reaction, whereas a slight deceleration of the reaction was observed for the period of 6-24 h (Fig. 4). This change in catalytic activity can be due to an increasing agglomeration of the catalyst particles with increasing time span after the initial dispersion by ultrasound or might indeed be caused by a change in the catalytic properties of the LFO catalyst over time. This aspect will be discussed later in the text (see section 3.2.4.).
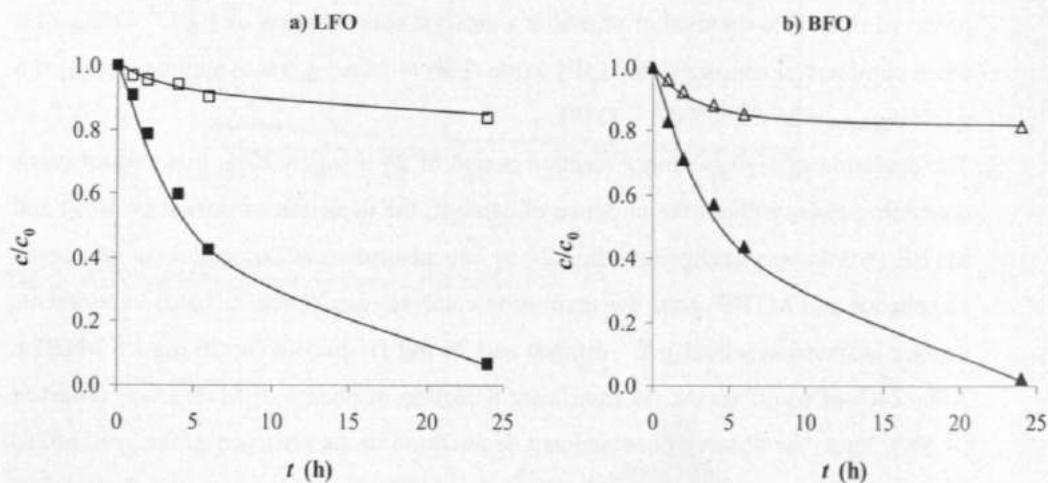

Fig. 3. Kinetics of phenol oxidation (filled symbols) and H_2O_2 decomposition (empty symbols) for **a)** LFO (■, □) and **b)** BFO (▲, △) as catalyst (c_{cat} = 0.1 g L^{-1}, c_{H2O2} = 3 g L^{-1}, $c_{0,phenol}$ = 25 mg L^{-1}, pH = 7.0 ± 0.2).

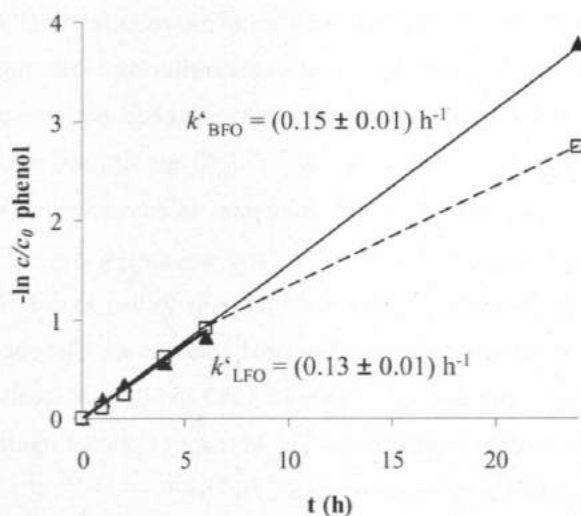**Fig. 4**: Pseudo-first-order kinetics plot for phenol degradation with LFO (□) and BFO (▲) ($c_{cat} = 0.1$ g L^{-1}, $c_{0,H2O2} = 3$ g L^{-1}, $c_{0,phenol} = 25$ mg L^{-1}, pH = 7.0 ± 0.2), thin solid line and k'_{BFO}: fit over the whole reaction period (0-24h) for BFO, thick solid line k'_{LFO}: fit for reaction period of 0-6 h for LFO, dashed line: illustrates deviation from first-order kinetics over longer reaction times.

In the next step, experiments under variable reaction conditions (H_2O_2 and catalyst concentrations, reaction temperature) were conducted. In these experiments, pseudo-first-order rate constants (k') for phenol degradation were determined for the initial reaction period (<6 h) and used for comparison, since reaction conditions (e.g., pH) could be well controlled in this interval and reasonable fitting results were obtained.

3.2.1. Optimization of initial H_2O_2 concentration

Previous research on Fenton-like oxidation has highlighted the existence of an optimum in the H_2O_2 concentration with respect to achievable rates of contaminant degradation. These observations can be explained by the fact that H_2O_2 is both, a source and a consumer of •OH. Under conditions where H_2O_2 is the dominant sink of •OH, it can be predicted that a further increase in H_2O_2 concentration will not result in an increase of contaminant degradation rates because the steady-state concentration of •OH remains unchanged [26].

The relative importance of phenol and H_2O_2 as •OH consumers can be estimated from the products of their second-order rate constants for reaction with •OH and their concentrations in the reaction system. In the experiments with variation of the initial H_2O_2 concentration (1, 3 and 10 g L^{-1}) the initial phenol concentration was kept constant at 25 mg L^{-1}. With $k_{OH,phenol} = 1.41 \times 10^{10}$ M^{-1} s^{-1} [27] and $k_{OH,H2O2} = 2.7 \times 10^{7}$ M^{-1} s^{-1} [26], phenol and H_2O_2 are almost equally important as consumers of •OH at 3 g L^{-1} H_2O_2 (with $k_{OH,phenol} \times c_{phenol} = 3.8 \times 10^{6}$ s^{-1} and $k_{OH,H2O2} \times c_{H2O2} = 2.4 \times 10^{6}$ s^{-1}, respectively). However, when the H_2O_2 concentration is further increased to 10 g L^{-1}, it becomes the dominant consumer of •OH compared with phenol. The observed optimum in the phenol degradation rate at 3 g L^{-1} H_2O_2 for LFO and BFO as catalysts (see Fig. 5) is in accordance with these considerations. The kinetics of phenol oxidation at various H_2O_2 concentrations is additionally shown in SI, Fig. S1.
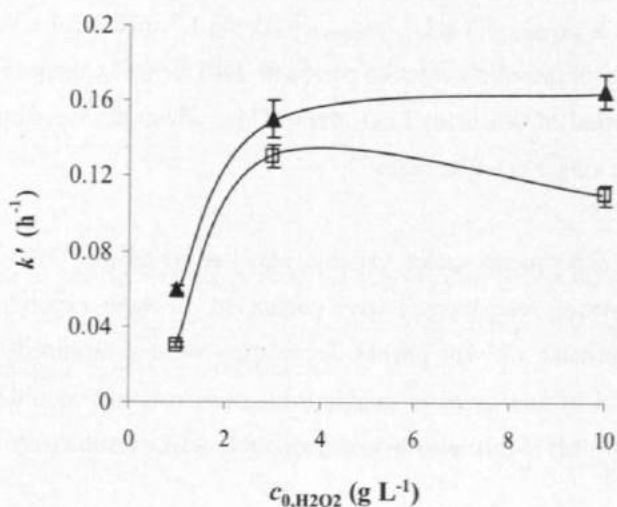
Fig. 5. Effect of H_2O_2 dose on the observed pseudo-first-order rate constants (k') of phenol degradation versus initial H_2O_2 dose for LFO (□) and BFO (▲) ($c_{cat} = 0.1$ g L^{-1}, $c_{0,H2O2} = 1.3$ and 10 g L^{-1}, $c_{0,phenol} = 25$ mg L^{-1}, pH = 7.0 ± 0.2).

3.2.2. Effect of pH value

The catalytic performance of LFO and BFO towards phenol oxidation was examined at pH = 5 and compared with the values obtained at pH = 7. In the LFO- and BFO-catalyzed Fenton system this slight decrease in pH value significantly enhanced the degradation rates of phenol (Fig. 6).
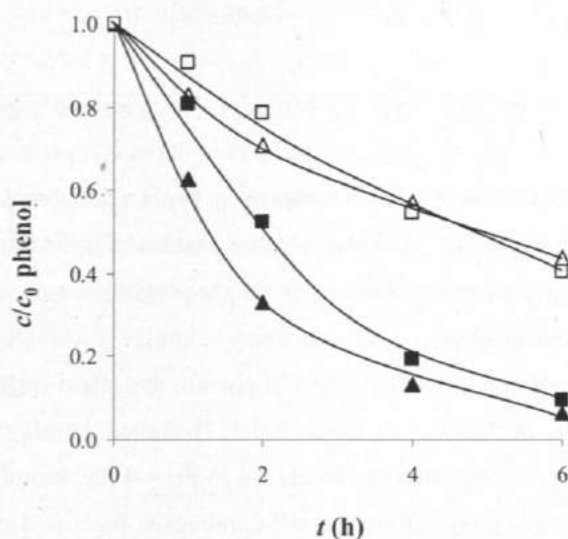
Fig. 6. Kinetics of phenol oxidation at pH = 5 (full symbols) and pH = 7 (empty symbols) for LFO (■, □) and BFO (▲, △) (c_{cat} = 0.1 g L^{-1}, $c_{0,phenol}$ = 25 mg L^{-1}, c_{H2O2} = 3 g L^{-1}, pH = 5.0 ± 0.2 or 7.0 ± 0.2).

The k' value for phenol degradation increased approximately by a factor of 3.5 for BFO ((0.51 ± 0.03) h^{-1}) and a factor of 3.1 for LFO ((0.40 ± 0.04) h^{-1}) at pH = 5.

In order to estimate the contribution of a homogeneous Fenton reaction caused by leached iron, the stability of LFO and BFO catalysts in aqueous media was examined at pH = 5 and pH = 7. After 24 h of vigorous stirring, the aqueous suspensions containing 1 g L^{-1} catalyst were filtered using a 1000 Da regenerated cellulose membrane and the filtrates were analyzed by means of ICP-MS measurements (Table 2).

Table 2 Concentration of dissolved metal species detected in the filtrates obtained after 24 h leaching of LFO and BFO (1 g L^{-1}) at pH = 5 and pH = 7.

Ions	LFO		BFO	
	pH = 5	pH = 7	pH = 5	pH = 7
La (mg L^{-1})	5.6	0.025	-	-
Fe (mg L^{-1})	< DL	< DL	0.014	< DL
Bi (mg L^{-1})	-	-	5×10^{-4}	< DL

Detection limit: DL$_{(La)}$ = 1 × 10^{-5} mg L^{-1}, DL$_{(Fe)}$ = 1 × 10^{-3} mg L^{-1}, DL$_{(Bi)}$ = 2 × 10^{-4} mg L^{-1}.

Iron was detected only in case of the BFO suspension at pH = 5, but still at an extremely low concentration (0.014 mg L^{-1}), which implies that no significant contribution of homogeneous Fenton reaction occurs even at the slightly acidic pH conditions. Interestingly, a significant amount of La was detected at pH = 5. Although dissolved La does not contribute to the catalytic oxidation of phenol, this effect might be crucial for the long-term stability of the catalyst. Faye et al. [17] studied the pH range of 2 to 4.5 and found a pronounced optimum between pH = 3 to pH = 4 for phenol degradation for their LaFeO$_3$ catalyst originating from the self-combustion process. However, the iron leaching detected (0.27 wt% corresponding to 2.7 mg L^{-1} at c_{LaFeO3} = 1 g L^{-1} catalyst) and the similarity in the optimum pH range to dissolved iron as catalyst, indicates that a homogeneous Fenton reaction played an important role in their system.

Luo et al. [19] studied the degradation of RhB with H$_2$O$_2$ using BFO as catalyst and were able to rule out any contribution of a homogeneous Fenton reaction in the pH range of 4 to 8. In this case a continuous increase in the rate constant for RhB degradation was observed when the pH was decreased from pH = 8 to pH = 3, with a moderate increase between pH = 7 and pH = 5 (factor of 1.5). While solution pH drastically influences the efficiency of homogeneous Fenton reaction (mainly due to the pH-induced changes in speciation of dissolved iron), the effect of pH on contaminant degradation by heterogeneous Fenton reactions is generally only moderate. In heterogeneous Fenton systems, pH effects can result from the following mechanisms: i) pH influence on surface adsorption of the organic contaminant (which is, however, mainly relevant for charged compounds), ii) the complex formation of H$_2$O$_2$ with active sites can be influenced by the acid/base equilibria at the catalyst surface and iii) changes

in iron(II,III) recycling due to the pH-dependent oxidation and reduction of iron by the hydroperoxyl radical and its conjugate base, $HO_2\bullet/O_2^-$ (Eq. 3).

The influential role of electrostatics on contaminant interactions with the catalyst surface (as described for charged contaminant molecules [19, 28]) should be of minor importance for phenol which is uncharged in the considered pH range. Thus, the acceleration of phenol degradation observed for BFO and LFO might be due to a superposition of the latter two of the above mentioned factors.

3.2.3. Effect of reaction temperature

In order to extend the operation range, the catalytic activity of LFO and BFO was examined at reaction temperatures of 20, 40 and 60 °C at pH = 7. A moderate increase in the reaction temperature lead to a strong acceleration of phenol oxidation with BFO, where the k' value increased by one order of magnitude (Fig. 7).
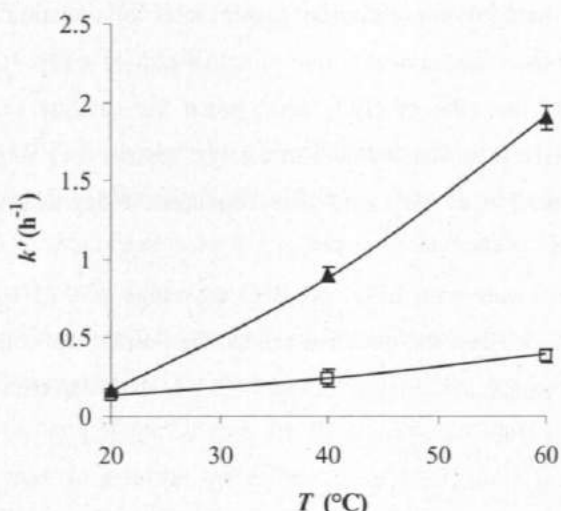
Fig. 7. Effect of the reaction temperature on the rate constant (k') of phenol degradation with LFO (□) and BFO (▲) (c_{cat} = 0.1 g L^{-1}, $c_{0,H2O2}$ = 3 g L^{-1}, $c_{0,phenol}$ = 25 mg L^{-1}, pH = 7.0 ± 0.2).

Hydrogen peroxide decomposition was enhanced in both reaction systems, *i.e.* the pseudo-first-order rate constants increased approximately by factors of 15 and 7 for BFO and LFO, respectively, when T was raised from 20 to 60 °C. However, the

oxidation of phenol catalyzed by LFO was less affected by the reaction temperature than BFO.

By plotting ln k' versus $1/T$ according to the Arrhenius equation (see SI, Fig. S2) apparent activation energies (E'_A) of 51 kJ mol^{-1} and 22 kJ mol^{-1} were calculated for the phenol oxidation catalyzed by BFO and LFO, respectively. For comparison, E'_A determined for RhB degradation catalyzed by BFO in [19] is 20.7 kJ mol^{-1}. The obtained values for E'_A are significantly higher than the range attributed to diffusion-controlled reactions (10-13 kJ mol^{-1}) [29], implying that in the perovskite-catalyzed reaction intrinsic chemical reactions dominate the overall rate. However, one has to stress that the heterogeneous Fenton-like oxidation is a complex system including various chemical reactions and equilibria, so that mechanistic interpretations of apparent activation energies are not straightforward.

3.2.4. Effect of the catalyst concentration

By increasing the catalyst concentration higher rates of contaminant removal are expected due to the increased concentration of active centers where •OH are produced. However, similar to the case of H_2O_2 dose, when the catalyst surface becomes a dominant sink of •OH, a further increase in catalyst surface area might not affect the steady-state concentration of •OH and thus contaminant degradation is not further accelerated [9].

In a series of experiments with LFO and BFO the range of 0.01-1 g L^{-1} of catalyst concentration was tested and the obtained pseudo-first-order rate constants for phenol oxidation at pH = 7 ($c_{0,phenol} = 25$ mg L^{-1}, $c_{0,H2O2} = 3$ g L^{-1}) are depicted in Fig. 8.
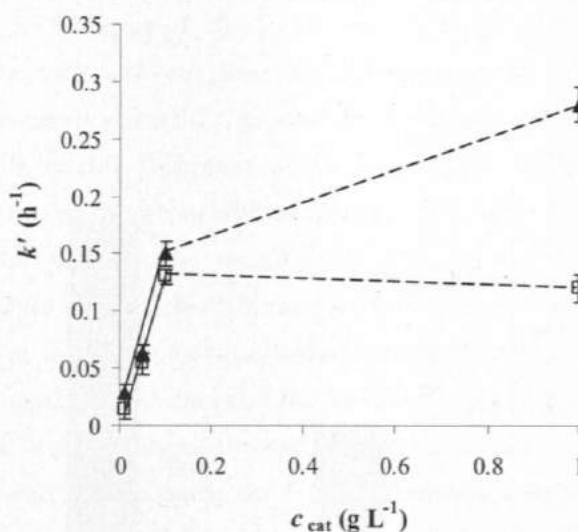
Fig. 8. Influence of increased catalyst concentration on the rate constant (k') of phenol oxidation with LFO ($\square$) and BFO ($\blacktriangle$) (c_{cat} = 0.01, 0.05, 0.1 and 1 g L^{-1}, $c_{0,H2O2}$ = 3 g L^{-1}, $c_{0,phenol}$ = 25 mg L^{-1}, pH = 7.0 ± 0.2).

For LFO and BFO the increase of k' for phenol removal was nearly proportional to the catalyst concentration in the range of 0.01-0.1 g L^{-1}. However, when the catalyst concentration was further raised to 1 g L^{-1}, k' was only moderately increased for BFO or even slightly decreased with LFO.

Considering the depletion of oxidant, only in the reaction with 1 g L^{-1} of BFO a high degree of H_2O_2 decomposition was monitored (85% of the oxidant was decomposed within 24 h). In the rest of the batches the H_2O_2 decomposition did not exceed 20% within 24 h. In order to estimate the efficiency of H_2O_2 utilization for contaminant degradation at various catalyst concentrations the parameter R_{50} (mol mol^{-1}) was introduced (Eq. 7). R_{50} defines the amount of H_2O_2 (n_{H2O2}) consumed per mol of phenol (n_{phenol}) degraded in the reaction period between t = 0 h and t_{50}, *i.e.* the time at which 50% of the phenol was degraded. The lower the R_{50} value the more efficient the oxidant is exploited.

$$R_{50} = \left(\frac{n_{H2O2}}{n_{phenol}} \right)_{t_{50}}$$

Eq. 7

Fig. 9 illustrates the efficiency of H_2O_2 utilization for phenol oxidation at catalyst concentrations of 0.1 and 1 g L^{-1}.
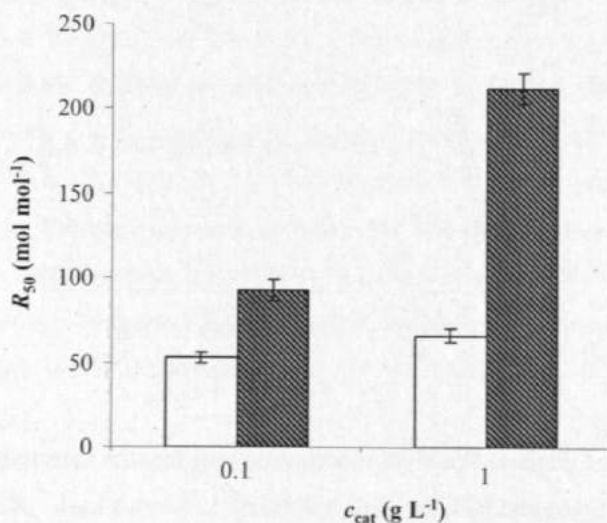
Fig. 9. Efficiency of H_2O_2 utilization at 0.1 and 1 g L^{-1} of LFO (empty columns) and BFO (dashed columns) (c_{cat} = 0.1 and 1 g L^{-1}, $c_{0,H2O2}$ = 3 g L^{-1}, $c_{0,phenol}$ = 25 mg L^{-1}, pH = 7.0 ± 0.2).

Compared to the stoichiometric amount of 14 moles H_2O_2 needed to mineralize one mol of phenol, the consumption of H_2O_2 in the heterogeneous systems with LFO and BFO is much higher, indicating the existence of productive (•OH producing) and parasitic pathways for H_2O_2 decomposition in parallel as generally discussed for heterogeneous Fenton reactions. Strong competition for consumption of •OH by other non-target species (H_2O_2, catalyst surface) can additionally contribute to inefficient utilization of H_2O_2 for contaminant degradation.

The results of Figs. 8 and 9 show that only a limited increase in contaminant degradation rates can be achieved by means of increasing catalyst concentrations. At the same time the efficiency of oxidant utilization becomes worse. This observation is not restricted to the perovskite catalyst but was previously described also for other Fenton catalysts [9, 29]. The increased consumption of •OH due to an increased concentration of individual catalyst particles requires that •OH produced on the surface of one particle will react with the surface of another particle. For individual catalyst nano- or

microparticles this is unlikely, since the lifetime of •OH in reaction solutions typically containing H_2O_2 in the range of 10^{-1} to 10^0 g L^{-1} is extremely short, not allowing diffusion into the bulk solution phase [9]. However, nanoparticles are prone to agglomeration processes, whereby fraction and conformation of the agglomerates formed depend on particle concentration. As a consequence, agglomerates can be formed which are loose enough to enable access of H_2O_2 to the active sites but tight enough to quench •OH, thereby reducing the efficiency of H_2O_2 utilization for contaminant degradation. The results obtained for BFO are in accordance with this hypothesis, since an increase in the catalyst concentration from 0.1 to 1 g L^{-1} resulted in faster H_2O_2 decomposition (k' increased by about one order of magnitude) but only slight acceleration of phenol degradation and thus less efficient H_2O_2 utilization. In case of LFO, neither phenol degradation nor H_2O_2 decomposition were increased to the expected extent when the catalyst concentration was raised to 1 g L^{-1}. Having in mind the result of La leaching described in section 3.2.2., we conducted an experiment where the filtrate obtained after 24 h of catalyst leaching (1 g L^{-1}) was used as reaction medium to which a new dose of fresh catalyst (0.1 g L^{-1}) and phenol were added and the reaction was initiated by hydrogen peroxide addition. Comparing the rate of phenol degradation in presence of the leachate with a reference experiment where fresh catalyst in deionized water was used, a considerable slowdown is noticed. Only 50% of phenol was removed within 24 h (see SI, Fig. S3). The significant inhibiting effect of the LFO leachate indicates the occurrence of a reorganization process at the LFO surface which involves the dissolution and re-deposition of La species and finally results in deterioration of the catalytic properties of the LFO surface. This time-dependent process might also contribute to the observed deceleration of phenol degradation (i.e. deviation from pseudo-first order kinetics) over longer reaction times (6-24 h) as described in section 3.2.

3.2.5. Catalyst stability and reusability

The stability of the BFO catalyst with respect to the contaminant degradation (in this case MTBE) and H_2O_2 utilization was examined in four consecutive runs at pH = 7. The measured data showed approximately constant removal of MTBE, i.e. about 80% of MTBE was degraded in 6 h (Fig. 10). The oxidation efficiency was characterized by

R_{50} values of about 120 which are depicted in the small figure in Fig. 10. The stoichiometric ratio of H_2O_2: MTBE for its complete mineralization is 15 mol mol^{-1}.
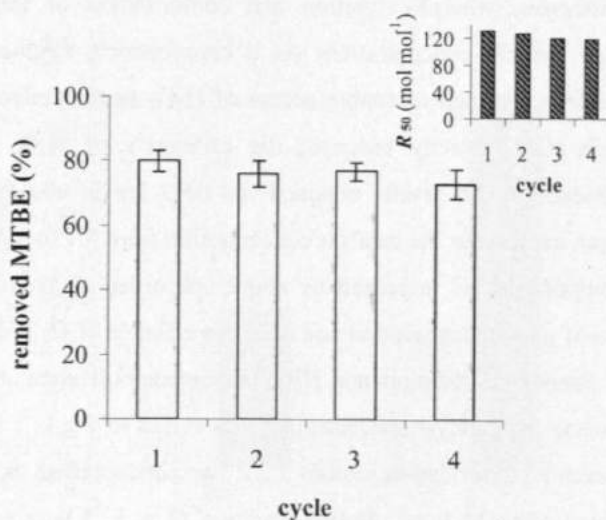
Fig. 10. MTBE removal (%) after 6 h in presence of BFO catalyst in four consecutive batch experiments, the small figure illustrates the R_{50} values obtained in each cycle (c_{cat} = 0.1 g L^{-1}, $c_{0,H2O2}$ = 5 g L^{-1}, $c_{0,MTBE}$ = 50 mg L^{-1}, pH = 7.0 ± 0.2, T = 40 ± 2 °C).

The pseudo-first order rate constant for MTBE degradation is (0.26 ± 0.03) h^{-1}, and thus lower than the value observed for phenol (k' = (0.91 ± 0.05) h^{-1} under the same conditions (c_{cat} = 0.1 g L^{-1}, $c_{0,H2O2}$ = 5 g L^{-1}, pH = 7.0 ± 0.2, T = 40 ± 2 °C). This is plausible since MTBE as aliphatic ether compound is less reactive towards electrophilic attack than phenol as aromatic compound. This is also reflected in the second order rate constants for reaction with •OH reported for the two compounds ($k_{OH,phenol}$ = 1.41 × 10^{10} M^{-1} s^{-1} [27], $k_{OH,MTBE}$ = 1.6 × 10^9 M^{-1} s^{-1} [30]).

A sample for the determination of leached metal species (Fe, Bi) was withdrawn at the end of the recycling experiment and filtered using a 1000 Da regenerated cellulose membrane. The ICP-MS measurements showed concentrations below the detection limits ($DL_{(Fe)}$ = 1 µg L^{-1}, $DL_{(Bi)}$ = 0.2 µg L^{-1}). In accordance with the results reported by Luo et al. [19] for reuse of BFO in RhB degradation, our results confirm that the BFO catalyst appears to be stable and can be reused without loss in catalytic activity.

3.3. Isotope fractionation study

One of the important questions on Fenton-like oxidation systems, regardless of homogeneous or heterogeneous, is that for the active, short-living oxidizing species. In addition to ‚direct' spectroscopic methods, the inter- or intramolecular selectivity of an oxidation can provide hints on the dominating active species. Different species create their own characteristic fingerprints. A particular case of such a fingerprint is the compound-specific stable isotope analysis (CSIA) of a chemical reaction [31].

Recently, we have applied the CSIA technique on biotic and abiotic transformation reactions of MTBE and ETBE [23] including heterogeneous Fenton-like oxidation catalyzed by LFO and BFO (see Supporting Information in [23]). The information value with respect to the type of reactive species formed by the perovskite catalysts stimulates a more detailed interpretation of these results in this paper.

The average enrichment factors ε_{bulk} [‰] for the elements carbon and hydrogen during oxidation of MTBE and ETBE were derived from Rayleigh plots [31] in the form of Eqs. 8 and 9:

$$\ln\left(\frac{\delta^{13}C_t + 1000}{\delta^{13}C_0 + 1000}\right) = \frac{\varepsilon_C}{1000} \cdot \ln f$$

Eq. 8

$$\ln\left(\frac{\delta^{2}H_t + 1000}{\delta^{2}H_0 + 1000}\right) = \frac{\varepsilon_H}{1000} \cdot \ln f$$

Eq. 9

where $\delta^{13}C_t$ and $\delta^{2}H_t$ are the isotope ratios ($^{13}C/^{12}C$ and $^{2}H/^{1}H$) of the residual substrate (expressed in the Delta notation) at a certain extent of degradation (i.e. at time t) and $\delta^{13}C_0$ and $\delta^{2}H_0$ the initial values (i.e. at $t = 0$). f is the time-dependent residual fraction of the substrate.

Table 3 shows ε_C and ε_H values for MTBE and ETBE oxidation by homogeneous Fenton reaction and heterogeneous Fenton-like reaction catalyzed by BFO and LFO. For comparison values for oxidation by potassium permanganate ($KMnO_4$) are also included.

Table 3 Average isotope enrichment factors ε_{bulk} [‰] for the oxidation of MTBE and ETBE in various oxidation systems.

Oxidation system	MTBE		ETBE		Reference
	$-\varepsilon_{C,bulk}$	$-\varepsilon_{H,bulk}$	$-\varepsilon_{C,bulk}$	$-\varepsilon_{H,bulk}$	
Homogeneous Fenton reaction	1.3 ± 0.1	30 ± 1	0.85 ± 0.25	18	[23][1]
BFO + H_2O_2	1.4	25	0.8	15	[23]
LFO + H_2O_2	1.6	24	1.3	15	[23]
$KMnO_4$	5.53	109	5.2	128	[23]

[1] Average of values reported for homogeneous Fenton initiated with Fe^{2+} and Fe^{3+}, respectively, in this reference

Obviously, the isotope fractionation fingerprints of the homogeneous Fenton oxidation and the two heterogeneous Fenton oxidation systems are similar. This suggests a similar pool of reactive species. The perceptible tendencies are in accordance with the general rules of isotope fractionation: i) the light molecules (containing exclusively ^1H and ^{12}C atoms) react faster than their heavy isotopologues (containing one ^2H or ^{13}C atom at natural abundance) and ii) the more reactive atoms of an element are in the substrate molecule, the lower the observable enrichment factors. In contrast, oxidation with $KMnO_4$, a much less reactive oxidant than •OH, is expectedly related with a much stronger fractionation effect than Fenton systems.

In order to not only compare the *relative* fractionation effects of the various oxidation systems but in addition to draw mechanistic conclusions from the *absolute* isotope enrichment factors it is useful to transform them into kinetic isotope effects (*KIEs*). *KIEs* are defined as the ratio of rate constants of two elementary reactions according to Eq. 10:

$$KIE = k_{light} / k_{heavy} \quad \text{e.g., } KIE_H = k_H / k_D \text{ and } KIE_C = k_{12C} / k_{13C} \qquad \text{Eq. 10}$$

wherein the rate constants k describe the attack of a reactive species on a specific position or bond. The main point in the transformation of bulk enrichment factors into apparent (= observable) kinetic isotope effects (*AKIEs*) is a statistic correction for the

numbers of atoms of the same element which are present in the substrate molecule (n) and in a reactive position (x) as described in Eq. 11:

$$AKIE \approx 1 \, / \, (1 + z \times n/x \times \varepsilon_{bulk}) \approx 1 \, / \, (1 + n \times \varepsilon_{bulk}) \qquad\qquad \text{Eq. 11}$$

z is the number of atoms that are in an intramolecular competition. For consideration of exclusively primary isotope effects it holds $z = x$ such that Eq. 11 can be used in its simplified version (right side of Eq. 11). This approach takes into account that at natural abundance only one heavy atom is present per molecule which ‚dilutes' the observable bulk fractionation effect. MTBE is attacked by •OH via H-abstraction from its methyl groups whereby the branching ratio between attack at the methoxy group and the *tert*-butyl side is about 3:2 [32]. Applying Eq. 11 will result in this case in an *AKIE* value which represents the average of the *KIE*s of the two types of bond breakage involved (at the primary carbon in the *tert*-butyl side and the methoxy group). For further discussion of the approximations contained in Eq. 11 see SI.

In order to test the hypothesis that •OH is the dominant reactive species in homogeneous and perovskite-catalyzed oxidation of the model compounds, hydrogen fractionation ($AKIE_{H}$) is considered here. Applying Eq. 11 with $n_{H} = 12$ in MTBE and $n_{H} = 14$ in ETBE for the range of $\varepsilon_{H,bulk}$ observed in the homogeneous and heterogeneous Fenton reaction it results:

$$KIE_{H,MTBE} = 1 \, / \, (1 - 12 \times 0.024...0.030) = 1.40...1.56 \qquad\qquad \text{Eq. 12}$$

$$KIE_{H,ETBE} = 1 \, / \, (1 - 14 \times 0.015...0.018) = 1.27...1.34 \qquad\qquad \text{Eq. 13}$$

There are only limited data available for KIE_{H} in reaction of organic compounds with hydroxyl radicals in the aqueous phase. From UV/H_2O_2 experiments with deuterated cyclohexane Pignatello et al. [33] determined a value of $KIE_{H} = 1.08 \pm 0.02$ which was not significantly different from the value determined for homogeneous Fenton degradation of this compound ($KIE_{H} = 1.06 \pm 0.08$) determined in the same study. Methanol oxidation by homogeneous Fenton reagent was reported to have a similar KIE_{H} of 1.08 ± 0.02 [30]. Thus, the magnitude of reported KIE_{H} differs in the order MTBE $\approx$ ETBE > cyclohexane $\approx$ methanol, even though the general reaction

mechanism for reaction of •OH with all these substrates is H-abstraction from sp^3-hybridized aliphatic carbon atoms. The variability of measured KIE_H-values might suggest that reactive species other than free •OH radicals may be active in the investigated oxidation systems as well, including the two homogeneous Fenton systems. However, this conclusion is not stringent as will be discussed in the following.

More literature data than for aqueous phase reactions are available for gas phase reactions of alkanes with •OH (see [34] and papers cited therein). Isotope fractionation effects in gas phase reactions of •OH are generally larger than those observed for aqueous phase reactions at the same temperature (e.g., $KIE_H = 2.59 \pm 0.16$ for cyclohexane oxidation in the gas phase at 292 K [35] compared to 1.08 in the aqueous phase) and thus cannot be directly compared. However, some trends can be expected to be similar in both phases. For gas phase reactions, the magnitude of KIE_H for H-abstraction correlates with the C-H(D) bond strength [36, 37]: The higher the bond strength the higher the KIE_H-value. The two ethers MTBE and ETBE contain three and four, respectively, non-activated methyl groups which have higher C-H bond strengths than those in cyclohexane and methanol [38]. This could lead to higher fractionation effects for the two ethers MTBE and ETBE, because H-abstraction from the methyl groups is a significant pathway for the •OH attack on these compounds. From this point of view, the above mentioned sequence in KIE_H becomes conceivable.

To sum up, bulk enrichment factors for hydrogen and carbon observed during LFO- and BFO-catalyzed oxidation of MTBE and ETBE as well as derived KIE_H values are in accordance with the hypothesis that •OH is the dominating reactive species in this heterogeneous Fenton-like system. Recently, further support of this hypothesis was provided by results on UV/H_2O_2 oxidation of MTBE and ETBE reported by Zhang et al. [39] which showed very similar $\varepsilon_{H,bulk}$ and $\varepsilon_{C,bulk}$ values as the homogeneous and perovskite-catalyzed Fenton systems. Nevertheless, we do not consider these isotope fractionation data as clear proof of an exclusive role of •OH radicals as the only hydrocarbons oxidizing species.

4. Conclusions

In conclusion, LFO and BFO perovskites were prepared by a sol-gel process with subsequent high-temperature calcination obtaining particles with a crystallite size of 60-

70 nm and SSA of 5.2 m^2 g^{-1} (LFO) and 3.2 m^2 g^{-1} (BFO). The obtained perovskite catalysts revealed high catalytic activities in heterogeneous Fenton-like oxidation of phenol and MTBE at neutral conditions. The contribution of leached metal species was confirmed to be negligible. A comparison with literature data for simple Fe(II,III) oxide nanoparticles shows that LFO and BFO perovskites possess a higher catalytic activity (normalized to catalyst mass concentration) when applied for phenol degradation at pH = 7.

Rate constants for phenol degradation were determined as (0.13 ± 0.01) h^{-1} and (0.15 ± 0.01) h^{-1} for LFO and BFO, respectively, at a catalyst concentration of 0.1 g L^{-1}, 3 g L^{-1} H$_2$O$_2$ and pH = 7. The rate constant for phenol degradation increased approximately three-fold for both perovskites when the reaction pH was slightly decreased to pH = 5. An increase in reaction temperature in the range of 20-60°C was also observed to accelerate contaminant degradation, wherein the BFO-catalyzed reaction was more affected than LFO.

While the catalytic activity of LFO appears to be affected by surface re-organization occurring in aqueous medium, BFO showed a very good stability. MTBE degradation in four consecutive runs using BFO as heterogeneous Fenton catalyst revealed constant catalytic activity and H$_2$O$_2$ utilization efficiency. The obtained results suggest that the performance of the AFeO$_3$ perovskite catalysts is influenced by i) the intrinsic properties of the perovskite (e.g., crystal structure, A-site cation or structural impurities) and ii) processes that occur spontaneously under the Fenton conditions (e.g., agglomeration effects and scavenging of reactive species). Finally, based on isotope fractionation results hydroxyl radicals have been suggested to be the major reactive species responsible for contaminant degradation in heterogeneous Fenton-like reaction with perovskite nanocatalysts.

Acknowledgement

References

[1]   G.V. Buxton, C.L. Greenstock, W.P. Helman, A.B. Ross, *J. Phys. Chem. Ref. Data* 17 (1988) 513-886.

[2]   S. Perathoner, G. Centi, *Top. Catal.* 33 (2005) 207-224.

[3]   E.G. Garrido-Ramirez, B.K.G. Theng, M.L. Mora, *Appl. Clay Sci.* 47 (2010) 182-192.

[4]   R. Gonzalez-Olmos, U. Roland, H. Toufar, F.D. Kopinke, A. Georgi, *Appl. Catal. B-Environ.* 89 (2009) 356-364.

[5]   S. Navalon, M. Alvaro, H. Garcia, *Appl. Catal. B-Environ.* 99 (2010) 1-26.

[6]   J.J. Wu, M. Muruganandham, J.S. Yang, S.S. Lin, *Catal. Commun.* 7 (2006) 901-906.

[7]   T. Zhou, Y.Z. Li, J. Ji, F.S. Wong, X.H. Lu, *Sep. Purif. Technol.* 62 (2008) 551-558.

[8]   P. Baldrian, V. Merhautova, J. Gabriel, F. Nerud, P. Stopka, M. Hruby, M.J. Benes, *Appl. Catal. B-Environ.* 66 (2006) 258-264.

[9]   K. Rusevova, F.D. Kopinke, A. Georgi, *Journal of Hazardous Materials* (accepted). DOI: 10.1016/j.jhazmat.2012.09.068

[10]   H. Tanaka, *Catal. Surv. Asia* 9 (2005) 63-74.

[11]   M.A. Pena, J.L.G. Fierro, *Chem. Rev.* 101 (2001) 1981-2017.

[12]   A. Ariafard, H.R. Aghabozorg, F. Salehirad, *Catal. Commun.* 4 (2003) 561-566.

[13]   M. Soleymani, A. Moheb, D. Babakhani, *Chem. Eng. Technol.* 34 (2011) 49-55.

[14]   Y.N. Lee, R.M. Lago, J.L.G. Fierro, J. Gonzalez, *Appl. Catal. A-Gen.* 215 (2001) 245-256.

[15]   H. Falcon, R.E. Carbonio, J.L.G. Fierro, *J. Catal.* 203 (2001) 264-272.

[16]   L.L. Ju, Z.Y. Chen, L. Fang, W. Dong, F.G. Zheng, M.R. Shen, *J. Am. Cer. Soc.* 94 (2011) 3418-3424.

[17]   J. Faye, E. Guelou, J. Barrault, J.M. Tatibouet, S. Valange, *Top. Catal.* 52 (2009) 1211-1219.

[18]   J.A. Melero, J.L. Sotelo, G. Ovejero, F. Martinez, A. Milieni, *Appl. Catal. B-Environ.* 47 (2004) 281-294.

[19]   W. Luo, L.H. Zhu, N. Wang, H.Q. Tang, M.J. Cao, Y.B. She, *Environ. Sci. Technol.* 44 (2010) 1786-1791.

[20]   J.L. Ding, X.M. Lu, H.M. Shu, J.M. Xie, H. Zhang, *Mater. Sci. Eng. B-Adv.* 171 (2010) 31-34.

[21]   S.M. Sun, W.Z. Wang, L. Zhang, M. Shang, *J. Phys. Chem. C.* 113 (2009) 12826-12831.

[22]   P.V. Gosavi, R.B. Biniwale, *Mater Chem Phys* 119 (2010) 324-329.

[23]   M. Rosell, R. Gonzalez-Olmos, T. Rohwerder, K. Rusevova, A. Georgi, F.D. Kopinke, H.H. Richnow, *Environ. Sci. Technol.* 46 (2012) 4757-4766.

[24]   S.N. Danilchenko, O.G. Kukharenko, C. Moseke, I.Y. Protsenko, L.F. Sukhodub, B. Sulkio-Cleff, *Cryst. Res. Technol.* 37 (2002) 1234-1240.

[25]   H.J. Su, L.Q. Jing, K.Y. Shi, C.H. Yao, H.G. Fu, *J Nanopart Res* 12 (2010) 967-974.

[26]   B.M. Voelker, W.P. Kwan, *Environ. Sci. Technol.* 37 (2003) 1150-1158.

[27]   A.K. De, B. Chaudhuri, S. Bhattacharjee, B.K. Dutta, *J. Hazard. Mater.* 64 (1999) 91-104.

[28]   W.P. Kwan, B.M. Voelker, *Environ. Sci. Technol.* 38 (2004) 3425-3431.

[29]   X.F. Xue, K. Hanna, M. Abdelmoula, N.S. Deng, *Appl. Catal. B-Environ.* 89 (2009) 432-440.

[30]   R. Gonzalez-Olmos, F. Holzer, F.D. Kopinke, A. Georgi, *Appl. Catal. A-Gen.* 398 (2011) 44-53.

[31]   M. Elsner, L. Zwank, D. Hunkeler, R.P. Schwarzenbach, *Environ. Sci. Technol.* 39 (2005) 6896-6916.

[32]   M.I. Stefan, J. Mack, J.R. Bolton, *Environ. Sci. Technol.* 34 (2000) 650-658.

[33]   J.J. Pignatello, D. Liu, P. Huston, *Environ. Sci. Technol.* 33 (1999) 1832-1839.

[34]   W.P. Hess, F.P. Tully, *J. Phys. Chem.* 93 (1989) 1944-1947.

[35]   A.T. Droege, F.P. Tully, *J. Phys. Chem.* 91 (1987) 1222-1225.

[36]   F.P. Tully, Chem. *Phys. Lett.* 143 (1988) 510-514.

[37]   D.F. Mcmillen, D.M. Golden, *Annu. Rev. Phys. Chem.* 33 (1982) 493-532.

[38]   D.R. Lide, Handbook of Chemistry and Physics, CRC Press, 75t Edition, 1994, p. 9-64.

[39]   N. Zhang, J. Schindelka, H. Herrmann, M. Rosell, S. H. Martín, H. H. Richnow, 2012. Book of Abstracts, *Joint European Stable Isotope Users Group Meeting*, JESIUM 2012, Leipzig, p-266

Procedure of oxidation experiments for isotope fractionation studies

The isotope fractionation measurements were carried out in 100 mL cylindrical glass vessels with screw-cap Mininert® valve. Stoichiometric Fenton reaction was performed at pH 3.0 ± 0.2 in solution containing equimolar concentrations of Fe^{2+} and H_2O_2 (10 mM of each) for oxidation of 100 mg L^{-1} MTBE and ETBE. Heterogeneous Fenton-like reaction with LFO and BFO was carried out at 40 ± 2 °C and pH = 7.0 ± 0.2. The reaction medium contained 1 g L^{-1} BFO or LFO and 100 mg L^{-1} MTBE or ETBE. Reaction was started by adding 5 g L^{-1} of H_2O_2 and placed on a heater with magnetic stirrer. The pH value of reaction suspensions was regulated by adding 0.1 M NaOH or 0.1 M HCl.

For the isotope fractionation measurements representative samples were filtered through 0.22 μm PTFE filters into 5 mL vials containing sodium thiosulphate for stopping the reaction. The samples were kept in a freezer at -20 °C until the analysis of the isotope composition was conducted. Carbon and hydrogen stable isotope compositions of the MTBE and ETBE were measured using a gas chromatography-combustion-isotope ratio monitoring mass spectrometry system (GC-C-IRM-MS) described in [1].

Fig. S1. Kinetics of phenol oxidation measured at various initial H_2O_2 concentrations for a) LFO and b) BFO: ▲ 10 g L^{-1}, □ 3 g L^{-1}, × 1 g L^{-1} H_2O_2 (c_{cat} = 0.1 g L^{-1}, $c_{0,phenol}$ = 25 mg L^{-1}, pH = 7.0 ± 0.2).
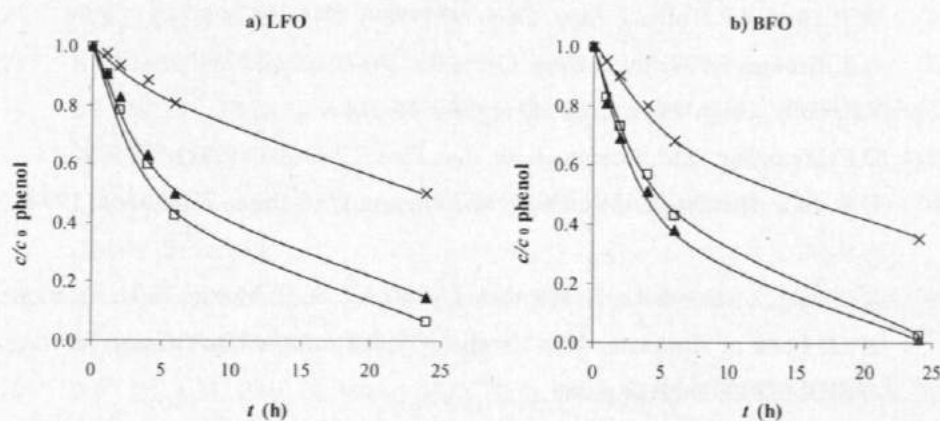
Fig. S2. Arrhenius plot: effect of the reaction temperature (20-60 °C) on the rate constant (k') of phenol degradation with LFO (□) and BFO (▲) ($c_{cat} = 0.1$ g L^{-1}, $c_{0,H2O2} = 3$ g L^{-1}, $c_{0,phenol} = 25$ mg L^{-1}, pH = 7.0 ± 0.2).
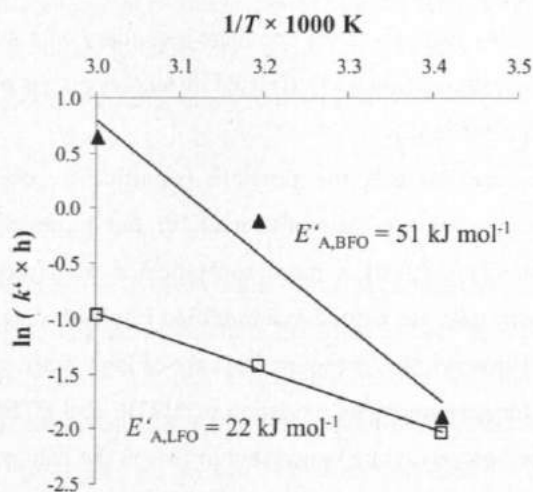
Fig. S3. Kinetics of phenol degradation in presence of the leachate (obtained after 24 h leaching of 1 g L^{-1} LFO) with freshly added LFO (○) and in a reference experiment in deionized water with freshly added LFO (●) ($c_{cat} = 0.1$ g L^{-1}, $c_{0,H2O2} = 3$ g L^{-1}, $c_{0,phenol} = 25$ mg L^{-1}, pH = 7.0 ± 0.2).
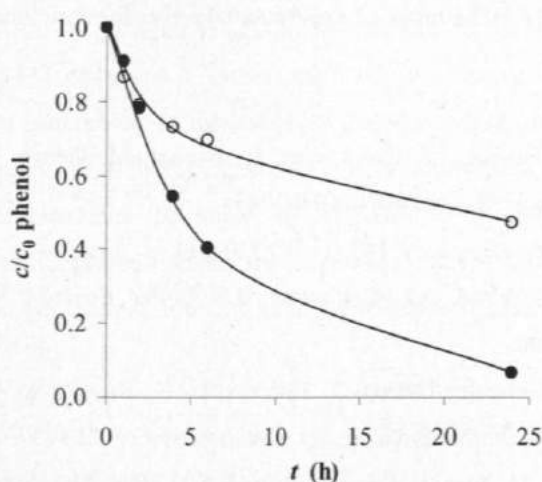
Further discussion of approximations applied for determination of apparent kinetic isotopes effects (*AKIEs*)

Applying Eq. 11 (introduced in the manuscript) for calculation of $AKIE_H$ from $\varepsilon_{bulk,H}$ includes the following approximations:

I) It is assumed that primary isotope effects dominate secondary ones such that the latter can be neglected. This approximation was validated by studies on gas phase reactions of alkanes with •OH as reported in [2].

II) The applied procedure neglects the possible (significant) 'overenrichment' of deuterium in the reactive position of a molecule in the presence of nonreactive positions. Elsner et al. [3] suggests a more sophisticated transformation procedure where the original isotope data are plotted in a modified Rayleigh diagram using $\varepsilon_{reactive\ position}$ rather than ε_{bulk}. However, this is required in case of large fractionation effects (as for instance observed for permanganate oxidation of MTBE and ETBE). Applying the more precise transformation procedure (suggested in [3]) to the data reported in [4] did not significantly alter the resulting $AKIE_H$ values compared to those obtained by applying Eq. 11 and reported here.

III) A uniform intramolecular isotope distribution in the initial substrates is assumed. McKelvie et al. [5] analyzed MTBE samples from various sources by means of quantitative site-specific ^{2}H-NMR spectroscopy. They revealed a significant depletion of ^{2}H in the methoxy group ($\delta^2H = -135 \pm 36$‰) compared to the tertiary butyl group ($\delta^2H = -92 \pm 14$‰). This affects the ε_{bulk} value in Eq. 9 (our original paper) by a factor of 1.037 which is usually in the range of experimental errors for enrichment factors.

References

[1]   M. Rosell, D. Barcelo, T. Rohwerder, U. Breuer, M. Gehre, H.H. Richnow, *Environ. Sci. Technol.* 41 (2007) 2036-2043.

[2]   F.P. Tully, *Chem. Phys. Lett.* 143 (1988) 510-514.

[3]   M. Elsner, J. Mckelvie, G.L. Couloume, B.S. Lollar, *Environ. Sci. Technol.* 41 (2007) 5693-5700.

[4]   M. Rosell, R. Gonzalez-Olmos, T. Rohwerder, K. Rusevova, A. Georgi, F.D. Kopinke, H.H. Richnow, *Environ. Sci. Technol.* 46 (2012) 4757-4766.

[5]   J.R. McKelvie, M. Elsner, A.J. Simpson, B.S. Lollar, M.J. Simpson, *Environ. Sci. Technol.* 44 (2010) 1062-1068.

7. Critical evaluation of the 2D-CSIA scheme for distinguishing fuel oxygenate degradation reaction mechanisms

Mònica Rosell, Rafael González-Olmos, Thore Rohwerder, Klara Rusevova, Anett Georgi, Frank-Dieter Kopinke and Hans H. Richnow

Abstract

Although the uniform initial hydroxylation of methyl *tert*-butyl ether (MTBE) and other oxygenates during aerobic biodegradation has already been proven by molecular tools, variations in carbon and hydrogen enrichment factors (ε_C and ε_H) have still been associated with different reaction mechanisms (McKelvie et al. *Environ. Sci. Technol.* 2009, *43*, 2793-2799). Here, we present new laboratory-derived ε_C and ε_H data on the initial degradation mechanisms of MTBE, ethyl *tert*-butyl ether (ETBE) and *tert*-amyl methyl ether (TAME) by chemical oxidation (permanganate, Fenton reagents), acid hydrolysis and aerobic bacteria cultures (species of *Aquincola*, *Methylibium*, *Gordonia*, *Mycobacterium*, *Pseudomonas* and *Rhodococcus*). Plotting of $\Delta\delta^2$H/ $\Delta\delta^{13}$C data from chemical oxidation and hydrolysis of ethers resulted in slopes (Λ values) of 22 ± 4 and between 6 and 12, respectively. With *A. tertiaricarbonis* L108, *R. zopfii* IFP 2005 and *Gordonia* sp. IFP 2009, ε_C was low ($<|-1|$‰) and ε_H insignificant. Fractionation obtained with *P. putida* GPo1 was similar to acid hydrolysis and *M. austroafricanum* JOB5 and *R. ruber* DSM 7511 displayed Λ values previously only ascribed to anaerobic attack. The fractionation patterns rather correlate with the employment of different P450, AlkB and other monooxygenases, likely catalyzing ether hydroxylation via different transition states. Our data questions the value of 2D-CSIA for a simple distinguishing of oxygenate biotransformation mechanisms, therefore caution and complementary tools are needed for proper interpretation of groundwater plumes at field sites.

1. Introduction

Fuel oxygenates have been providing added value to the petrol industry for decades. Methyl *tert*-butyl ether (MTBE) has been used since the 1970's as gasoline additive due to its high octane number and its oxygen content which led to a reduction in emissions of exhaust pollutants. Today, in the era of climate change concerns and renewable energy ambitions, fuel oxygenates still play a major role. Since 2003, due to the promotion of the use of biofuels through tax incentives (Directive 2003/30/EC), some European MTBE refiners converted their plants to synthesize ethyl *tert*-butyl ether (ETBE) using bio-ethanol from agricultural feedstocks. Moreover, the new EU Renewable Energy Directive (2009/28/EC) contemplates the feasibility of bio-MTBE production using bio-methanol based on crude glycerin, a waste product from biodiesel production [1]. Overall, the estimated current annual production capacity of fuel ethers in Europe is approximately 6 million tones, split between almost 70 production plants and these compounds make up about 4% of the gasoline supply [2]. Despite the promotion of best practices for handling fuel ethers, their widespread use in gasoline caused contamination of groundwater tables worldwide [3, 4]. Similar to MTBE, ETBE and *tert*-amyl methyl ether (TAME) showed recently to cause odor and flavor problems making water sources unpalatable at very low concentrations (ETBE with 1–2 µg/L and MTBE and TAME from 7 to 16 µg/L) [5]. Mainly due to these public concerns, fuel oxygenate ethers are now partially or absolutely banned in some states of USA and substituted by ethanol [6]. However, drinking water resources will be threatened for a long time, as fuel oxygenates are recalcitrant to microbial attack particularly by the limited concentrations of oxygen typically found in fuel-contaminated aquifers [7].

In that respect, reliable methods for detecting *in situ* fuel oxygenates biodegradation and insights into the functioning of the responsible microorganisms are crucial for improving remediation technologies based on the activities of such degrading microorganisms. In recent years, compound-specific stable isotope analysis (CSIA) has been used as an important tool for monitoring biodegradation of organic contaminants in environmental systems [8, 9] and for characterizing the initial reaction mechanisms [10]. The reaction-dependent compound-specific isotope enrichment factors (ε) can be quantified using a modified form of the Rayleigh distillation equation under defined laboratory conditions [11] and converted to the apparent kinetic isotope effect (AKIE) to obtain information on the transition state of the bond cleavage reaction. The kinetic

isotope effect (KIE) allows obtaining information on rate limitation and bond change of enzymatic reactions [12]. In environmental studies, isotope fractionation is used to characterize environmental processes and to predict reaction mechanisms, however, recent results on the diversity of isotopic fractionation during bacterial fuel oxygenate degradation question whether the extent of fractionation can be used to identify specific metabolic reactions [13].

The aerobic microbial MTBE degradation is initiated by a hydroxylation of the methyl group of the ether by a monooxygenase catalyzed reaction [14] and the breaking of the C-H bond would be expected to lead to similar carbon and hydrogen isotope effects. However, there are three different clusters of isotopic fractionation patterns found for aerobic MTBE degradation: (i) high fractionation of carbon and hydrogen was observed for *Methylibium* strains PM1 and R8 with ε_C and ε_H ranging from -2.0 to -2.4‰ and -33 to -40‰, respectively; (ii) similar carbon but higher hydrogen fractionation ($\varepsilon_H = -100‰$) was discovered for *Pseudonocardia tetrahydrofuranoxydans* K1; (iii) whereas much lower carbon fractionation ($\varepsilon_C \leq |-0.5|‰$) and practically non-detectable hydrogen fractionation was observed for *Aquincola tertiaricarbonis* L108 and *Rhodococcus ruber* IFP 2001 [13, 15, 16]. Although this diversity in observed isotope effects questions the uniform hydroxylation step, studies on knockout mutants have clearly proven the involvement of monooxygenases in the initial attack of MTBE in the high-fractionating strain PM1 [17] and in the low-fractionating strains L108 and IFP 2001 [18, 19]. Therefore, low fractionation is likely associated with more efficient C-H bond breaking combined with rate determining non-fractionating steps involved in typically multistep processes of enzymatically catalyzed hydroxylation, thus masking the intrinsic isotope effect. However, as this suppression should equally affect isotopic fractionation of both elements, two-dimensional (2D)-CSIA graphs are thought to cancel these effects (when a reaction is committed to catalysis and become irreversible) and the ratio of hydrogen to carbon isotope fractionation should be able to distinguish between hydroxylation and other enzymatic reactions [10]. Considering analytical errors for determining low ε_H values, the fractionation observed with strains L108 and IFP 2001 may indeed give a similar slope as observed with strains PM1 and R8. However, it is clear that the two-dimensional scheme is not really applicable for very low isotopic fractionation. The different slopes (Λ) found for strain K1 ($\Lambda = 48$) vs. *Methylibium* spp. ($\Lambda = 18$) would lead to question the generally accepted assumption of a uniform hydroxylation

mechanism for aerobic bacteria. Although the authors considered the high hydrogen enrichment factor of strain K1 consistent with the one they previously measured for abiotic oxidation of MTBE by permanganate (ε_H = -109‰), no information about ε_C or Λ was provided [20]. It is not clear, therefore, how a mechanism can be predicted for aerobic ether-degrading bacteria against alternative reaction mechanisms, such as the acid hydrolysis S_N1 (Λ = 11) and hydrolysis by (enzymatic) nucleophilic attack S_N2 suggested for the anaerobic degradation pathway (Λ = 1.2) [21]. In addition, the wide variability of enrichment factors ε_C from -0.37 to -2.29‰ and ε_H from <|-5| to -66‰ as well as Λ values in the range from 12 to 45 found in several aerobic mixed cultures from contaminated sites suggest the coexistence and activity of all the described degradation mechanisms within environmental microbial communities [15, 22-26]. These findings seriously complicate evaluation of *in situ* biodegradation of MTBE and other fuel oxygenates by 2D-CSIA. Therefore, additional studies are needed to elucidate how CSIA could be used for assessing fuel oxygenate biodegradation at groundwater contaminated sites.

Although there are isotope fractionation data for MTBE, there are few studies with ETBE and TAME. Therefore knowledge on the variability of isotopic fractionation among abiotic and biotic processes is needed for a proper evaluation of fuel oxygenate biodegradation employing CSIA for characterizing potentially contaminated sites in the future. For that purpose, we performed systematic work with a total of 10 pure strains (six of them were never tested before for isotopic fractionation studies) including *Aquincola*, *Methylibium*, *Gordonia*, *Mycobacterium*, *Pseudomonas* and *Rhodococcus* species which are able to grow aerobically on or cometabolically degrade MTBE, ETBE or TAME and compared their isotopic patterns with the results obtained in abiotic chemical oxidation experiments (permanganate vs. Fenton with $Fe^{2+/3+}$ and H_2O_2) as well as acid hydrolysis (HCl) in order to better understand their enzymatic mechanisms. Moreover, the present results could be useful to evaluate whether Fenton-like transformation of fuel oxygenates produces a significant isotopic fractionation pattern that can be used to monitor *in situ* chemical oxidation (ISCO), and to determine whether this pattern can be used to differentiate between biotic and abiotic transformation at a field site.

2. Materials and Methods

2.1. Chemicals

All the chemicals and organic solvents were either purchased from Sigma-Aldrich (Munich, Germany) or Merck (Darmstadt, Germany) at analytical grade quality.

2.2. Abiotic oxidation reactions

Stoichiometric Fenton (with Fe^{2+}) and catalytic Fenton-like (with Fe^{3+}) reactions were carried out at $22 \pm 2°C$ in 100-mL reactors, covered with foil paper in order to avoid photo-reactions, at pH 3 using solutions of $FeSO_4 \cdot 7\ H_2O$ or $Fe(NO_3)_3$, respectively, to oxidize 100 mg/L of each fuel oxygenate. In the stoichiometric Fenton reaction, equimolar concentrations of Fe^{2+} and H_2O_2 were used (10 mM of each). In order to avoid quenching of hydroxyl radicals by excess H_2O_2, H_2O_2 was added stepwise (1 mM each 5 min). In the catalytic Fenton-like reaction, an excess of H_2O_2 with respect to Fe^{3+} was used (0.03 mM Fe^{3+}; 100 mM H_2O_2). Permanganate oxidation reaction was also carried out at $22 \pm 2°C$ in 100-mL reactors using a solution of 0.11 M of $KMnO_4$ to oxidize 250 mg/L of each fuel oxygenate. All the oxidation experiments were carried out with an individual fuel oxygenate compound, except one experiment with permanganate which was done with a mixture of 100 mg/L of MTBE and ETBE. For sampling, always 2-mL aliquots were taken in 5-mL vials over time. Sodium thiosulfate was added in order to stop the reaction (200 mM). Afterwards, the concentration of MTBE and ETBE was determined (see below). Samples were kept in the freezer at -20 °C before analysis of isotopic fractionation. In addition, heterogeneous Fenton-like reactions with orthoferrites such as $BiFeO_3$ and $LaFeO_3$ in the presence of H_2O_2 at neutral pH and $22 \pm 2°C$ were tested for MTBE and ETBE and can be found in the Supporting Information (SI).

2.3. Acid hydrolysis experiments

Hydrolysis was conducted in 100-mL serum bottles sealed with butyl rubber stoppers and incubated on a shaker at 30°C. The reaction was started by adding 100 μL of each pure fuel oxygenate to 100 mL of different dilutions of HCl (1, 3 or 5 M prepared from a Combi-Titrisol® 5M HCl, Merck, Darmstadt, Germany). At each sampling event, 3-mL aliquots were removed with a syringe and each 1-mL subsample was transferred into 20-mL headspace vials for duplicate headspace GC analysis [27] or one 10-mL vial

for the stable isotope analysis, all of them containing 1 mL of the corresponding molarity of NaOH and cooled on ice to avoid losses during neutralization. Such a procedure served to quench the reaction and ensured that samples were free of volatile corrosive compounds.

2.4. Bacterial strains and cultivation conditions

Aquincola tertiaricarbonis L108 [28, 29] and *Methylibium* sp. R8 [16] were obtained from the strain collection of the UFZ department of Environmental Microbiology. *Methylibium petroleiphilum* PM1 [30, 31] were purchased from the American Type Culture Collection (ATCC BAA-1232). *Mycobacterium austroafricanum* IFP 2012, *Rhodococcus zopfii* IFP 2005, *Gordonia* sp. IFP 2009 and *Rhodococcus ruber* IFP 2001 were provided by F. Fayolle-Guichard (IFP Energies nouvelles, France). *Rhodococcus ruber* DSM 7511 was obtained from the German Collection of Microorganisms and Cell Cultures (DSMZ) and *Mycobacterium austroafricanum* JOB5 and *Pseudomonas putida* GPo1 from the collection of Institute Pasteur (CIP 105723 and CIP 105816, respectively). In general, the bacteria were grown in 1-L glass bottles filled with about 25% (v/v) mineral medium as described elsewhere [32] ensuring oxic conditions, 10% of inoculum (v/v) and appropriate growth substrate/s (see details in SI Table S1) on a rotary shaker at 30°C. After 5 days, cells were harvested by centrifugation (8500 rpm, 10 min at 4°C), washed with mineral salt solution and suspended at a high density. For resting-cell experiments, 60 mL of cell suspension were placed in 240-mL serum bottles, supplemented with vitamins and cobalt as for growing, 10-20 μL of each fuel oxygenate (MTBE, ETBE or TAME) and if necessary additional substrates for cometabolic degradation or enzyme inducers (see SI Table S1), closed immediately with butyl rubber stoppers and incubated as above. Control bottles were always prepared in parallel and were monitored for substrate concentrations and isotopic composition in order to evaluate abiotic losses or cross-contamination. Samples for substrate concentration, isotopic composition and pH were taken periodically according to Rosell et al. [27] until complete degradation (when possible).

2.5. Analytical methods

Monitoring of concentrations (fuel oxygenates and corresponding main degradation products) was performed using a headspace-gas chromatography system with flame

ionization detector (HS-GC-FID) as described elsewhere [27] except for the chemical oxidation experiments where a mass spectrometer was used as detector [33]. Carbon and hydrogen stable isotopic composition of the fuel oxygenates were measured in all cases using gas chromatography-combustion-isotope ratio monitoring mass spectrometry systems (GC-C-IRM-MS) described in our previous work [16]. A Zebron ZB1 column (60 m length x 0.32 mm ID x 1 μm film thickness; Phenomenex, Aschaffenburg, Germany) was used for separation. Each sample was analyzed via headspace sampling in triplicate.

2.6. Stable isotope definitions and calculations

Carbon and hydrogen isotopic compositions are reported as $\delta^{13}C$ and δ^2H values in parts per thousand (‰) relative to Vienna Pee Dee Belemnite standard (V-PDB) and Vienna Standard Mean Ocean Water (V-SMOW), respectively

$$\delta[\text{‰}] = \left(\frac{R_{sample}}{R_{reference}} - 1 \right) \times 1000 \tag{1}$$

where R_{sample} and $R_{reference}$ are the atomic ratios of the heavy isotope to the light isotope ($^{13}C/^{12}C$ or $^2H/^1H$) in the sample and the international standard, respectively. A simplified Rayleigh equation for a closed system [11] was used to quantify the isotopic fractionation,

$$\ln\left(\frac{R_t}{R_0} \right) = \frac{\varepsilon}{1000} \cdot \ln\left(\frac{C_t}{C_0} \right) \tag{2}$$

where the isotopic enrichment factor (ε) describes the relationship between changes in isotopic composition $R_t/R_0 = (\delta_t + 1000)/(\delta_0 + 1000)$ and the concentrations during the course of the experiment. When possible, 2D-CSIA was applied to the data sets. To correct for differences in the initial isotopic composition ($\delta^{13}C_0$ and δ^2H_0) of MTBE, isotopic shifts for hydrogen ($\Delta\delta^2H$) and carbon ($\Delta\delta^{13}C$) were calculated by subtracting the isotopic signature at time t from the initial value ($\Delta\delta = \delta_t - \delta_0$). The slope of a linear regression of $\Delta\delta^2H$ vs. $\Delta\delta^{13}C$ describes the relationship between carbon and hydrogen fractionation (Λ).

$$\varLambda = \frac{\Delta\delta^2 H}{\Delta\delta^{13}C} \approx \frac{\varepsilon_H}{\varepsilon_C} \tag{3}$$

Each sample was measured at least in triplicate and all linear regression parameters including the 95% confidence intervals (CI) were obtained by the function "Linear Fit" using errors (standard deviation of measured data sets or corresponding propagated errors in both axes) as weight in OriginPro® 7.5.

3. Results

3.1. Chemical oxidation of MTBE and ETBE

By means of the stoichiometric Fenton reaction (10 mM Fe^{2+} and stepwise addition of 10 mM of $H_2\dot{O}_2$) $\geq$ 99% removal of MTBE and ETBE was achieved in less than 1 h (See SI Figure S1). The catalytic Fenton-like reaction (initiated with 0.03 mM Fe^{3+} and 100 mM H_2O_2) resulted in slower degradation of MTBE and ETBE (> 20 h required for $\geq$ 95% removal). ETBE reacts slightly faster than MTBE in both reaction systems. Fitting of the fuel oxygenate oxidation by pseudo-first order kinetics gives a ratio of the rate constants between MTBE and ETBE of 0.68 and 0.56 for the Fenton and Fenton-like reactions, respectively. This is in good agreement with the ratio of 0.59 previously reported with OH-radicals [34]. In the reactions with permanganate, the removal of fuel oxygenates followed pseudo-first order kinetics (for 3 experiments R^2 = 0.93-0.995). The half-lives for MTBE and ETBE were 17.8 h and 0.81 h, respectively (see SI Figure S1). The ratio of the rate constants is 0.046. Permanganate selectively oxidizes the carbon atom adjacent to the ether bond under formation of an ester, whereby H-abstraction is the first step. In general, MnO_4^- has a higher reactivity with primary alkyl than with methyl carbon atoms in ethers [35, 36]. Thus ETBE is expected to degrade faster than MTBE, which is confirmed by our results.

The Rayleigh approach (equation 2) was applied to quantify the isotopic fractionation. The highest MTBE carbon and hydrogen isotopic fractionation during chemical oxidation of $\Delta\delta^{13}C$ = (15.6 ± 0.1)‰ and $\Delta\delta^2 H$ = (387 ± 7)‰ was observed after 94% conversion by permanganate corresponding to ε_C and ε_H values of (-5.53 ± 0.04)‰ and (-109 ± 4)‰, respectively (see Table 1). In contrast, lower MTBE carbon and hydrogen isotopic fractionation was detected during the Fenton and Fenton-like oxidation

reactions. Low values for the kinetic deuterium isotope effect (KDIE) in the range of 1.06 to 1.08 have been also reported for other reactions where H-abstraction from aliphatic carbon by hydroxyl radicals is considered as the predominant degradation pathway [37, 38]. In our study, no significant differences were found between ε_C (-1.2 ± 0.2)‰ vs. (-1.4 ± 0.1)‰ and ε_H (-29 ± 6)‰ vs. (-31 ± 9)‰ values obtained when using Fe^{2+} or Fe^{3+}, respectively. Moreover, when plotting the respective $\Delta\delta^2H$ vs. $\Delta\delta^{13}C$ values (equation 3) for the three tested oxidation reactions, comparable 2D-CSIA slopes, Λ, were obtained fitting into a range between 20 and 25 (mean Λ of 22 ± 4 for MTBE oxidation, $R^2 = 0.94$, n = 43, see Figure 1). Independently of the different reaction rates, analogous isotopic enrichment factors were found for MTBE and ETBE during each type of oxidation. A similar mean Λ of 23 ± 2 was also calculated for ETBE oxidation with a good correlation ($R^2 = 0.9$) when plotting all the values together (n = 11, Figure S2 in SI). Comparable results were also obtained when using orthoferrites as solid catalysts (see Table S2 in SI).

3.2. Acid hydrolysis of fuel oxygenates

Dissolved fuel oxygenate concentrations decreased exponentially with time in the eight batch experiments ($R^2 = 0.82$-0.9997) obtaining in all cases concomitant accumulation of main degradation products *tert*-butyl alcohol (TBA) and *tert*-amyl alcohol (TAA) from 46 to 94% of its parental compound (see SI Figure S2). At 30°C and in the presence of 5 M HCl, MTBE was hydrolyzed with a half-life of 0.64 h, whereas ETBE and TAME reacted even faster (0.35 and 0.03 h, respectively). In order to lower the hydrolysis rates for better monitoring of the reactions, further experiments were performed with lower HCl concentrations (3M and 1M). In this way, the half-life of MTBE at 1M HCl increased to 34 h, while ETBE and TAME required 17 and 8.5 h, respectively. For the three compounds, degradation >99% was achieved (see Table 1). Pronounced MTBE carbon and hydrogen isotopic fractionation of $\Delta\delta^{13}C = (28.58 ± 0.05)$‰ and $\Delta\delta^2H = (106 ± 12)$‰ was observed after 99.3% and 92% conversion, respectively, which corresponded to ε_C value of (-6.05 ± 0.03)‰ and ε_H value of (-43 ± 4)‰, when combining all data points (see Table 1). The data fitted the Rayleigh-type linear fractionation model with R^2 of 0.997 and 0.99, respectively, indicating that no significant difference in isotopic fractionation was detected at different acid concentrations. The corresponding 2D-CSIA slope, Λ, was 6.2 ± 0.5 ($R^2 = 0.997$)

(equation 3). However, values closer to those previously published for MTBE were obtained for ETBE and TAME (see more details in Table 1) with Λ of 9.0 ± 0.3 ($R^2 = 0.99$) and 11.5 ± 0.2 ($R^2 = 0.999$), respectively.

Table 1. Comparison of fuel oxygenates carbon and hydrogen isotopic enrichment factors (ε) and 2-D CSIA slopes (Λ) caused by different chemical oxidation reactions and acid hydrolysis experiments. When possible the respective 95% confidence intervals (± 95% CI) are provided.

Reaction	Target	ε_C [‰]	±95% CI [‰]	R^2	D [%]	N	ε_H [‰]	±95% CI [‰]	R^2	D [%]	N	Λ ± 95% CI	ref.
Chemical oxidation													
Oxidation by permanganate (n=1)	MTBE	?					-109	9	0.98	90	16	?	20
(n=3)	MTBE	-5.53	0.04	0.98	94	24	-109	4	0.92	94	24	20.1 ± 0.5	this study
(n=2)	ETBE	-5.2	0.1	0.996	99	6	-128	24	0.97	97	5	24 ± 4	this study
Oxidation Fenton (Fe^{2+}) (n=2)	MTBE	-1.2	0.2	0.90	99.1	11	-29	6	0.92	71	9	22 ± 4	this study
(n=1)	ETBE	-0.6	0.2	0.996	95	4	-18	-	0.82	66	3	23	this study
Oxidation Fenton (Fe^{3+}) (n=2)	MTBE	-1.4	0.1	0.95	97	12	-31	9	0.74	85	10	25 ± 5	this study
(n=1)	ETBE	-1.1	0.1	0.998	98	5	-18	-	1.00	92	3	17	this study
Acid hydrolysis (S_N1)													
2M HCl	MTBE	-4.9	0.6	0.995	88	6	-55	7	0.99	88	6	11 ± 1	20
5M (n=1) and 1M HCl (n=1)	MTBE	-6.05	0.03	0.997	99.3	17	-43	4	0.99	92	12	6.2 ± 0.5	this study
5M (n=1), 3M (n=1) and 1M HCl (n=1)	ETBE	-5.1	0.1	0.99	99	14	-47	2	0.96	99	14	9.0 ± 0.3	this study
5M (n=1), 3M (n=1) and 1M HCl (n=1)	TAME	-5.48	0.08	0.997	99	12	-66	2	0.8	97	9	11.5 ± 0.2	this study

n: number of experiments, N: number of data points; na: not analyzed or not applicable; ns: not significant; CI is 95% Confidence Interval; D%: maximum percentage of substrate initial/partial degradation (do not confuse with complete mineralization to CO_2) which could be analyzed for the corresponding isotopic composition taking into account different detection limits for carbon and hydrogen.
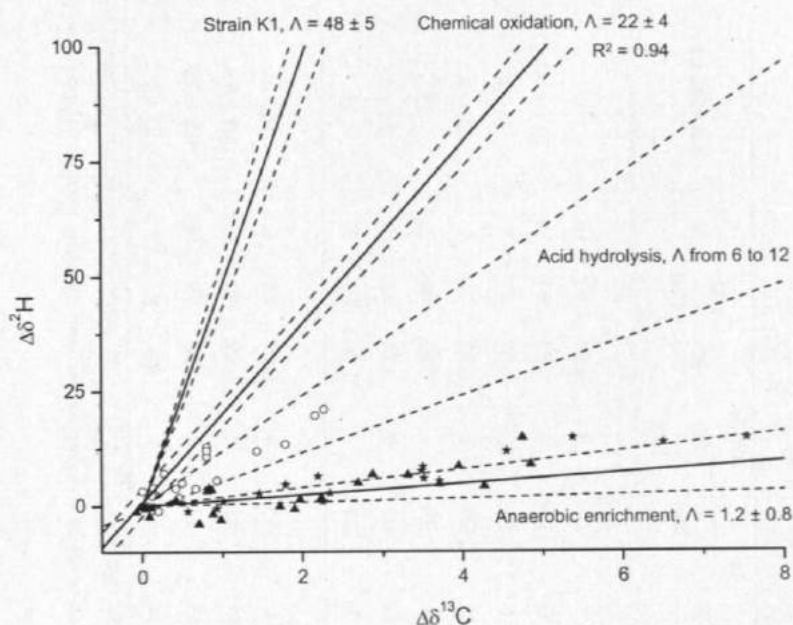
Figure 1. MTBE two dimensional plot of hydrogen versus carbon isotopic shifts for the so far discovered initial reaction mechanisms including (i) the mean slope (Λ value) for chemical oxidation (by plotting together permanganate and the two Fenton reactions in this study), (ii) the acid hydrolysis (S_N1-type, Λ range according to Elsner et al. [20] and our study), (iii) the S_N2-type hydrolysis suggested for an anaerobic enrichment culture [20, 21] although a $\Lambda = 6$ has been also reported for an anaerobic enrichment culture when adding syringic acid as co-substrate [25] (not shown) and (iv) the isotopic pattern discovered for strain K1 [13]. Linear regression curves (solid lines) allow comparison within the 95% confidence intervals (CI) (dashed lines). Measured values for strains GPo1 (circles), JOB5 (triangles) and DSM 7511 (stars) are shown. Previously studied strains PM1 and R8 fit to the chemical oxidation pattern (not shown) [15, 16]. Due to not measurable hydrogen fractionation, strains L108, IFP 2001 [16] and IFP 2012 are not shown.

3.3. Aerobic biodegradation of fuel oxygenates

In growing and resting-cell experiments with *A. tertiaricarbonis* L108, TAME was completely degraded without TAA accumulation and with low carbon fractionation of $\varepsilon_C = (-0.4 \pm 0.1)$‰. Hydrogen fractionation was too low to be detectable with our methods. With *R. zopfii* IFP 2005 and *Gordonia* sp. IFP 2009, cometabolic MTBE and TAME degradation did not reach more than 30% after 2 weeks which was insufficient for determining isotopic fractionation. In contrast, ETBE degradation required only some hours. Both strains accumulated the ether metabolites TBA and TAA stoichiometrically. The ETBE carbon fractionation was low with $\varepsilon_C = (-0.4 \pm 0.1)$‰ and (-0.62 ± 0.03)‰ for strains IFP 2005 and IFP 2009, respectively, and no significant ^{2}H enrichment was detected. The two *Methylibium* strains PM1 and R8 could grow on TAME and displayed identical carbon fractionation of $\varepsilon_C = (-1.9 \pm 0.1)$‰. For two of the four batch experiments with strain PM1, the hydrogen fractionation was measured resulting in ε_H of (-52 ± 2)‰ and Λ of 25 ± 1 ($R^2 = 0.86$).

With *P. putida* GPo1, it was difficult to reach high degrees of degradation for MTBE and TAME (ETBE was not tested due to known low rates [39]). The best results were obtained after (i) growing the cells on glucose with dicyclopropylketone (DCPK) (the alternative growing substrate n-octane was difficult to wash out and inhibited temporarily fuel oxygenate degradation), (ii) several additions of glucose during the resting-cell experiments and (iii) the use of larger bottles (500 mL) for increasing the headspace volume and thus the oxygen supply. Under these conditions, the maximum degradation for MTBE and TAME reached 80 and 59%, respectively, along with the corresponding stoichiometric accumulation of TBA and TAA (*tert*-butyl formate, TBF, was not detected). A new MTBE fractionation pattern was discovered with intermediate carbon fractionation of $\varepsilon_C = (-1.4 \pm 0.1)$‰ and low hydrogen fractionation of $\varepsilon_H = (-11 \pm 2)$‰ resulting in a distinct Λ of 8 ± 1 ($R^2 = 0.85$). For TAME, the values were found in the same order of magnitude (see Table 2 for details).

Table 2. Carbon and hydrogen isotopic enrichment factors (ε) of fuel oxygenates and 2-D CSIA slopes (Λ) during biodegradation by aerobic pure strains grouped due to similar isotopic fractionation pattern. When possible the respective 95% confidence intervals (± 95% CI) are provided.

Strain	Target	ε_C [‰]	±95% CI [‰]	R^2	D [%]	N	ε_H [‰]	±95% CI [‰]	R^2	D [%]	N	Λ ± 95% CI	ref.
Aquincola tertiaricarbonis L108[*]	MTBE	-0.48	0.05	0.94	96	34	ns (-0.2)	8	0.00	82	29	na	16
	ETBE	-0.67	0.04	0.93	98.9	69	-11.4	0.6	0.7	99.7	74	14 ± 1	16
(n=1)	TAME	-0.4	0.1	0.9	98	11	ns (+5)	11	0.5	94	7	na	this study
Rhodococcus ruber IFP 2001[*]	MTBE	-0.28	0.06	0.81	97	27	ns (+5)	20	0.14	88	24	na	16
	ETBE	-0.8	0.2	0.96	98	23	-10	2	0.8	98	23	10 ± 3	16
Gordonia sp. IFP 2009 (n=3)	ETBE	-0.62	0.03	0.995	98	15	ns (-10)	11	0.2	93	9	na	this study
Rhodococcus zopfii IFP 2005 (n=2)	ETBE	-0.4	0.1	0.98	91	7	na					na	this study
Methylibium petroleiphilum PM1	MTBE	-2.0 to -2.4	0.1 to 0.3	0.88 to 0.98	93	39	-33 to -37	4 to 5	0.90 to 0.99	80 to 90	26	18 ± 3	10,15
(n=4)	TAME	-1.89	0.06	0.998	99	20	-52	2	0.9	91	10	25 ± 1	this study
Methylibium sp. R8[*]	MTBE	-2.3	0.1	0.98	98	40	-40	4	0.95	91	36	17 ± 1	16,24
(n=2)	TAME	-1.9	0.1	0.99	99	12	na					na	this study

Strain	Target	ε_C [‰]	±95% CI [‰]	R^2	D [%]	N	ε_H [‰]	±95% CI [‰]	R^2	D [%]	N	$\Lambda \pm 95\%$ CI	ref.
Pseudonocardia tetrahydrofuranoxydans K1 (n=5)	MTBE	-2.3	0.2	0.99	96	12	-100	10	0.99	92	11	48 ± 5	13
(n=3)	ETBE	-1.7	0.2	0.99		9	-73	7	0.97		5	49 ± 4	13
	TAME	-1.1	0.2	0.9	59	32	-18	5	0.9	59	17	13 ± 3	this study
Mycobacterium austroafricanum IFP 2012 (n=5)	MTBE	-2.64	0.08	0.96	96	52	ns (+1)	2	0.02	92	43	na	this study
(n=5)	TAME	-2.16	0.05	0.995	96	41	ns (-0.2)	6	0.2	95	27	na	this study
Mycobacterium austroafricanum JOB5 (n=3)	MTBE	-2.50	0.04	0.994	96	31	-4.2	0.9	0.6	86	24	1.7 ± 0.3	this study
(n=3)	TAME	-2.12	0.05	0.998	99	20	ns (+3)	2	0.5	97	18	na	this study
Rhodococcus ruber DSM7511 (n=4)	MTBE	-2.48	0.06	0.997	99	27	-7	3	0.86	95	22	2.4 ± 0.8	this study
(n=2)	ETBE	-1.5	0.1	0.98	95	20	-11	2	0.8	95	20	7 ± 1	this study
(n=3)	TAME	-2.01	0.08	0.995	99	27	ns (-3)	3	0.05	85	22	na	this study

n: number of experiments, N: number of data points; na: not analyzed or not applicable; ns: not significant; CI is 95% Confidence Interval; D%: maximum percentage of substrate initial/ partial degradation (do not confuse with complete mineralization to CO_2) which could be analyzed for the corresponding isotopic composition taking into account different detection limits for carbon and hydrogen.

*Original data was recalculated according to Rosell et al. [27] and in the case of several experiments (e.g. growing and resting cells), the data was combined.

With *M. austroafricanum* IFP 2012, degradation of the three fuel oxygenates was performed with TBA-grown resting cells. Although this strain is able to grow on MTBE, an inhibition of degradation at high concentration was observed by Francois et al. [40]. At an initial concentration of 480 μM (approx. 42 mg/L) when the degradation products (TBF and TBA) reached high concentrations, the MTBE degradation rate slowed down and stopped. Due to limited sensitivity of the isotope analysis, our resting-cells experiments were performed initially at MTBE concentrations 5 times higher (200 mg/L) compared to previous experiments [40]. We obtained a similar behavior and after 8 h when MTBE conversion was around 50%, TBF and TBA accumulated at about 4 and 44%, respectively, of initial parental concentration. At this point, the MTBE degradation slowed down and stopped at 66% after 9 days. Higher degradation levels were obtained in subsequent batch experiments by (i) reducing MTBE initial concentration to 100 mg/L (92% after the same incubation time) or/and (ii) adding acetate or glucose at 0.5 g/L at the beginning of the experiment (substantial reduction of experimental time and lower TBF concentrations). Comparable TAME degradation rates were observed under the same conditions whereas ETBE was always weakly degraded to a maximum 27% of the initial concentration. In all cases, the metabolites did not become degraded until the parental compound was almost depleted. In the case of the related strain *M. austroafricanum* JOB5, the fuel oxygenate degradation was strictly cometabolic in the presence of 0.5 g/L glucose. Although the main degradation products (TBA, TBF or TAA) were accumulated similarly to the experiment with strain IFP 2012; the degradation of TAME was around 5 times faster than of MTBE by strain JOB5. As with strains GPol and IFP 2012, ETBE was poorly degraded (4% in 50 days) and accompanied by TBA formation. Whereas the carbon isotopic fractionation of ε_C (-2.5 ± 0.1)‰ was similar to the values obtained with the *Methylibium* strains, the hydrogen isotopic fractionation was extremely low ($\varepsilon_H < |-5|‰$) leading to a very small Λ value when it was possible to calculate it ($\Lambda = 1.7 ± 0.3$ for strain JOB5, $R^2 = 0.6$). The same tendency was obtained for TAME degradation (see Table 2). Similar isotopic values were observed for *R. ruber* DSM 7511 during MTBE and TAME degradation. Strain DSM 7511 could not grow on ETBE, but it was able to degrade it completely in the presence of 0.5 g/L glucose.

4. Discussion

4.1. Chemical model reactions

MTBE hydrogen fractionation was observed for all oxidation reactions tested (by permanganate, Fenton and Fenton-like reagents). However, the highest ε_H values were obtained by permanganate, fitting exactly the fractionation reported by Elsner et al. [20] for the same reaction. Interestingly, we observed also significant carbon fractionation for the latter process, while ε_C values for the Fenton reactions were much lower. Although individual enrichment factors for permanganate vs. Fenton reactions were different, they all gave the same Λ value. It was suggested that permanganate performs selective oxidation of C-H bonds next to an ether group, whereas Fenton's reagent is known to oxidize C-H bonds in a less selective fashion [20, 35]. The ratio of the rate constants for OH-radical attack at the methyl and *tert*-butyl groups of MTBE was reported to be 3:2 [41]. However, by means of CSIA, the exact mechanism can not be distinguished. The similar fractionation pattern with ETBE may point to a similar mechanism of C-H bond cleavage upon these reactions. Moreover, the use of iron in different oxidation states and species ($Fe^{2+/3+}$ and solid Fe(III)-oxide) has an insignificant effect on the bulk isotope fractionation of the ethers and, therefore, it is not possible to distinguish between these reactions . This might be explained by the fact that hydroxyl radicals are the dominant reactive species in all of the tested Fenton reactions (see further discussion on ferryl species in the SI).

It is not evident why our results of the acid hydrolysis as a model for S_N1 reactions with various concentrations of HCl at 30°C were slightly different from those obtained by Elsner et al. [20] when using 2 M HCl at room temperature. However, the enrichment factors are in the same order of magnitude and differences of less than 1‰ (taking into account the 95% CI) might be attributed to lower precision obtained at a lower ether removal of 88%. Additional experiments are needed to understand the extent of variability associated with this reaction.

4.2. Bacterial isotopic fractionation challenges the simple use of the 2D-CSIA concept

The variability of carbon and hydrogen isotopic patterns observed during bacterial fuel ether degradation can only partially be explained by the chemical model reactions such as oxidation and hydrolysis (see Figure 1 as well as S2 and S3 in the SI). The MTBE

pattern observed for the two *Methylibium* spp. (strains PM1 and R8) correlates with the assumed oxidation of the methyl group. In addition, the low carbon and insignificant hydrogen fractionation obtained with strains IFP 2005 and 2009 may be interpreted by masking effects due to more efficient hydroxylation catalysis, as has already been assumed for MTBE and ETBE attack by strains L108 and IFP 2001 [26, 27]. In contrast, the isotopic pattern discovered for strain K1 with such a high Λ value cannot be explained by oxidation reactions such as by permanganate, as it was suggested previously by comparing only the hydrogen fractionation [20], or by any other chemical reaction tested. In addition, from a mechanistic point of view, the Λ value (8 ± 1) found for strain GPo1 would be interpreted as S_N1 hydrolysis reaction mechanism (Λ from 5.7 to 12) [20]. This tendency was also observed for TAME degradation (see Figure S3 in SI). However, by testing OCT plasmid-deficient variants, it has unambiguously been proven that strain GPo1 employs a non-heme diiron alkane hydroxylase of the AlkB-type for attacking ether oxygenates [39]. More serious, MTBE isotopic patterns obtained with the aerobic strains IFP 2012 and JOB5 exhibited a Λ value fitting to the obtained values of an anaerobic enrichment culture ($\Lambda = 1.2 \pm 0.8$) which was suggested to be an initial hydrolysis step via an S_N2 mechanism at the $H_3C\text{-}O$ group [20, 21]. However, the formation of TBF during MTBE degradation by these strains clearly indicates the activity of hydroxylases in the initial fuel ether attack. Further, the involvement of another AlkB-type monooxygenase has been suggested for strains IFP 2012 and JOB5 as well as in other mycobacterial strains [40, 42, 43]. Likewise puzzling is the fractionation observed with strain DSM 7511. While the MTBE Λ value fitted to the anaerobic pathway slope (but also to the aerobic strain JOB5, see Figure 1), for ETBE a behavior closer to the acid hydrolysis (see Figure S2 in SI) was observed, suggesting different enzymatic mechanisms for the initial attack of each ether by this strain.

4.3. Biochemistry of C-H bond cleavage and transition state considerations

Considering the substantial evidence collected for the uniform hydroxylation step in the initial attack of fuel ethers by aerobic bacterial strains [14], hydrolysis reactions or other oxygen-independent processes can be ruled out. Hence, the interpretation of isotopic fractionation patterns only by the 2D-CSIA scheme without taking the extent of isotope fractionation into account is obviously misleading. For example, the significant diversity of fuel ether-attacking hydroxylase enzymes documented thus far cannot be

ignored [14, 17, 44]. Consequently, accepting the well-known fact that different enzymes can catalyze identical reactions via different transition states (see recent review [45]) is a more straightforward explanation for the observed variability in isotopic fractionation.

The almost absence of isotopic fractionation observed for MTBE, ETBE and TAME degradation by strains L108, IFP 2001, IFP 2005 and IFP 2009 correlates well with the finding that in all these strains the P450 monooxygenase EthB is involved in the initial C-H bond breaking [19, 26, 46]. All four strains share EthB enzymes with nearly identical amino acid sequences, showing 98 to 99% identity. This high degree of similarity suggests nearly identical catalysis and substrate specificities allowing degradation of all ethers tested. Nevertheless, different transition states may still occur, as the interaction with the amino acid residues in the active site of the P450 enzymes likely vary for the different ether substrates. However, as C-H bond breaking is obviously not rate-limiting, the intrinsic isotope effects are nearly completely suppressed in all cases. Consequently, only slight variations in isotopic fractionation were observed.

Interpretation of the isotopic fractionation observed with strain K1 is more difficult. This strain [47] and the closely related strain *Pseudonocardia* sp. ENV478 [48] attack MTBE most likely by a four-component monooxygenase involved in degradation of tetrahydrofuran [13, 49], as only cells pre-grown on this cyclic ether compound show significant MTBE conversion to TBA. In addition, it has already been argued that the extremely high hydrogen fractionation found with strain K1 is consistent with the effects found for abiotic oxidation [13], supporting the involvement of a hydroxylation step. However, the published Λ value of about 50 is not reached by any of the tested oxidation reactions (Table 1). Hence, an effect simulating an "asymmetric masking" significantly affecting only the carbon isotopic fractionation must be postulated. Similar observations have been made with C-H bond breaking in the course of dehydrogenase reactions [50-52] and may suggest that chemical reactions should be taken with caution as a reference to predict mechanisms of enzymatic reactions. High deuterium fractionation was related to a transition state early in the reaction coordinate resembling more the substrate, while ^{13}C isotope effects were stronger in later transition states where the bond breaking is more advanced [50]. Therefore, an early transition state (maximum hydrogen but reduced carbon fractionation) might be the case for the catalysis of the hydroxylating enzymes involved in ether attack in strain K1. Interestingly, Λ values

obtained for ETBE and TAME with strain K1 were also close to 50, suggesting very similar transition states for all substrates.

Finally, we need a better understanding of the fractionation patterns observed with bacterial strains employing non-heme diiron alkane monooxygenases of the AlkB-type and possibly other types of hydroxylases. Strain PM1 uses the AlkB-type enzyme, MdpA, in the initial attack on MTBE [17]. This enzyme is also present in the closely related strain R8 and both strains show identical MdpA sequences [26]. In addition, both strains degrade MTBE with similar efficiency but are not able to attack ETBE [53]. Therefore, it is likely that MdpA is also involved in ether degradation in strain R8. Accordingly, the identical MTBE and TAME isotopic fractionation obtained for these strains would indicate similar transition states in MdpA catalysis in both strains. Potential masking of isotopic effects, if present, seem to affect equally carbon and hydrogen as Λ value fit the expected symmetric intrinsic isotopic effects of the C-H bond breaking. In contrast, totally different Λ values were obtained with the other strains where employment of AlkB-like monooxygenases has been suggested. This finding might be surprising at first glance, as all these enzymes belong to the same enzyme family and show significant sequence similarity including the four conserved motifs of iron-complexing histidine residues (see SI Figure S4). However, phylogenetic analysis has already revealed that MdpA, the AlkB from strain GPo1 and the mycobacterial enzymes form distinct groups [17, 54]. Particularly, amino acid residues of the second transmembrane domain directly interacting with the substrate deviate among the different AlkB enzymes [17, 55] (see TM helix 2 in SI Figure S4). Consequently, variations in substrate specificity are observed, as MdpA and the AlkB from strain GPo1 can only attack ethers, while the mycobacterial strains which likely also employ AlkB enzymes have a broader substrate spectrum including also the alcohols TBA and TAA. Highly likely, all these factors will influence transition state structure and, consequently, isotopic fractionation patterns. Significant differences between transition states have already been found for homologous enzymes with 87% sequence identity and 100% conserved catalytic sites [45]. In the case of fuel oxygenate degradation, with strains belonging to the same genus, i. e. *Methylibium*, *Pseudomonas* or *Mycobacterium*, similar fractionation patterns were obtained, indicating a correlation between functional and phylogenetic relationships. In this respect, it can be speculated whether the *Mycobacterium*-related Gram-positive strain DSM 7511 also employs the

mycobacterial AlkB enzyme for ether degradation, as isotopic fractionation for MTBE corresponds well with the values obtained with strains IFP 2012 and JOB5. The higher ETBE $\Lambda = 7 \pm 1$ for the *Rhodococcus* strain may indicate the presence of a P450 hydroxylase, as this fractionation is in the same range of magnitude than the one of strain IFP 2001 ($\Lambda = 10 \pm 3$). Indeed, a common feature of many alkane degraders is that they contain multiple alkane hydroxylases with overlapping substrate ranges [56]. In particular, a study with 27 alkyl ether utilizing rhodococci strains proved that 26 of them contained multiple alkB genes encoding non-heme iron alkane monooxygenases as well as diverse P450 systems [57]. Since involvement of other hydroxylating enzymes (including AlkB monooxygenases) cannot be ruled out for strains IFP 2012 and JOB5 [43], isotopic fractionation patterns could also be the result of catalysis by multiple hydroxylases. However, identical 2D-CSIA slopes obtained with the latter strains correlate with the exclusive use of a single AlkB enzyme. The slightly different Λ values observed with strain DSM 7511 may also correspond to minor changes in transition states of the same enzyme due to molecular size differences of MTBE and ETBE.

4.4. Recommendations for biodegradation evaluation

Our study clearly shows that the 2D-CSIA scheme on its own cannot distinguish between aerobic and anaerobic fuel oxygenate degradation pathways (as it was previously assumed by Zwank et al. [58]) or between biotic and abiotic degradation in the case of ISCO applications at contaminated field sites. Our finding rather questions whether previous studies reporting low Λ values were really caused by anaerobic degradation processes. For example, Van Breukelen et al. [59] has criticized the conclusions of Zwank et al. [58] showing that biodegradation at the target field site was unlikely exclusively associated with anaerobic degradation based on his improved 2D-CSIA interpretation. Kuder et al. [21] plotted together isotopic data from nine different contaminated sites close to gasoline stations in the USA ($\Lambda = 1.3$), but anoxic conditions were only proved by microcosm experiments from one of them. Recently, Kujawinski et al. [60]classified as aerobic and anaerobic different sections of the same MTBE/ TAME contamination plume based on (i) the dissolved oxygen values (above or under 1 mg/L respectively) and (ii) the slope of the 2D-CSIA plot. However, some oxic samples fell clearly into the previously assumed anaerobic trend and some bacteria can effectively

degrade MTBE below 0.5 mg/L of oxygen [27]. Although the detection of high carbon fractionation with ε_C values $\geq|-6|‰$ may still be indicative for anaerobic ether attack (see summary in Youngster et al. [25]), geochemical information e.g. redox conditions and availability of other electron acceptors now becomes crucial to validate interpretation of 2D-CSIA analysis. Further insights may be obtained in future studies when a third element (oxygen fractionation, $^{18}O/^{16}O$) is included in the CSIA concept. However, a routine methodology for the analysis of oxygen enrichment factors in bacterial degradation experiments and environmental aqueous samples by GC-C-IRMS has not been developed. More conveniently, 2D-CSIA should be applied together with molecular biological tools such as monitoring the expression of key enzymes [26, 61] or stable isotope probing approaches [24, 62] for a more reliable characterization of fuel oxygenate degradation. In addition, detection of key metabolites may be helpful. In this respect, it was recently discovered that strains PM1, R8 and L108 emit highly volatile alkenes during fuel oxygenate degradation [53]. As these compounds can easily be measured by simple GC devices, a further line of evidence on fuel ether biodegradation activities may be derived by analyzing gas samples from contaminated sites.

Acknowledgement

References

(1)   The European Fuel Oxygenates Association (EFOA) Technological developments. http://www.efoa.eu/en/markets/ether-market-drivers-and-future-developments/technological-developments.aspx (November 2011).

(2)   The European Fuel Oxygenates Association (EFOA) Ether Facts and Figures. http://www.efoa.eu/en/markets/ether-facts-and-figures.aspx (October 2011).

(3)   Rosell, M.; Lacorte, S.; Barcelo, D. Occurrence and Fate of MTBE in the Aquatic Environment Over the Last Decade. In *Fuel Oxygenates*, Barceló, D., Ed. Springer-Verlag: Berlin Heidelberg, Germany, 2007; Vol. 5, Part R, pp 31–55.

(4)   Fayolle-Guichard, F.; Durand, J.; Cheucle, M.; Rosell, M.; Michelland, R. J.; Tracol, J. P.; Le Roux, F.; Grundman, G.; Atteia, O.; Richnow, H. H.; Dumestre, A.; Benoit, Y. Study of an aquifer contaminated by ethyl tert-butyl ether (ETBE): site characterization and on-site bioremediation. *J. Hazard. Mater.* 2012, *201- 202*, 236– 243.

(5)   van Wezel, A.; Puijker, L.; Vink, C.; Versteegh, A.; de Voogt, P. Odour and flavour thresholds of gasoline additives (MTBE, ETBE and TAME) and their occurrence in Dutch drinking water collection areas. *Chemosphere* 2009, *76* (5), 672-676.

(6)   Weaver, J. W.; Exum, L. R.; Prieto, L. M. *Gasoline Composition Regulations Affecting LUST Sites*; EPA/600/R-10/001; Office of Research and Development, United States Environmental Protection Agency: Washington, DC, USA, January, 2010.

(7)   Müller, R. H.; Rohwerder, T.; Harms, H. Carbon conversion efficiency and limits of productive bacterial degradation of methyl tert-butyl ether and related compounds. *Appl. Environ. Microbiol.* 2007, *73* (6), 1783-1791.

(8)   Meckenstock, R. U.; Morasch, B.; Griebler, C.; Richnow, H. H. Stable isotope fractionation analysis as a tool to monitor biodegradation in contaminated aquifers. *J. Contam. Hydrol.* 2004, *75* (3-4), 215-255.

(9)   Schmidt, T. C.; Zwank, L.; Elsner, M.; Berg, M.; Meckenstock, R. U.; Haderlein, S. B. Compound-specific stable isotope analysis of organic

contaminants in natural environments: a critical review of the state of the art, prospects, and future challenges. *Anal. Bioanal. Chem.* 2004, *378* (2), 283-300.

(10) Elsner, M.; Zwank, L.; Hunkeler, D.; Schwarzenbach, R. P. A new concept linking observable stable isotope fractionation to transformation pathways of organic pollutants. *Environ. Sci. Technol.* 2005, *39* (18), 6896-6916.

(11) Mariotti, A.; Germon, J. C.; Hubert, P.; Kaiser, P.; Letolle, R.; Tardieux, A.; Tardieux, P. Experimental-determination of nitrogen kinetic isotope fractionation - some principles - illustration for the denitrification and nitrification processes. *Plant Soil* 1981, *62* (3), 413-430.

(12) Northrop, D. B. The Expression of Isotope Effects on Enzyme-Catalyzed Reactions. *Annu. Rev. Biochem.* 1981, *50*, 103-131.

(13) McKelvie, J. R.; Hyman, M.; Elsner, M.; Smith, C. A.; Aslett, D.; Lacrampe-Couloume, G.; Sherwood Lollar, B. Isotopic fractionation of MTBE suggests different initial reaction mechanisms during aerobic biodegradation. *Environ. Sci. Technol.* 2009, *43* (8), 2793–2799.

(14) Lopes Ferreira, N.; Malandain, C.; Fayolle-Guichard, F. Enzymes and genes involved in the aerobic biodegradation of methyl tert-butyl ether (MTBE). *Appl. Microbiol. Biotechnol.* 2006, *72* (2), 252-262.

(15) Gray, J. R.; Lacrampe-Couloume, G.; Gandhi, D.; Scow, K. M.; Wilson, R. D.; Mackay, D. M.; Sherwood Lollar, B. Carbon and hydrogen isotopic fractionation during biodegradation of methyl tert-butyl ether. *Environ. Sci. Technol.* 2002, *36* (9), 1931-1938.

(16) Rosell, M.; Barcelo, D.; Rohwerder, T.; Breuer, U.; Gehre, M.; Richnow, H. H. Variations in 13C/12C and D/H enrichment factors of aerobic bacterial fuel oxygenate degradation. *Environ. Sci. Technol.* 2007, *41* (6), 2036-2043.

(17) Schmidt, R.; Battaglia, V.; Scow, K.; Kane, S.; Hristova, K. R. Involvement of a novel enzyme, MdpA, in methyl tert-butyl ether degradation in *Methylibium petroleiphilum* PM1. *Appl. Environ. Microbiol.* 2008, *74* (21), 6631-6638.

(18) Breuer, U.; Bäjen, C.; Rohwerder, T.; Müller, R. H.; Harms, H. In *MTBE degradation genes of an Ideonella-like bacterium L108*, 3rd European Conference on MTBE and Other Fuel Oxygenates, Antwerp, Belgium, 2007; Bastiaens, L., Ed. VITO: Antwerp, Belgium, 2007; p 103.

(19)   Chauvaux, S.; Chevalier, F.; Le Dantec, C.; Fayolle, F.; Miras, I.; Kunst, F.; Beguin, P. Cloning of a genetically unstable cytochrome P-450 gene cluster involved in degradation of the pollutant ethyl tert-butyl ether by Rhodococcus ruber. *J. Bacteriol.* 2001, *183* (22), 6551-6557.

(20)   Elsner, M.; McKelvie, J.; Couloume, G. L.; Sherwood Lollar, B. Insight into methyl tert-butyl ether (MTBE) stable isotope Fractionation from abiotic reference experiments. *Environ. Sci. Technol.* 2007, *41* (16), 5693-5700.

(21)   Kuder, T.; Wilson, J. T.; Kaiser, P.; Kolhatkar, R.; Philp, P.; Allen, J. Enrichment of stable carbon and hydrogen isotopes during anaerobic biodegradation of MTBE: Microcosm and field evidence. *Environ. Sci. Technol.* 2005, *39* (1), 213-220.

(22)   Hunkeler, D.; Butler, B. J.; Aravena, R.; Barker, J. F. Monitoring biodegradation of methyl tert-butyl ether (MTBE) using compound-specific carbon isotope analysis. *Environ. Sci. Technol.* 2001, *35* (4), 676-681.

(23)   Lesser, L. E.; Johnson, P. C.; Aravena, R.; Spinnler, G. E.; Bruce, C. L.; Salanitro, J. P. An evaluation of compound-specific isotope analyses for assessing the biodegradation of MTBE at Port Hueneme, CA. *Environ. Sci. Technol.* 2008, *42* (17), 6637-6643.

(24)   Bastida, F.; Rosell, M.; Franchini, A. G.; Seifert, J.; Finsterbusch, S.; Jehmlich, N.; Jechalke, S.; von Bergen, M.; Richnow, H. H. Elucidating MTBE degradation in a mixed consortium using a multidisciplinary approach. *FEMS Microbiol. Ecol.* 2010, *73*, 370–384.

(25)   Youngster, L. K. G.; Rosell, M.; Richnow, H. H.; Häggblom, M. M. Assessment of MTBE biodegradation pathways by two-dimensional isotope analysis in mixed bacterial consortia under different redox conditions. *Appl. Microbiol. Biotechnol.* 2010, *88* (1), 309-317.

(26)   Jechalke, S.; Rosell, M.; Martinez-Lavanchy, P. M.; Perez-Leiva, P.; Rohwerder, T.; Vogt, C.; Richnow, H. H. Linking Low-level stable isotope fractionation to expression of the cytochrome P450 Monooxygenase-encoding ethB gene for elucidation of methyl tert-butyl ether biodegradation in aerated treatment pond systems. *Appl. Environ. Microbiol.* 2011, *77* (3), 1086-1096.

(27)   Rosell, M.; Finsterbusch, S.; Jechalke, S.; Hübschmann, T.; Vogt, C.; Richnow, H. H. Evaluation of the Effects of Low Oxygen Concentration on Stable Isotope

Fractionation during Aerobic MTBE Biodegradation. *Environ. Sci. Technol.* 2010, *44* (1), 309-315.

(28)   Lechner, U.; Brodkorb, D.; Geyer, R.; Hause, G.; Hartig, C.; Auling, G.; Fayolle-Guichard, F.; Piveteau, P.; Müller, R. H.; Rohwerder, T. *Aquincola tertiaricarbonis* gen. nov., sp nov., a tertiary butyl moiety-degrading bacterium. *Int. J. Syst. Evol. Microbiol.* 2007, *57*, 1295-1303.

(29)   Müller, R. H.; Rohwerder, T.; Harms, H. Degradation of fuel oxygenates and their main intermediates by *Aquincola tertiaricarbonis* L108. *Microbiol.-Sgm* 2008, *154*, 1414-1421.

(30)   Nakatsu, C. H.; Hristova, K.; Hanada, S.; Meng, X. Y.; Hanson, J. R.; Scow, K. M.; Kamagata, Y. *Methylibium petroleiphilum* gen. nov., sp nov., a novel methyl tert-butyl ether-degrading methylotroph of the *Betaproteobacteria. Int. J. Syst. Evol. Microbiol.* 2006, *56*, 983-989.

(31)   Kane, S. R.; Chakicherla, A. Y.; Chain, P. S. G.; Schmidt, R.; Shin, M. W.; Legler, T. C.; Scow, K. M.; Larimer, F. W.; Lucas, S. M.; Richardson, P. M.; Hristova, K. R. Whole-genome analysis of the methyl tert-butyl ether-degrading beta-proteobacterium *Methylibium petroleiphilum* PM1. *J. Bacteriol.* 2007, *189* (5), 1931-1945.

(32)   Rohwerder, T.; Breuer, U.; Benndorf, D.; Lechner, U.; Müller, R. H. The alkyl tertiary butyl ether intermediate 2-hydroxyisobutyrate is degraded via a novel cobalamin-dependent mutase pathway. *Appl. Environ. Microbiol.* 2006, *72*, 4128-4135.

(33)   Gonzalez-Olmos, R.; Roland, U.; Toufar, H.; Kopinke, F. D.; Georgi, A. Fe-zeolites as catalysts for chemical oxidation of MTBE in water with H2O2. *Appl. Catal. B-Environ.* 2009, *89* (3-4), 356-364.

(34)   Karpel Vel Leitner, N.; Papailhou, A. L.; Croue, J. P.; Peyrot, J.; Dore, M. Oxidation of methyl tert-butyl ether (MTBE) and ethyl tert-butyl ether (ETBE) by ozone and combined ozone/hydrogen peroxide. *Ozone-Sci.*1994, *16* (1), 41-54.

(35)   Schmidt, H. J.; Schafer, H. J. Oxidation of Hydrocarbons with Benzyl(Triethyl)Ammonium Permanganate. *Angew. Chem.-Int.* 1979, *18* (1), 68-69.

(36) Waldemer, R. H.; Tratnyek, P. G. Kinetics of contaminant degradation by permanganate. *Environ. Sci. Technol.* 2006, *40* (3), 1055-1061.

(37) Gonzalez-Olmos, R.; Holzer, F.; Kopinke, F. D.; Georgi, A. Indications of the reactive species in a heterogeneous Fenton-like reaction using Fe-containing zeolites. *Appl. Catal. A-Gen.* 2011, *398* (1-2), 44-53.

(38) Pignatello, J. J.; Liu, D.; Huston, P. Evidence for an additional oxidant in the photoassisted Fenton reaction. *Environ. Sci. Technol.* 1999, *33* (11), 1832-1839.

(39) Smith, C. A.; Hyman, M. R. Oxidation of methyl tert-butyl ether by alkane hydroxylase in dicyclopropylketone-induced and n-octane-grown Pseudomonas putida GPo1. *Appl. Environ. Microbiol.* 2004, *70* (8), 4544-4550.

(40) Francois, A.; Garnier, L.; Mathis, H.; Fayolle, F.; Monot, F. Roles of tert-butyl formate, tert-butyl alcohol and acetone in the regulation of methyl tert-butyl ether degradation by Mycobacterium austroafricanum IFP 2012. *Appl. Microbiol. Biotechnol.* 2003, *62* (2-3), 256-262.

(41) Stefan, M. I.; Mack, J.; Bolton, J. R. Degradation pathways during the treatment of methyl tert-butyl ether by the UV/H2O2 process. *Environ. Sci. Technol.* 2000, *34* (4), 650-658.

(42) Johnson, E. L.; Smith, C. A.; O'Reilly, K. T.; Hyman, M. R. Induction of methyl Tertiary butyl ether (MTBE)-oxidizing activity in Mycobacterium vaccae JOB5 by MTBE. *Appl. Environ. Microbiol.* 2004, *70* (2), 1023-1030.

(43) House, A. J.; Hyman, M. R. Effects of gasoline components on MTBE and TBA cometabolism by Mycobacterium austroafricanum JOB5. *Biodegradation* 2010, *21* (4), 525-541.

(44) Smith, C. A.; Hyman, M. R. Oxidation of gasoline oxygenates by closely related non-haem-iron alkane hydroxylases in Pseudomonas mendocina KR1 and other n-octane-utilizing Pseudomonas strains. *Environ. Microbiol. Rep.* 2010, *2* (3), 426-432.

(45) Schramm, V. L. Enzymatic transition state theory and transition state analogue design. *J. Biol. Chem.* 2007, *282* (39), 28297-28300.

(46) Malandain, C.; Fayolle-Guichard, F.; Vogel, T. M. Cytochromes P450-mediated degradation of fuel oxygenates by environmental isolates. *Fems Microbiol. Ecol* 2010, *72* (2), 289-296.

(47) Kämpfer, P.; Kohlweyer, U.; Thiemer, B.; Andreesen, J. R. Pseudonocardia tetrahydrofuranoxydans sp nov. *Int. J. Syst. Evol. Microbiol.* 2006, *56*, 1535-1538.

(48) Vainberg, S.; McClay, K.; Masuda, H.; Root, D.; Condee, C.; Zylstra, G. J.; Steffan, R. J. Biodegradation of ether pollutants by Pseudonocardia sp strain ENV478. *Appl. Environ. Microbiol.* 2006, *72* (8), 5218-5224.

(49) Thiemer, B.; Andreesen, J. R.; Schrader, T. Cloning and characterization of a gene cluster involved in tetrahydrofuran degradation in Pseudonocardia sp strain K1. *Arch. Microbiol.* 2003, *179* (4), 266-277.

(50) Botting, N. P. Isotope effects in the elucidation of enzyme mechanisms. *Nat. Prod. Rep.* 1994, *11* (4), 337-353.

(51) Scharschmidt, M.; Fisher, M. A.; Cleland, W. W. Variation of transition-state structure as a function of the nucleotide in reactions catalyzed by dehydrogenases .1. liver alcohol-dehydrogenase with benzyl alcohol and yeast aldehyde dehydrogenase with benzaldehyde. *Biochemistry* 1984, *23* (23), 5471-5478.

(52) Hermes, J. D.; Morrical, S. W.; Oleary, M. H.; Cleland, W. W. Variation of transition-state structure as a function of the nucleotide in reactions catalyzed by dehydrogenases .2. formate dehydrogenase. *Biochemistry* 1984, *23* (23), 5479-5488.

(53) Schäfer, F.; Muzica, L.; Schuster, J.; Treuter, N.; Rosell, M.; Harms, H.; Müller, R. H.; Rohwerder, T. Formation of alkenes via degradation of tert-alkyl ethers and alcohols by aquincola tertiaricarbonis L108 and methylibium spp. *Appl. Environ. Microbiol.* 2011, *77* (17), 5981-5987.

(54) Lopes Ferreira, N.; Mathis, H.; Labbe, D.; Frederic, M.; Greer, C. W.; Fayolle-Guichard, F. n-Alkane assimilation and tert-butyl alcohol (TBA) oxidation capacity in Mycobacterium austroafricanum strains. *Appl. Microbiol. Biotechnol.* 2007, *75* (4), 909-919.

(55) van Beilen, J. B.; Smits, T. H. M.; Roos, F. F.; Brunner, T.; Balada, S. B.; Rothlisberger, M.; Witholt, B. Identification of an amino acid position that determines the substrate range of integral membrane alkane hydroxylases. *J. Bacteriol.* 2005, *187* (1), 85-91.

(56) van Beilen, J. B.; Funhoff, E. G. Alkane hydroxylases involved in microbial alkane degradation. *Appl. Microbiol. Biotechnol.* 2007, *74* (1), 13-21.

(57) Kim, Y. H.; Engesser, K. H.; Kim, S. J. Physiological, numerical and molecular characterization of alkyl ether-utilizing rhodococci. *Environ. Microbiol.* 2007, *9* (6), 1497-1510.

(58) Zwank, L.; Berg, M.; Elsner, M.; Schmidt, T. C.; Schwarzenbach, R. P.; Haderlein, S. B. New evaluation scheme for two-dimensional isotope analysis to decipher biodegradation processes: Application to groundwater contamination by MTBE. *Environ. Sci. Technol.* 2005, *39* (4), 1018-1029.

(59) Van Breukelen, B. M. Extending the Rayleigh equation to allow competing isotope fractionating pathways to improve quantification of biodegradation. *Environ. Sci. Technol.* 2007, *41* (11), 4004-4010.

(60) Kujawinski, D. M.; Stephan, M.; Jochmann, M. A.; Krajenke, K.; Haas, J.; Schmidt, T. C. Stable carbon and hydrogen isotope analysis of methyl tert-butyl ether and tert-amyl methyl ether by purge and trap-gas chromatography-isotope ratio mass spectrometry: Method evaluation and application. *J. Environ. Monitor.* 2010, *12* (1), 347-354.

(61) Baldwin, B. R.; Biernacki, A.; Blair, J.; Purchase, M. P.; Baker, J. M.; Sublette, K.; Davis, G.; Ogles, D. Monitoring gene expression to evaluate oxygen infusion at a gasoline-contaminated site. *Environ. Sci. Technol.* 2010, *44* (17), 6829-6834.

(62) Busch-Harris, J.; Sublette, K.; Roberts, K. P.; Landrum, C.; Peacock, A. D.; Davis, G.; Ogles, D.; Holmes, W. E.; Harris, D.; Ota, C.; Yang, X.; Kolhatkar, A. bio-traps coupled with molecular biological methods and stable isotope probing demonstrate the in situ biodegradation potential of MTBE and TBA in gasoline-contaminated aquifers. *Ground Water Monit.* 2008, *28* (4), 47-62.

Supporting Information

Table S1. Details for growing and resting cells cultivation (strains in alphabetical order).

Strain	Growing cells			Resting cells		
	Growth substrate/s	Additional inducer	Target compound	Co-substrate	Additional inducer
Aquincola tertiaricarbonis L108	MTBE or TAME	-	TAME	-	-
Gordonia sp. IFP2009	ETBE (with or without 0.5 g/L acetate)	-	ETBE	with or without 0.5 g/L acetate	-
		-	MTBE	acetate (0.5 g/L)	-
		-	TAME	acetate (0.5 g/L)	-
Methylibium petroleiphilum PM1	MTBE or TAME	-	TAME	-	-
Methylibium sp. R8	MTBE or TAME	-	na	-	-
Mycobacterium austroafricanum IFP2012	TBA	-	ETBE	acetate or glucose (0.5 g/L)	-
		-	MTBE	acetate or glucose (0.5 g/L)	-
		-	TAME	acetate or glucose (0.5 g/L)	-
Mycobacterium austroafricanum JOB5	MTBE plus glucose (0.5 g/L)	-	ETBE	glucose (0.5 g/L)	-
		-	MTBE	glucose (0.5 g/L)	-
		-	TAME	glucose (0.5 g/L)	-
Pseudomonas putida GPo1	0.05% (v/v) n-octane or 0.5 g/L glucose plus inducer	1 mM DCPK	ETBE	glucose (0.5 g/L)	1 mM DCPK
			MTBE	glucose (0.5 g/L)	1 mM DCPK
			TAME	glucose (0.5 g/L)	1 mM DCPK
Rhodococcus ruber DSM7511	MTBE plus glucose (0.5 g/L)	-	ETBE	glucose (0.5 g/L)	-
		-	MTBE	glucose (0.5 g/L)	-
		-	TAME	glucose (0.5 g/L)	-
Rhodococcus zopfii IFP2005	ETBE (with or without 0.5 g/L acetate or glucose)	-	ETBE	acetate or glucose (0.5 g/L)	-
		-	MTBE	acetate or glucose (0.5 g/L)	-
		-	TAME	acetate or glucose (0.5 g/L)	-

na: not analyzed

DCPK: dicyclopropylketone

ETBE: ethyl *tert*-butyl ether

MTBE: methyl *tert*-butyl ether

TAME: *tert*-amyl methyl ether

TBA: *tert*-butyl alcohol

Figure S1. Chemical degradation of fuel oxygenates with, a) Fenton reaction (10 mM H_2O_2 / 10 mM Fe^{2+}, pH 3) b) Fenton-like reaction (100 mM H_2O_2 / 0.03 mM Fe^{3+}, pH 3) c) permanganate (0.11 M $KMnO_4$) and d) acid hydrolysis (1 M HCl). Blanks of the target compounds in deionized water were always prepared in parallel and were monitored to evaluate external losses to the studied reaction. Conditions detailed in the manuscript.
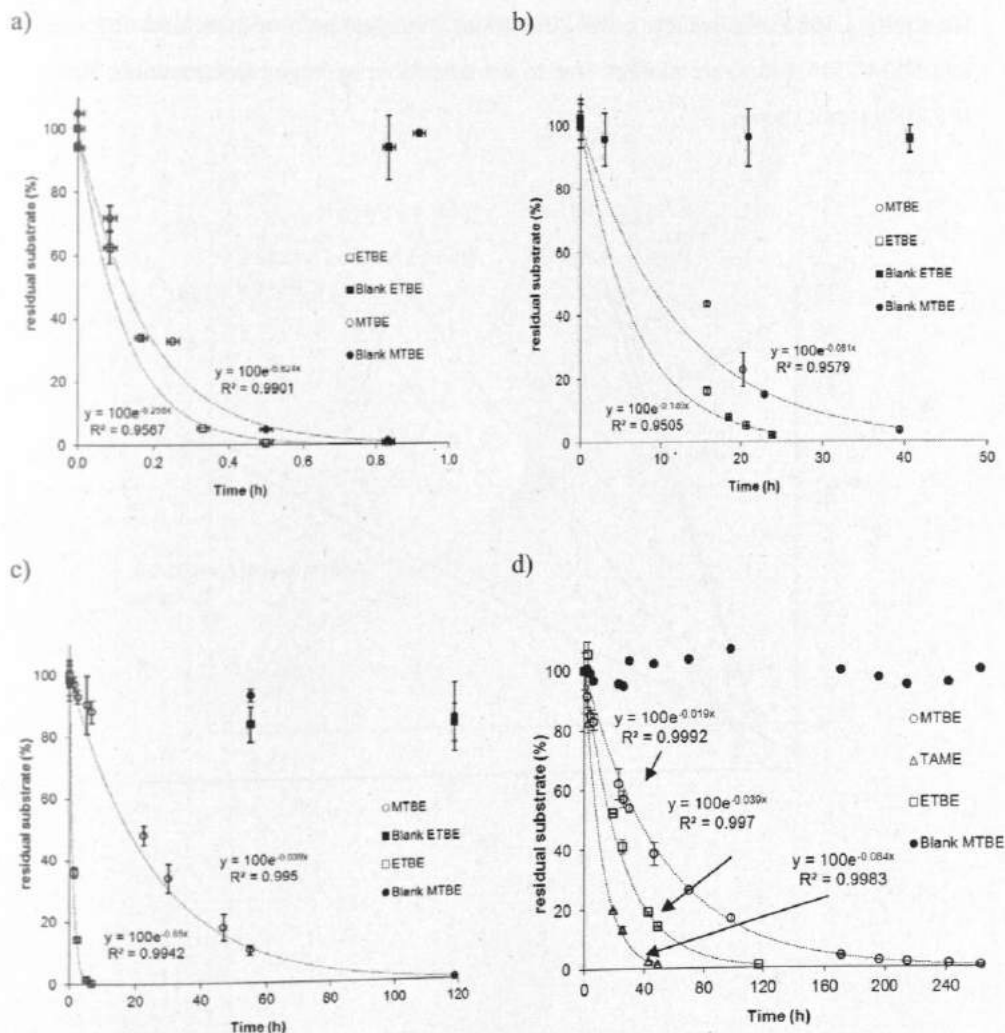
Figure S2. ETBE two dimensional plot of hydrogen versus carbon isotopic shifts for the so far discovered initial reaction mechanisms including (i) the mean slope (Λ value) for chemical oxidation (by plotting together permanganate and the two Fenton reactions of this study), (ii) the acid hydrolysis (S_N1-type, Λ from the present study) and (iii) the isotopic pattern discovered for strain K1 [1]. No anaerobic culture or S_N2-type hydrolysis has been reported so far. Linear regression curves (solid lines) allow comparison within the 95% confidence intervals (CI) (dashed lines). Measured values for strains L108 (solid squares), IFP 2001 (open triangles) both original data from [2] and DSM 7511 (stars) are plotted. Due to not detectable hydrogen fractionation, strain IFP 2009 is not shown.
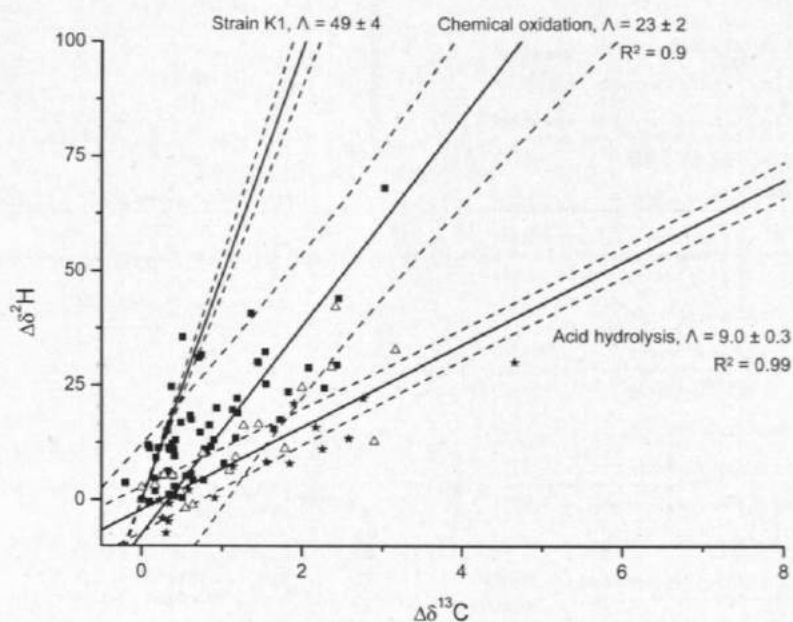
Figure S3. TAME two dimensional plot of hydrogen versus carbon isotopic shifts for the so far discovered initial reaction mechanisms including (i) the isotopic pattern of strain PM1 which might represent the oxidation of the methyl group, (ii) the acid hydrolysis (S_N1-type) and (iii) the isotopic pattern discovered for strain K1 [1]. No 2D-CSIA study with anaerobic cultures or S_N2-type hydrolysis has been reported so far. Linear regression curves (solid lines) allow comparison within the 95% confidence intervals (CI) (dashed lines). Measured values for strain GPo1 (open circles) are plotted. Due to not detectable hydrogen fractionation, strains L108, IFP 2012, JOB5 and DSM7511 are not shown.
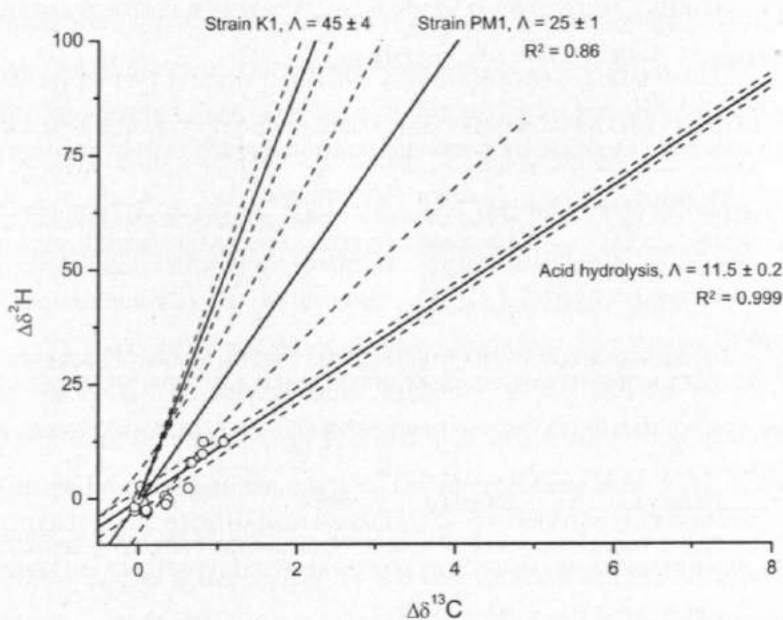
Figure S4. ClustalW2 alignment of amino acid sequences of AlkB enzymes from *Pseudomonas* (strain GPo1, CAB54050), *Methylibium* (strain PM1, Mpe_B0606) and *Mycobacterium* (strain IFP 2173, FJ009005, identical to the IFP 2012 published sequence) suggested to be involved in fuel oxygenate attack. Topology is indicated as proposed by van Beilen et al. [3] for the AlkB of strain GPo1. While iron-binding histidine residues of motifs A to D are conserved in all sequences (highlighted in bold), significant sequence variability is found in the transmembrane (TM) helices forming the substrate-binding pocket. Particularly, the bulky tryptophane residue W55 in strain GPo1, which is located in the middle of TM helix 2, is replaced by smaller residues in strains PM1 and IFP 2173 (highlighted in black).

```
              CYTOPLASM        TM helix 1          TM helix 2
GPo1_AlkB    MLEKHRVLDS----APEYVDKKKYLWILSTLWPATPMIG---IWLANETGW----GIFYG 49
PM1_AlkB     MISSLPNNDSGGSGETRYRDMKRYAWPIGVLWPMLPAIG---IAAAQLTGK----AAFYW 53
IFP2173_AlkB ----MSKPD-----VEQWRDKKRYLWLMGLIAPTALFVMLPLIWALNQFGWHVAAQVPLW 51
               *   .:**.**.:.*  :  *  :  *

              TM helix 2        CYTOPLASM          TM helix 3
GPo1_AlkB    LVLLVWYGALPLLDAMFGEDFNNPPEEVVPKLEKERYYRVLTYLTVPMHYAALIVSAWWV
             109
PM1_AlkB     LAPFLTFVVIPLLDMVIGSSQKNPPESAIKALEDDNYYRNLTFVTVPVHYLSMITGAWAV 113
IFP2173_AlkB IGPILLYILLPALDLKFGPDGQNPPDEVMERLENDKYYRYCTYLYIPFQYASVIMGAYLF 111
             :  ::  :*  ** .*  .***.  **..*** *:..*..* ..* *:.

                   TM helix 4              motif A    CYTOPLASM
GPo1_AlkB    GTQPMSWLEIGA---------LALSLGIVNGLALNTGHELGHKKETFDRWMAKIVLAVVG 160
PM1_AlkB     GTLDLTGLNYAG---------ICISVGLANGLAIVTSHELGHKKDALERWMSKICLAVTA 164
IFP2173_AlkB TASDLGWLGFEGGLSWPAKIGLALSVGLLGGVGINTAHEMGHKKDSLERWLAKITLAQTL
             171
               :  *  .     ..*.+.  *..  *.**.****....**..** **

                  motif B
GPo1_AlkB    YGHFFIEHNKGHHRDVATPMDPATSRMGESIYKFSIREIP-GAFIRAWGLEEQRLSRRGQ 219
PM1_AlkB     YGQYMIDHNRGHHRDVATPEDSSSARMGEGIYFFALRELPYTGFIRPWRLEKERLARSGK
             224
IFP2173_AlkB YGHFYIEHNRGHHVRVATPEDPASARFGETFWEFLPRSVF-GSLKSAWELEAKRLERAGK
             230
             **.. *.**.*** **** *.....*.** .. * *.   . * **.** * *.

                  TM helix 5          TM helix 6       motif C
GPo1_AlkB    SVWSFDNEILQPMIITVILYAVLLALFGPKMLVFLPIQMAFGWWQLTSANYIEHYGLLRQ 279
PM1_AlkB     GPWTLENEFLQPALISLVFYGALIVWLGSSIIPYLLATAFGGYWFLVIADYIEHYGLLRQ 284
IFP2173_AlkB SKWHWSNDVLNAWAMSVVLYGALIAVFGWALIPYILISAVFGFTLLEAVNYLEHYGLLRK
             290
             . *  .*.*.  .....*..*. .*  .. ..   *. *  .*.*******.

              CYTOPLASM        motif D
GPo1_AlkB    KMEDGRYEHQKPHHSWNSNHIVSNLVLFHLQRHSDHHAHPTRSYQSLRDFPGLPALPTGY
             339
PM1_AlkB     KLPDGRYERVRPEHSWNTDHIASNVIYFHVQRHSDHHAFPTRSYQALRSYSDVPTMPSGY
             344
IFP2173_AlkB KLDNGRYERCAPVHSWNSDHIVTNLFLYHLQRHSDHHANPTRRYQTLRSMEGAPNLPSGY
             350
             *:.****. * ****..**.*. .*.******** *** **.**  *.*.**

GPo1_AlkB    PGAFLMAMIPQWFRSVMDPKVVDWAGGDLNKIQIDDSMRETYLKKFGTSSAGHSSSTSAV
             399
PM1_AlkB     PGMIWLCHIPPLFRAVMDPLLLKQYDGDLTKINIDPGKRSKLFRRYANQLAQPVRD---- 400
IFP2173_AlkB ASMIGLTYFPPLWRRMMDHRVLAHYGGDITQVNIQPRVRDKVLARYGAAADERSREEKKA
             410
             . :: .*  .*.**  ..  **..::*:  *. : ::

GPo1_AlkB    AS------------ 401
PM1_AlkB     --------------
IFP2173_AlkB ADERSREEQGGKA 423
```

Heterogeneous Fenton-like reactions

In addition to the Fenton (catalyzed by Fe^{2+}) and Fenton-like (catalyzed by Fe^{3+}) reactions, orthoferrites $BiFeO_3$ and $LaFeO_3$ were used as heterogeneous catalysts in a system with H_2O_2 for MTBE and ETBE oxidation. Relative to the homogeneous Fenton-like catalysts, these heterogeneous catalysts are active over a wider pH range [4]. It is often assumed that heterogeneous Fenton-like reactions proceed by the formation of hydroxyl radicals at the surface iron species of the catalyst, but no direct evidence for this hypothesis exists so far. As an alternative mechanism, the formation of high-valent iron-oxo species, i.e. ferryl (Fe(IV)=O) has been suggested, whereby the reaction pH might be a decisive factor for the possible reaction pathways (see e.g. discussion in [5, 6]).

Orthoferrites were synthesized by a sol-gel method [7, 8] and characterized by X-ray diffraction (XRD). Batch experiments were carried out in cylindrical glass vessels (100 mL) with Mininert® valves. The reaction medium was prepared by adding 1 g/L $BiFeO_3$ or $LaFeO_3$ to a solution containing 100 mg/L MTBE or ETBE. Before the reaction was started by adding 3 g/L H_2O_2 into the reaction medium, samples were sonicated for 10 min and afterwards placed on a heater with magnetic stirrer. The pH of the reaction medium was kept in the range of pH 6.5-7.0 and the reaction temperature was $40 \pm 2°C$. The concentration of organic compounds was monitored by GC-MS headspace analysis and representative samples for the analysis of the isotopic fractionation were filtrated through 0.22 μm filter into 5-mL vials containing sodium thiosulfate used for stopping the reaction. The samples were kept in the freezer at -20 °C before the analysis of the isotopic fractionation.

Values for ε_C, ε_H and Λ determined for the heterogeneous Fenton reaction using the orthoferrites (see Table S1) are not significantly different from values obtained for the homogeneous Fenton and Fenton-like reactions (Table 1 in the manuscript). This is in line with the hypothesis that hydroxyl radicals might be the predominant reactive species formed from H_2O_2 also in case of the orthoferrite catalysts whereas a significant contribution of the ferryl species (Fe(IV)=O) for which higher fractionation effects could be expected (as discussed in [5]), is less likely. Moreover, the different pH (pH 3 vs. neutral) is not affecting the isotopic fractionation, confirming that acid hydrolysis is not playing any role in the Fenton experiments. Since this heterogeneous Fenton-like reaction obviously does not represent another type of reaction mechanism for the

oxidation of the fuel oxygenates, it was not additionally included in Figure 1. However, further research on isotopic fractionation produced by ferryl species should be done as they are postulated as active species in the iron centers of the hydroxylase enzymes employed by fuel oxygenate-degrading bacteria [9] and in order to confirm the expected higher fractionation and/or different involved reaction mechanism.

Table S2. Comparison of MTBE and ETBE carbon and hydrogen isotopic enrichment factors (ε) and 2D-CSIA slopes (Λ) caused by heterogeneous Fenton-like reactions. When possible the respective 95% confidence intervals ($\pm$ 95% CI) are provided.

Reaction	Target	ε_C [‰]	±95% CI [‰]	R²	D [%]	N	ε_H [‰]	±95% CI [‰]	R²	D [%]	N	$\Lambda \pm$ 95% CI
BiFeO$_3$ (n=1)	MTBE	-1.4	0.2	0.993	94	5	-25	-	0.996	85	3	16
(n=1)	ETBE	-0.8	0.2	0.98	94	6	-15	9	0.993	94	5	18 ± 8
LaFeO$_3$ (n=1)	MTBE	-1.6	0.4	0.996	89	5	-24	6	0.997	85	4	15 ± 3
(n=1)	ETBE	-1.3	0.2	0.977	98	6	-15	-	0.81	83	3	11

n: number of experiments, N: number of data points; CI is 95% Confidence Interval; D%: maximum percentage of substrate initial/partial degradation (do not confuse with complete mineralization to CO_2) which could be analyzed for the corresponding isotopic composition taking into account different detection limits for carbon and hydrogen.

References

(1)   McKelvie, J. R.; Hyman, M.; Elsner, M.; Smith, C. A.; Aslett, D.; Lacrampe-Couloume, G.; Sherwood Lollar, B. Isotopic fractionation of MTBE suggests different initial reaction mechanisms during aerobic biodegradation. *Environ. Sci. Technol.* 2009, *43* (8), 2793–2799.

(2)   Rosell, M.; Barcelo, D.; Rohwerder, T.; Breuer, U.; Gehre, M.; Richnow, H. H. Variations in 13C/12C and D/H enrichment factors of aerobic bacterial fuel oxygenate degradation. *Environ. Sci. Technol.* 2007, *41* (6), 2036-2043.

(3)   van Beilen, J. B.; Smits, T. H. M.; Roos, F. F.; Brunner, T.; Balada, S. B.; Rothlisberger, M.; Witholt, B. Identification of an amino acid position that determines the substrate range of integral membrane alkane hydroxylases. *J. Bacteriol.* 2005, *187* (1), 85-91.

(4)   Caudo, S.; Centi, G.; Genovese, C.; Perathoner, S. Homogeneous versus heterogeneous catalytic reactions to eliminate organics from waste water using H_2O_2. *Top. Catal.* 2006, *40* (1-4), 207-219.

(5)   Gonzalez-Olmos, R.; Holzer, F.; Kopinke, F. D.; Georgi, A. Indications of the reactive species in a heterogeneous Fenton-like reaction using Fe-containing zeolites. *Appl. Catal. A-Gen.* 2011, *398* (1-2), 44-53.

(6)   Pham, A. L.-T.; Lee, C.; Doyle, F. M.; Sedlak, D. L. A silica-supported iron oxide catalyst capable of activating hydrogen peroxide at neutral pH values. *Environ. Sci. Technol.* 2009, *43* (23), 8930-8935.

(7)   Luo, W.; Zhu, L. H.; Wang, N.; Tang, H. Q.; Cao, M. J.; She, Y. B. Efficient removal of organic pollutants with magnetic nanoscaled $BiFeO_3$ as a reusable heterogeneous Fenton-like catalyst. *Environ. Sci. Technol.* 2010, *44* (5), 1786-1791.

(8)   Shabbir, G.; Qureshi, A. H.; Saeed, K. Nano-crystalline $LaFeO_3$ powders synthesized by the citrate-gel method. *Mater. Lett.* 2006, *60* (29-30), 3706-3709.

(9)   Hamdane, D.; Zhang, H. M.; Hollenberg, P. Oxygen activation by cytochrome P450 monooxygenase. *Photosynth. Res.* 2008, *98* (1-3), 657-666.

8. Summary

Chemical oxidation processes have emerged as a powerful and versatile tool for treatment of organically contaminated water streams. Remediation of polluted groundwater by means of *in situ* chemical oxidation (ISCO) became a widely applied approach in the last three decades. Especially potassium permanganate ($KMnO_4$) has emerged as an effective oxidant for treatment of zones contaminated with chlorinated solvents. Hydroxyl radicals (•OH) generated by e.g., Fenton reaction are on the other hand highly suitable when dealing with clean up of wastewaters and industrial effluents, which are often loaded with different types of recalcitrant pollutants. Although ISCO with $KMnO_4$ and Fenton oxidation are considered as efficient treatment techniques with respect to the contaminant degradation, in a large scale they face several shortcomings. Thus, the main aim of the present study is to propose and test novel strategies, where integration of colloidal reagents and catalysts plays the key role.

In the first manuscript, a new $KMnO_4$ reagent with slow-release properties is introduced, which could be applied as oxidant in a reactive barrier for efficient plume remediation. Manganese dioxide (MnO_2) was tested as a suitable coating for $KMnO_4$ particles because of its insolubility in water, adsorptive and catalytic properties and environmental compatibility. The MnO_2-coated $KMnO_4$ particles (MCP) were synthesized by i) partial reduction of solid $KMnO_4$ using the acid-catalyzed reaction with n-propanol or ii) the comproportionation of Mn(VII) and Mn(II) in n-propanol as reaction medium. The obtained particles were characterized by scanning electron microscopy and BET analysis, where the MCP revealed higher specific surface area (approx. $40 \ m^2 \ g^{-1}$) than the native $KMnO_4$ ($0.04 \ m^2 \ g^{-1}$).

The longevity of MCP was tested in column experiments and showed that for MCP with a residual $KMnO_4$ fraction of 70 wt%, the duration of permanganate release under flow-through conditions was prolonged by a factor of 10 compared to native $KMnO_4$. Although the coating process was successful, the release prolongation is considered to be rather moderate. This is probably due to the non-uniform structure of the synthesized MnO_2 coating, which contains relatively wide defects in form of cracks. Experiments on the oxidation of benzaldehyde as a model compound in dry dichloromethane as solvent, which is a representative for non-polar non-aqueous phase liquids (NAPL), revealed that the reaction does not take place with native $KMnO_4$, but only with MCP. It is

obvious that MnO_2 plays a significant role in oxidation processes in non-aqueous media and this property can be utilized for treatment of NAPL-contaminated zones. Moreover, this study indicates that the invented MCP can be applied in other heterogeneous systems, where an oxidant in solid phase is required.

The second and third manuscripts are focused on the replacement of conventional Fenton reagent (*i.e.* dissolved iron as catalyst) by iron-containing nanocatalysts in order to improve the overall performance and versatility of the Fenton process for contaminant degradation.

Two different types of minerals have been elucidated as suitable nanocatalysts in the heterogeneous Fenton-like reaction: i) magnetic Fe(II,III) oxides such as magnetite (Fe_3O_4), which contain Fe^{II} and Fe^{III} in their structure, are environmentally compatible, and easy to separate due to their magnetic properties and ii) orthoferrites with perovskite structure, in particular $LaFeO_3$ (LFO) and $BiFeO_3$ (BFO), which due to their well-defined structure and intrinsic redox properties have found an application in advanced technologies such as solid oxide fuel cells, electrode materials, chemical sensors and catalysts (mainly for gas phase reactions).

Magnetite and both perovskite catalysts were prepared by co-precipitation and sol-gel method respectively. Transition electron microscopy (TEM) images confirmed crystallite sizes in the nanometer range for magnetite and commercial Fe(II,III) oxide, whereas in case of perovskites aggregates of single nanoparticles were observed. This can be attributed to aggregation phenomena caused by the applied high temperature calcination. BET analysis revealed relatively low specific surface areas for LFO (5.2 m^2 g^{-1}) and BFO (3.2 m^2 g^{-1}) in comparison with magnetite (95 m^2g^{-1}) or commercial Fe(II,III) oxide (45 m^2g^{-1}).

The catalytic activity of the prepared materials was tested in batch experiments using phenol as a model contaminant and hydrogen peroxide as oxidant. In batch experiments carried out at room temperature and pH = 7, LFO and BFO perovskites revealed a higher catalytic activity (normalized to catalyst mass concentration) and more efficient utilization of H_2O_2 in comparison to various Fe(II,III) oxides. For instance, for the half-life of phenol values of 2.5, 5 and > 24 h were determined for BFO, LFO and commercial Fe(II,III) oxide, respectively, under identical reaction conditions ($c_{0,phenol}$ = 25 mg L^{-1}, $c_{0,H2O2}$ = 3 g L^{-1}, and c_{cat} = 1 g L^{-1}, pH = 7 ± 0.2). Obviously, the catalytic

activity of BFO and LFO is even more superior when considering surface-normalized rate coefficients.

It has been shown that nano-sized magnetite is susceptible to fast oxidation under Fenton conditions and is converted into maghemite (γ-Fe_2O_3), starting from the surface and continuing to the core of the particle. The presence of residual Fe(II) in the nanoparticle core appears to be of minor importance for the catalytic activity in phenol degradation by H_2O_2. However, if the Fe(II) content was raised above the stoichiometric ratio of magnetite (achieved by reduction of commercial Fe(II,III) oxide with $NaBH_4$), then only the non-productive decomposition of H_2O_2 was accelerated. Furthermore, the catalyst surface of Fe(II,III) oxides emerged as an important scavenger of reactive species, since it was observed that the reaction rates of phenol oxidation were relatively insensitive to catalyst concentration in the range of 1-10 g L^{-1}, whereby particle agglomeration seems to play a key role. Thus, based on the obtained results, magnetite has catalytic properties for H_2O_2 activation, however, its intrinsic catalytic activity appears to be rather low, *i.e.* not adequate for practical application.

LFO and BFO were further investigated under various reaction conditions, in particular variation of catalyst and H_2O_2 concentration, reaction pH and temperature. Additionally, the stability and reusability of the catalysts were tested, which is a prerequisite for further practical application. In summary, BFO revealed a better catalytic performance than LFO when reaction conditions such as catalyst concentration or temperature were varied in order to achieve high phenol degradation rates. For example, an increase in the reaction temperature from 20 °C to 60 °C improved the catalyst activity of BFO by a factor of 10, whereas LFO showed only a very slight improvement. In 4 consecutive batch runs BFO revealed a constant catalytic activity, whereby the concentration of methyl *tert*-butyl ether (MTBE) was reduced by 80% within 6 h of reaction at 40 °C. The higher activity of the BFO perovskite can be attributed to the structural and intrinsic properties of the material, where the synthesis step can play a crucial role (e.g., existing surface defects in the structure or impurities).

The last manuscript deals with the mechanistic aspects of the heterogeneous Fenton-like system using perovskite nanocatalysts. It is often assumed that heterogeneous Fenton-like reactions proceed via •OH, in a similar manner as the homogeneous Fenton reaction. However, clear evidence is missing so far. In this study the reactive species involved during LFO- and BFO-catalyzed Fenton-like reactions at neutral pH

conditions were investigated by analyzing the carbon and hydrogen isotope fractionation coupled to the oxidation of two model compounds (MTBE and ethyl *tert*-butyl ether, ETBE). The obtained isotope fractionation results of the perovskite-catalyzed reaction have been compared to other abiotic chemical oxidation systems, in particular permanganate, homogeneous Fenton- and Fenton-like (Fe^{3+} + H_2O_2) oxidation. The strong similarity in the observed C- and H-fractionation indicates that the perovskite-catalyzed oxidation follows the same pathway as the homogeneous Fenton reaction, which means that it involves •OH as dominant reactive species. In addition, the C- and H-bulk enrichment factors determined for these abiotic oxidation reactions formed a reference for evaluating biodegradation pathways for fuel oxygenates applied by various bacteria strains.

Zusammenfassung

Chemische Oxidationsprozesse sind ein leistungsfähiges und vielseitiges Instrument zur Behandlung von mit organischen Schadstoffen kontaminierten Wasserströmen. Die Grundwasserreinigung durch In-situ chemische Oxidation (ISCO) wurde in den letzten drei Jahrzehnten vermehrt angewendet. Besonders Kaliumpermanganat ($KMnO_4$) hat sich als ein wirksames Oxidationsmittel zur Behandlung von Kontaminationszonen von chlorierten Lösungsmitteln bewährt. Die Anwendung von Hydroxylradikalen (•OH), die z. B. durch die Fenton-Reaktion erzeugt werden, ist auf der anderen Seite sehr gut geeignet, wenn es um die Behandlung von kontaminierten Wässern, wie zum Beispiel industriellen Abwässern geht, die oft mit verschiedenen Arten von schwer abbaubaren Schadstoffen beladen sind. Obwohl ISCO mit $KMnO_4$ und Fenton-Oxidation als effiziente Behandlungstechniken bezüglich des Abbaus organischer Schadstoffe betrachtet werden, weisen sie bei Anwendung im großen Maßstab verschiedene Nachteile auf. Daher ist das Hauptziel der vorliegenden Studie neue Strategien zur Verbesserung dieser Techniken vorzuschlagen und zu testen, wobei der Einsatz von kolloidalen Reagenzien und Katalysatoren eine Schlüsselrolle spielt.

Im ersten Manuskript wird die Entwicklung eines neuen Kaliumpermanganat-Reagenz mit der Eigenschaft einer langsamen Permanganat-Freisetzung beschrieben, das als Oxidationsmittel in einer reaktiven Barriere für die effiziente Sanierung von Schadstofffahnen eingesetzt werden kann. Mangandioxid (MnO_2), wurde aufgrund seiner Unlöslichkeit in Wasser, seiner adsorptiven und katalytischen Eigenschaften sowie Umweltverträglichkeit als Coating-Material getestet. Die mit MnO_2 beschichteten $KMnO_4$-Partikel (MCP) wurden synthetisiert durch i) partielle Reduktion des festen $KMnO_4$ mittels säure-katalysierter Reaktion mit n-Propanol sowie ii) Synproportionierung von Mn^{7+} und Mn^{2+} in n-Propanol als Reaktionsmedium. Die erhaltenen Partikel wurden durch Rasterelektronenmikroskopie (SEM) und BET-Analyse charakterisiert, wobei MCP offenbar eine höhere spezifische Oberfläche (ca. 40 $m^2 \, g^{-1}$) als unbehandeltes $KMnO_4$ (0,04 $m^2 \, g^{-1}$) aufweist. Die Langlebigkeit der MCP wurde in Säulen-Experimenten getestet und es zeigte sich, dass für MCP mit einem Restgehalt an $KMnO_4$ von 70 Ma.-% die Dauer der Permanganat-Freisetzung unter Durchflussbedingungen im Vergleich zu unbehandeltem $KMnO_4$ um einen Faktor von 10 verlängert wurde. Obwohl die Modifizierung erfolgreich war, wird die

Freisetzungsverlängerung bzw. Lebensdauer der MCP als eher moderat eingeschätzt. Dies ist wahrscheinlich auf die uneinheitliche Struktur der synthetisierten MnO_2-Beschichtung zurückzuführen, die relativ breite Defekte in Form von Rissen enthält.

Experimente zur Oxidation von Benzaldehyd als Modellverbindung in trockenem Dichlormethan als Lösungsmittel, das eine typische unpolare nicht-wässrige Flüssigkeit (NAPL) repräsentiert, ergaben, dass die Reaktion nur mit MCP nicht aber mit unbehandeltem $KMnO_4$ stattfindet. Offensichtlich spielt MnO_2 bei Oxidationsprozessen in nicht-wässrigen Medien eine bedeutende Rolle und diese Eigenschaft kann zur Behandlung von kontaminierten NAPL-Zonen eingesetzt werden. Außerdem ist der Einsatz der entwickelten MCP in anderen heterogenen Systemen denkbar, wo ein Oxidationsmittel in fester Phase erforderlich ist.

Schwerpunkt des zweiten und dritten Manuskripts ist der Ersatz des konventionellen Fenton-Reagenz (d.h. gelöstes Eisen als Katalysator) durch eisenhaltige Nanokatalysatoren mit dem Ziel, die Leistungsfähigkeit und das Anwendungsspektrum des Fenton-Prozesses für den Schadstoffabbau zu verbessern. Zwei verschiedene Arten von Mineralien wurden auf ihre Eignung als Nanokatalysatoren in der heterogenen Fenton-Reaktion untersucht:

i) magnetische Fe(II,III)-Oxide wie Magnetit (Fe_3O_4), die Fe^{II} und Fe^{III} in ihrer Struktur enthalten, sowie umweltverträglich und aufgrund ihrer magnetischen Eigenschaften einfach abtrennbar sind und

ii) Orthoferrite mit Perowskitstruktur, wie $LaFeO_3$ (LFO) und $BiFeO_3$ (BFO), die aufgrund ihrer klar definierten Struktur und intrinsischen Redoxeigenschaften bereits eine Anwendung in modernen Technologien z.B. als Materialien für Brennstoffzellen, Elektroden, chemische Sensoren und Katalysatoren (hauptsächlich für Gasphasenreaktionen) gefunden haben.

Magnetit und beide Perowskit-Katalysatoren wurden durch Co-Präzipitation und Sol-Gel-Verfahren hergestellt. Durch Transmissions-Elektronenmikroskopie (TEM) wurden Kristallitgrößen im Nanometerbereich für Magnetit und kommerzielles Fe(II,III)-Oxid bestätigt, während im Fall der Perowskite Aggregate aus einzelnen Nanopartikeln beobachtet wurden. Dies ist auf Aggregationsphänomene während der Hochtemperatur-Kalzinierung zurückzuführen. Die BET-Analyse ergab relativ niedrige spezifische Oberflächen (SSA) für $LaFeO_3$ (5,2 $m^2\,g^{-1}$) und $BiFeO_3$ (3,2 $m^2\,g^{-1}$) im Vergleich zum hergestellten Magnetit (95 $m^2\,g^{-1}$) und kommerziellen Fe(II,III)-Oxid (45 $m^2\,g^{-1}$).

Die katalytische Aktivität der hergestellten Materialien wurde in Batch-Experimenten unter Verwendung von Phenol als Modellverbindung und Wasserstoffperoxid als Oxidationsmittel getestet. In Batch-Experimenten bei Raumtemperatur und pH = 7, zeigten LaFeO$_3$ und BiFeO$_3$ eine höhere katalytische Aktivität (normiert auf die Katalysator-Massenkonzentration) und eine effizientere Nutzung von H$_2$O$_2$ im Vergleich zu den getesten einfachen Fe(II,III)-Oxiden.

Beispielsweise wurden Halbwertszeiten von Phenol von 2,5; 5 und > 24 h für BFO, LFO und kommerzielles Fe(II,III)-Oxid unter jeweils gleichen Reaktionsbedingungen bestimmt ($c_{0,phenol}$ = 25 mg L^{-1}, $c_{0,H2O2}$ = 3 g L^{-1}, and c_{cat} = 1 g L^{-1}, pH = 7 ± 0.2). Betrachtet man Oberflächen-normierte Geschwindigkeitskonstanten, so wird die Überlegenheit von BFO und LFO hinsichtlich ihrer katalytischen Aktivität gegenüber einfachen Fe(II,III)-oxiden noch deutlicher.

Es wurde weiterhin nachgewiesen, dass nanoskaliges Magnetit unter Fenton-Bedingungen einer schnellen Oxidation unterliegt und ausgehend von der Oberfläche bis hin zum Kern des Partikels in Maghemit (γ-Fe$_2$O$_3$) umgewandelt wird. Die Anwesenheit von Fe(II)-Resten im Nanopartikelkern scheint von untergeordneter Bedeutung für die katalytische Aktivität bei der Phenoloxidation mit H$_2$O$_2$ zu sein. Wenn jedoch der Fe(II)-Gehalt über das stöchiometrische Verhältnis von Magnetit angehoben wurde (durch Reduktion von kommerziellem Fe(II,III)- Oxid mit NaBH$_4$), wurde lediglich die nicht-produktive Zersetzung von H$_2$O$_2$ nicht jedoch der Phenolabbau beschleunigt. Weiterhin wurde die Katalysatoroberfläche von Fe(II,III)-Oxiden als wichtiger Verbraucher von reaktiven Spezies identifiziert, da beobachtet wurde, dass die Reaktionsgeschwindigkeit der Phenoloxidation relativ unempfindlich gegenüber einer Erhöhung der Katalysatorkonzentration im Bereich von 1-10 g L^{-1} ist, wobei die Partikelagglomeration eine wichtige Rolle zu spielen scheint. Basierend auf den erhaltenen Ergebnissen kann somit die Schlussfolgerung gezogen werden, dass Magnetit katalytische Eigenschaften für die H$_2$O$_2$-Aktivierung besitzt, jedoch erscheint seine intrinsische katalytische Aktivität als relativ gering, d.h. nicht ausreichend für die praktische Anwendung.

LFO und BFO wurden weiter unter verschiedenen Reaktionsbedingungen, insbesondere Variation der Katalysator- und H$_2$O$_2$-Konzentration, Reaktions-pH-Wert und Temperatur untersucht. Zusätzlich wurde die Stabilität und Wiederverwendbarkeit der Katalysatoren getestet, was eine Voraussetzung für die weitere praktische Anwendung

ist. Zusammengefasst ist festzustellen, dass BFO im Vergleich zu LFO bessere katalytische Eigenschaften aufwies, wenn Reaktionsbedingungen, wie Katalysatorkonzentration oder Temperatur variiert wurden, um hohe Reaktionsgeschwindigkeiten für den Phenolabbau zu erreichen. Zum Beispiel verbessert eine Erhöhung der Reaktionstemperatur von 20 °C auf 60 °C die Katalysatoraktivität von BFO um einen Faktor von 10, während LFO nur eine geringe Verbesserung zeigte. In vier aufeinanderfolgenden Reaktionen zeigte BFO eine konstante katalytische Aktivität, wobei in jedem Lauf die Konzentration des Modelschadstoffs Methyl-*tert*-butylether (MTBE) innerhalb von 6 h Reaktion bei 40 °C um 80% verringert wurde. Die höhere Aktivität des BFO-Perowskits wird auf die intrinsischen Eigenschaften des Materials zurückgeführt, wobei die Syntheseprozedur eine entscheidende Rolle spielen könnte (z.B. durch Bildung von Strukturdefekten und Fehlstellen an der Oberfläche oder Verunreinigungen).

Das letzte Manuskript beschäftigt sich mit den mechanistischen Aspekten der heterogenen Fenton-artigen Reaktion mit Perowskit-Nanokatalysatoren. Es wird oft angenommen, dass heterogene Fenton-artige Reaktionen in einer ähnlichen Weise wie die homogene Fenton-Reaktion über •OH als reaktive Spezies verlaufen. Bisher fehlen allerdings klare Beweise. In dieser Studie wurde die mit der Oxidation von zwei Modellverbindungen (MTBE und Ethyl-tert-butylether, ETBE) gekoppelte Kohlenstoff- und Wasserstoff-Isotopenfraktionierung untersucht, um Hinweise auf die reaktiven Spezies in LFO-und BFO-katalysierten Fenton-artigen Reaktionen bei neutralen pH-Bedingungen zu erhalten. Die beobachteten Fraktionierungseffekte für die Perowskit-katalysierte Reaktion wurden mit denen anderer chemischer Oxidationsprozesse (Permanganatoxidation, homogene Fenton- und Fenton-artige Oxidation (Fe^{3+} + H_2O_2)) verglichen. Die starke Ähnlichkeit in den beobachteten C-und H-Fraktionierungsfaktoren lässt vermuten, dass die Perowskit-katalysierte Oxidation über denselben Reaktionsweg wie die homogene Fenton-Reaktion, d.h. über •OH als dominierende reaktive Spezies, verläuft. Darüber hinaus dienten die für die abiotischen Oxidationsreaktionen ermittelten C- und H-Fraktionierungsfaktoren als Referenz für die Beurteilung der durch verschiedene Bakterienstämme genutzten Abbauwege für die Krafstoffzusatzstoffe MTBE und ETBE.

Bibliography

Ariafard, A., Aghabozorg, H.R., Salehirad, F., 2003. Hydrogen peroxide decomposition over $La_{0.9}Sr_{0.1}Ni_{1-x}Cr_xO_3$ perovskites. *Catal. Commun.* 4, 561-566.

Arnold, W.A., Ball, W.P., Roberts, A.L., 1999. Polychlorinated ethane reaction with zero-valent zinc: pathways and rate control. *J. Contam. Hydrol.* 40, 183-200.

Auffan, M., Rose, J., Bottero, J.Y., Lowry, G.V., Jolivet, J.P., Wiesner, M.R., 2009. Towards a definition of inorganic nanoparticles from an environmental, health and safety perspective. *Nature Nanotechnology* 4, 634-641.

Auffan, M., Rose, J., Proux, O., Borschneck, D., Masion, A., Chaurand, P., Hazemann, J.L., Chaneac, C., Jolivet, J.P., Wiesner, M.R., Van Geen, A., Bottero, J.Y., 2008. Enhanced adsorption of arsenic onto maghemites nanoparticles: As(III) as a probe of the surface structure and heterogeneity. *Langmuir* 24, 3215-3222.

Baldrian, P., Merhautova, V., Gabriel, J., Nerud, F., Stopka, P., Hruby, M., Benes, M.J., 2006. Decolorization of synthetic dyes by hydrogen peroxide with heterogeneous catalysis by mixed iron oxides. *Appl. Catal. B-Environ.* 66, 258-264.

Baldwin, B.R., Biernacki, A., Blair, J., Purchase, M.P., Baker, J.M., Sublette, K., Davis, G., Ogles, D., 2010. Monitoring gene expression to evaluate oxygen infusion at a gasoline-contaminated site. *Environ. Sci. Technol.* 44, 6829-6834.

Bastida, F., Rosell, M., Franchini, A.G., Seifert, J., Finsterbusch, S., Jehmlich, N., Jechalke, S., von Bergen, M., Richnow, H.H., 2010. Elucidating MTBE degradation in a mixed consortium using a multidisciplinary approach. *FEMS Microbiol. Ecol.* 73, 370-384.

Bazylinski, D.A., Frankel, R.B., Konhauser, K.O., 2007. Modes of biomineralization of magnetite by microbes. *Geomocrobiol. J.* 24, 465-475.

Bhatnagar, A., Minocha, A.K., 2006. Conventional and non-conventional adsorbents for removal of pollutants from water - A review. *Indian J. Chem. Techn.* 13, 203-217.

Botting, N.P., 1994. Isotope Effects in the Elucidation of Enzyme Mechanisms. *Nat. Prod. Rep.* 11, 337-353.

Breuer, U., Bäjen, C., Rohwerder, T., Müller, R.H., Harms, H., 2007. MTBE degradation genes of an Ideonella-like bacterium L108. *3rd European Conference on MTBE and Other Fuel Oxygenates, Atwerp, Belgium, 2007; Bastiaens; L., Ed.; VITO: Antwerp, Belgium*, 103.

Busch-Harris, J., Sublette, K., Roberts, K.P., Landrum, C., Peacock, A.D., Davis, G., Ogles, D., Holmes, W.E., Harris, D., Ota, C., Yang, X.M., Kolhatkar, A., 2008. Bio-Traps Coupled with Molecular Biological Methods and Stable Isotope Probing Demonstrate the In Situ Biodegradation Potential of MTBE and TBA in Gasoline-Contaminated Aquifers. *Ground Water Monit. Rem.* 28, 47-62.

Buxton, G.V., Greenstock, C.L., Helman, W.P., Ross, A.B., 1988. Critical review of rate constants for reactions of hydrated electrons, hydrogen atoms and hydroxyl radicals (OH/O^-) in aqueous solution. *J. Phys. Chem. Ref. Data* 17, 513-886.

Chan, K.H., Chu, W., 2003. Modeling the reaction kinetics of Fenton's process on the removal of atrazine. *Chemosphere* 51, 305-311.

Chauvaux, S., Chevalier, F., Le Dantec, C., Fayolle, F., Miras, I., Kunst, F., Beguin, P., 2001. Cloning of a genetically unstable cytochrome P-450 gene cluster involved in degradation of the pollutant ethyl tert-butyl ether by Rhodococcus ruber. *J. Bacteriol.* 183, 6551-6557.

Costa, R.C.C., Lelis, M.F.F., Oliveira, L.C.A., Fabris, J.D., Ardisson, J.D., Rios, R.R.V.A., Silva, C.N., Lago, R.M., 2006. Novel active heterogeneous Fenton system based on $Fe_{3-x}M_xO_4$ (Fe, Co, Mn, Ni): The role of M^{2+} species on the reactivity towards H_2O_2 reactions. *J. Hazard. Mater.* 129, 171-178.

Crimi, M.L., Siegrist, R.L., 2004. Impact of reaction conditions on MnO2 genesis during permanganate oxidation. *J. Environ. Eng.* 130, 562-572.

Danilchenko, S.N., Kukharenko, O.G., Moseke, C., Protsenko, I.Y., Sukhodub, L.F., Sulkio-Cleff, B., 2002. Determination of the bone mineral crystallite size and lattice strain from diffraction line broadening. *Cryst. Res. Technol.* 37, 1234-1240.

Dash, S., Patel, S., Mishra, B.K., 2009. Oxidation by permanganate: synthetic and mechanistic aspects. *Tetrahedron* 65, 707-739.

De, A.K., Chaudhuri, B., Bhattacharjee, S., Dutta, B.K., 1999. Estimation of ·OH radical reaction rate constants for phenol and chlorinated phenols using UV/H_2O_2 photo-oxidation. *J. Hazard. Mater.* 64, 91-104.

De Windt, W., Aelterman, P., Verstraete, W., 2005. Bioreductive deposition of palladium (0) nanoparticles on Shewanella oneidensis with catalytic activity towards reductive dechlorination of polychlorinated biphenyls. *Environ. Microbiol.* 7, 314-325.

Deng, J.H., Jiang, J.Y., Zhang, Y.Y., Lin, X.P., Du, C.M., Xiong, Y., 2008. FeVO$_4$ as a highly active heterogeneous Fenton-like catalyst towards the degradation of Orange II. *Appl. Catal. B-Environ.* 84, 468-473.

Dhakshinamoorthy, A., Navalon, S., Alvaro, M., Garcia, H., 2012. Metal Nanoparticles as Heterogeneous Fenton Catalysts. *Chemsuschem* 5, 46-64.

Ding, J.L., Lu, X.M., Shu, H.M., Xie, J.M., Zhang, H., 2010. Microwave-assisted synthesis of perovskite ReFeO3 (Re: La, Sm, Eu, Gd) photocatalyst. *Mater. Sci. Eng. B-Adv.* 171, 31-34.

Droege, A.T., Tully, F.P., 1987. Hydrogen-Atom Abstraction from Alkanes by OH .6. Cyclopentane and Cyclohexane. *J. Phys. Chem.* 91, 1222-1225.

Eisenberg, G., 1943. Colorimetric determination of hydrogen peroxide. *Ing. Eng. Chem. Anal. Ed.* 15, 327-328.

Elsner, M., Mckelvie, J., Couloume, G.L., Lollar, B.S., 2007. Insight into methyl tert-butyl ether (MTBE) stable isotope Fractionation from abiotic reference experiments. *Environ. Sci. Technol.* 41, 5693-5700.

Elsner, M., Zwank, L., Hunkeler, D., Schwarzenbach, R.P., 2005. A new concept linking observable stable isotope fractionation to transformation pathways of organic pollutants. *Environ. Sci. Technol.* 39, 6896-6916.

Espinosa, A., Serrano, A., Llavona, A., de la Morena, J.J., Abuin, M., Figuerola, A., Pellegrino, T., Fernandez, J.F., Garcia-Hernandez, M., Castro, G.R., Garcia, M.A., 2012. On the discrimination between magnetite and maghemite by XANES measurements in fluorescence mode. *Meas. Sci. Technol.* 23.

European Commission, Nanomaterials, http://ec.europa.eu/environment/chemicals/nanotech/index.htm.

Falcon, H., Carbonio, R.E., Fierro, J.L.G., 2001. Correlation of oxidation states in LaFe$_x$Ni$_{1-x}$O$_{3+\delta}$ oxides with catalytic activity for H$_2$O$_2$ decomposition. *J. Catal.* 203, 264-272.

Faye, J., Guelou, E., Barrault, J., Tatibouet, J.M., Valange, S., 2009. LaFeO$_3$ Perovskite as new and performant catalyst for the wet peroxide oxidation of organic pollutants in ambient conditions. *Top. Catal.* 52, 1211-1219.

Fayolle-Guichard, F., Durand, J., Cheucle, M., Rosell, M., Michelland, R.J., Tracol, J.P., Le Roux, F., Grundman, G., Atteia, O., Richnow, H.H., Dumestre, A., Benoit, Y., 2012. Study of an aquifer contaminated by ethyl tert-butyl ether

(ETBE): Site characterization and on-site bioremediation. *J. Hazard. Mater.* 201, 236-243.

Ferreira, N.L., Malandain, C., Fayolle-Guichard, F., 2006. Enzymes and genes involved in the aerobic biodegradation of methyl tert-butyl ether (MTBE). *Appl. Microbiol. Biotechnol.* 72, 252-262.

Francois, A., Garnier, L., Mathis, H., Fayolle, F., Monot, F., 2003. Roles of tert-butyl formate, tert-butyl alcohol and acetone in the regulation of methyl tert-butyl ether degradation by Mycobacterium austroafricanum IFP 2012. *Appl. Microbiol. Biotechnol.* 62, 256-262.

Garrido-Ramirez, E.G., Theng, B.K.G., Mora, M.L., 2010. Clays and oxide minerals as catalysts and nanocatalysts in Fenton-like reactions - A review. *Appl. Clay Sci.* 47, 182-192.

Gavaskar, A.R., 1999. Design and construction techniques for permeable reactive barriers. *J. Hazard. Mater.* 68, 41-71.

Gavaskar, A.R., Sass, B., Gupta, N., Drescher, E., Yoon, W.-S., Sminchak, J., Hicks, J., Condit, W., 2002. Final report evaluating the longevity and hydraulic performance of permeable reative barriers at department of defense sites. Battelle Press, Columbus, Ohio.

Georgi, A., Gonzalez-Olmos, R., Kohler, R., Kopinke, F.D., 2010. Fe-Zeolites as catalysts for wet peroxide oxidation of organic groundwater contaminants: mechanistic studies and applicability tests. *Sep. Sci. Technol.* 45, 1579-1586.

Georgi, A., Kopinke, F.D., 2005. Interaction of adsorption and catalytic reactions in water decontamination processes Part I. Oxidation of organic contaminants with hydrogen peroxide catalyzed by activated carbon. *Appl. Catal. B-Environ.* 58, 9-18.

Godart, C., Latroche, M., Fretigny, C., Levyclement, C., 1992. EXAFS Studies of synthetic gamma-MnO_2 and related pryolusite and ramsdellite minerals. *Phys. Status Solidi A.* 132, 253-268.

Gonzalez-Olmos, R., Georgi, A., Roland, U., Toufar, H., Kopinke, F.D., 2009a. Fe-zeolites as catalysts for chemical oxidation of MTBE in water with H_2O_2. *Appl. Catal. B-Environ.* 89, 356-364.

Gonzalez-Olmos, R., Holzer, F., Kopinke, F.D., Georgi, A., 2011. Indications of the reactive species in a heterogeneous Fenton-like reaction using Fe-containing zeolites. *Appl. Catal. A-Gen.* 398, 44-53.

Gonzalez-Olmos, R., Roland, U., Toufar, H., Kopinke, F.D., Georgi, A., 2009b. Fe-zeolites as catalysts for chemical oxidation of MTBE in water with H2O2. *Appl. Catal. B-Environ.* 89, 356-364.

Gorski, C.A., Scherer, M.M., 2009. Influence of magnetite stoichiometry on Fe(II) uptake and nitrobenzene reduction. *Environ. Sci. Technol.* 43, 3675-3680.

Gosavi, P.V., Biniwale, R.B., 2010. Pure phase LaFeO$_3$ perovskite with improved surface area synthesized using different routes and its characterization. *Mater. Chem. Phys.* 119, 324-329.

Gray, J.R., Lacrampe-Couloume, G., Gandhi, D., Scow, K.M., Wilson, R.D., Mackay, D.M., Lollar, B.S., 2002. Carbon and hydrogen isotopic fractionation during biodegradation of methyl tert-butyl ether. *Environ. Sci. Technol.* 36, 1931-1938.

Greenwood, N.N., Earnshaw, A., 1997. Chemistry of the Elements. Butterworth Heinemann.

Guimaraes, I.R., Oliveira, L.C.A., Queiroz, P.F., Ramalho, T.C., Pereira, M., Fabris, J.D., Ardisson, J.D., 2008. Modified goethites as catalyst for oxidation of quinoline: Evidence of heterogeneous Fenton process. *Appl. Catal. A-Gen.* 347, 89-93.

Guo, L.Q., Chen, F., Fan, X.Q., Cai, W.D., Zhang, J.L., 2010. S-doped alpha-Fe$_2$O$_3$ as a highly active heterogeneous Fenton-like catalyst towards the degradation of acid orange 7 and phenol. *Appl. Catal. B-Environ.* 96, 162-168.

Haber, F., Weiss, J., 1934. The catalytic decomposition of hydrogen peroxide by iron salts. *Proc. R. Soc. London, Ser. A.* 147, 332-351.

Hammel, C.F., Tuzinski, P.A., Boren, R.M., 2002. Pretreatment and Regeneration of Oxides of Manganese. United States Patent 7041270.

Hanna, K., Kone, T., Medjahdi, G., 2008. Synthesis of the mixed oxides of iron and quartz and their catalytic activities for the Fenton-like oxidation. *Catal. Commun.* 9, 955-959.

Harriot, P., 1962. Mass transfer to particles: Part I. Suspended in agitated tanks. *AIChE J.* 8, 93-101.

Hartmann, M., Kullmann, S., Keller, H., 2010. Wastewater treatment with heterogeneous Fenton-type catalysts based on porous materials. *J. Mater. Chem.* 20, 9002-9017.

Heiderscheidt, J.L., Crimi, M., Siegrist, R.L., Singletary, M.A., 2008. Optimization of full-scale permanganate ISCO system operation: laboratory and numerical studies. *Ground Water Monit. R.* 28, 72-84.

Hermes, J.D., Morrical, S.W., Oleary, M.H., Cleland, W.W., 1984. Variation of transition-state structure as a function of the nucleotide in reactions catalyzed by dehydrogenases .2. formate dehydrogenase. *Biochemistry* 23, 5479-5488.

Herney-Ramirez, J., Vicente, M.A., Madeira, L.M., 2010. Heterogeneous photo-Fenton oxidation with pillared clay-based catalysts for wastewater treatment: A review. *Appl. Catal. B-Environ.* 98, 10-26.

Hess, W.P., Tully, F.P., 1989. Hydrogen-Atom Abstraction from Methanol by OH. *J. Phys. Chem.* 93, 1944-1947.

Hildebrand, H., Kuhnel, D., Potthoff, A., Mackenzie, K., Springer, A., Schirmer, K., 2010. Evaluating the cytotoxicity of palladium/magnetite nano-catalysts intended for wastewater treatment. *Environ. Pollut.* 158, 65-73.

Hildebrand, H., Mackenzie, K., Kopinke, F.D., 2009. Highly Active Pd-on-magnetite nanocatalysts for aqueous phase hydrodechlorination reactions. *Environ. Sci. Technol.* 43, 3254-3259.

Horak, D., Babic, M., Mackova, H., Benes, M.J., 2007. Preparation and properties of magnetic nano- and microsized particles for biological and environmental separations. *J. Sep. Sci.* 30, 1751-1772.

House, A.J., Hyman, M.R., 2010. Effects of gasoline components on MTBE and TBA cometabolism by Mycobacterium austroafricanum JOB5. *Biodegradation* 21, 525-541.

Huang, K.C., Hoag, G.E., Chheda, P., Woody, B.A., Dobbs, G.M., 1999. Kinetic study of oxidation of trichloroethylene by potassium permanganate. *Environ. Eng. Sci.* 16, 265-274.

Huling, S.G., Pivetz, B.E., 2006. In-situ Chemical Oxidation - Engineering Issue. http://www.epa.gov/nrmrl/pubs/600r06072/600r06072.pdf.

Human Development Reports, United Nations Development Programme (UNDP), 2006.

Hunkeler, D., Butler, B.J., Aravena, R., Barker, J.F., 2001. Monitoring biodegradation of methyl tert-butyl ether (MTBE) using compound-specific carbon isotope analysis. *Environ. Sci. Technol.* 35, 676-681.

Hvolbaek, B., Janssens, T.V.W., Clausen, B.S., Falsig, H., Christensen, C.H., Norskov, J.K., 2007. Catalytic activity of Au nanoparticles. *Nano Today* 2, 14-18.

Iwahori, K., Yamashita, I., 2007. Bio-template synthesis of nanoparticle by cage-shaped protein supramolecule, apoferritin. *J. Clust. Sci.* 18, 358-370.

Jechalke, S., Rosell, M., Martinez-Lavanchy, P.M., Perez-Leiva, P., Rohwerder, T., Vogt, C., Richnow, H.H., 2011. Linking low-level stable isotope fractionation to expression of the cytochrome P450 monooxygenase-encoding ethB gene for elucidation of methyl tert-butyl ether biodegradation in aerated treatment pond systems. *Appl. Environ. Microbiol.* 77, 1086-1096.

Johnson, E.L., Smith, C.A., O'Reilly, K.T., Hyman, M.R., 2004. Induction of methyl tertiary butyl ether (MTBE)-oxidizing activity in Mycobacterium vaccae JOB5 by MTBE. *Appl. Environ. Microbiol.* 70, 1023-1030.

Ju, L.L., Chen, Z.Y., Fang, L., Dong, W., Zheng, F.G., Shen, M.R., 2011. Sol-gel synthesis and photo-Fenton-like catalytic activity of $EuFeO_3$ nanoparticles. *J. Am. Ceram. Soc.* 94, 3418-3424.

Kampfer, P., Kohlweyer, U., Thiemer, B., Andreesen, J.R., 2006. Pseudonocardia tetrahydrofuranoxydans sp nov. *Int. J. Syst. Evol. Microbiol.* 56, 1535-1538.

Kane, S.R., Chakicherla, A.Y., Chain, P.S.G., Schmidt, R., Shin, M.W., Legler, T.C., Scow, K.M., Larimer, F.W., Lucas, S.M., Richardson, P.M., Hristova, K.R., 2007. Whole-genome analysis of the methyl tert-butyl ether-degrading beta-proteobacterium Methylibium petroleiphilum PM1. *J. Bacteriol.* 189, 4973-4973.

Kang, N., Hua, I., Rao, P.S.C., 2004. Production and characterization of encapsulated potassium permanganate for sustained release as an in situ oxidant. *Ind. Eng. Chem. Res.* 43, 5187-5193.

Kim, Y.H., Engesser, K.H., Kim, S.J., 2007. Physiological, numerical and molecular characterization of alkyl ether-utilizing rhodococci. *Environ. Microbiol.* 9, 1497-1510.

Koenigsberg, S.S., Sandefur, C.A., 1999. The use of oxygen release compound for the accelerated bioremediation of aerobically degradable contaminants: the advent of time-release electron acceptors. *Remed. J.* 10, 3-29.

Kuder, T., Wilson, J.T., Kaiser, P., Kolhatkar, R., Philp, P., Allen, J., 2005. Enrichment of stable carbon and hydrogen isotopes during anaerobic biodegradation of MTBE: Microcosm and field evidence. *Environ. Sci. Technol.* 39, 213-220.

Kujawinski, D.M., Stephan, M., Jochmann, M.A., Krajenke, K., Haas, J., Schmidt, T.C., 2010. Stable carbon and hydrogen isotope analysis of methyl tert-butyl ether and tert-amyl methyl ether by purge and trap-gas chromatography-isotope ratio mass spectrometry: Method evaluation and application. *J. Environ. Monitor.* 12, 347-354.

Kwan, W.P., Voelker, B.M., 2004. Influence of electrostatics on the oxidation rates of organic compounds in heterogeneous Fenton systems. *Environ. Sci. Technol.* 38, 3425-3431.

Lago, R.M., Costa, R.C.C., Moura, F.C.C., Ardisson, J.D., Fabris, J.D., 2008. Highly active heterogeneous Fenton-like systems based on Fe^0/Fe_3O_4 composites prepared by controlled reduction of iron oxides. *Appl. Catal. B-Environ.* 83, 131-139.

Lechner, U., Brodkorb, D., Geyer, R., Hause, G., Hartig, C., Auling, G., Fayolle-Guichard, F., Piveteau, P., Muller, R.H., Rohwerder, T., 2007. Aquincola tertiaricarbonis gen. nov., sp nov., a tertiary butyl moiety-degrading bacterium. *Int. J. Syst. Evol. Microbiol.* 57, 1295-1303.

Lee, C., Sedlak, D.L., 2008. Enhanced formation of oxidants from bimetallic nickel-iron nanoparticles in the presence of oxygen. *Environ. Sci. Technol.* 42, 8528-8533.

Lee, E.S., Schwartz, F.W., 2007. Characteristics and applications of controlled-release $KMnO_4$ for groundwater remediation. *Chemosphere* 66, 2058-2066.

Lee, E.S., Woo, N.C., Schwartz, F.W., Lee, B.S., Lee, K.C., Woo, M.H., Kim, J.H., Kim, H.K., 2008. Characterization of controlled-release $KMnO_4$ (CRP) barrier system for groundwater remediation: A pilot-scale flow-tank study. *Chemosphere* 71, 902-910.

Lee, Y.N., Lago, R.M., Fierro, J.L.G., Gonzalez, J., 2001. Hydrogen peroxide decomposition over $Ln_{1-x}A_xMnO_3$ (Ln = La or Nd and A = K or Sr) perovskites. *Appl. Catal. A-Gen.* 215, 245-256.

Lesser, L.E., Johnson, P.C., Aravena, R., Spinnler, G.E., Bruce, C.L., Salanitro, J.P., 2008. An evaluation of compound-specific isotope analyses for assessing the

biodegradation of MTBE at Port Hueneme, CA. *Environ. Sci. Technol.* 42, 6637-6643.

Levenspiel O., 1972. Chemical Reaction Engineering. Chapter 14: Solid-catalyzed reactions, J. Wiley&Sons, New York.

Lopes Ferreira, N., Mathis, H., Labbe, D., Frederic, M., Greer, C.W., Fayolle-Guichard, F., 2007. n-Alkane assimilation and tert-butyl alcohol (TBA) oxidation capacity in Mycobacterium austroafricanum strains. *Appl. Microbiol. Biotechnol.* 75, 909-919.

Luo, W., Zhu, L.H., Wang, N., Tang, H.Q., Cao, M.J., She, Y.B., 2010. Efficient removal of organic pollutants with magnetic nanoscaled $BiFeO_3$ as a reusable heterogeneous Fenton-like catalyst. *Environ. Sci. Technol.* 44, 1786-1791.

Ma, S.B., Lee, Y.H., Ahn, K.Y., Kim, C.M., Oh, K.H., Kim, K.B., 2006. Spontaneously deposited manganese oxide on acetylene black in an aqueous potassium permanganate solution. *J. Electrochem. Soc.* 153, C27-C32.

Mackenzie, K., Schierz, A., Georgi, A., Kopinke, F.D., 2008. Colloidal activated carbon and carbo-iron - Novel materials for in-situ groundwater treatment. *Global Nest J.* 10, 54-61.

MacKinnon, L.K., Thomson, N.R., 2002. Laboratory-scale in situ chemical oxidation of a perchloroethylene pool using permanganate. *J. Contam. Hydrol.* 56, 49-74.

Magario, I., Einschlag, F.S.G., Rueda, E.H., Zygadlo, J., Ferreira, M.L., 2012. Mechanisms of radical generation in the removal of phenol derivatives and pigments using different Fe-based catalytic systems. *J. Mol. Catal. A-Chem.* 352, 1-20.

Malandain, C., Fayolle-Guichard, F., Vogel, T.M., 2010. Cytochromes P450-mediated degradation of fuel oxygenates by environmental isolates. *FEMS Microbiol. Ecol.* 72, 289-296.

Mariotti, A., Germon, J.C., Hubert, P., Kaiser, P., Letolle, R., Tardieux, A., Tardieux, P., 1981. Experimental-determination of nitrogen kinetic isotope fractionation - some principles - illustration for the denitrification and nitrification processes. *Plant Soil* 62, 413-430.

Martin, R., Navalon, S., Alvaro, M., Garcia, H., 2011. Optimized water treatment by combining catalytic Fenton reaction using diamond supported gold and biological degradation. *Appl. Catal. B-Environ.* 103, 246-252.

Matta, R., Hanna, K., Kone, T., Chiron, S., 2008. Oxidation of 2,4,6-trinitrotoluene in the presence of different iron-bearing minerals at neutral pH. *Chem. Eng. J.* 144, 453-458.

McKelvie J.R., Elsner M., Simpson A.J., Lollar B.S., Simpson M.J. 2010. Quantitative site-specific ^{2}H NMR investigation of MTBE: Potential for assessing contaminant sources and Fate. *Environ. Sci. Technol.* 44, 1062-1068.

McKelvie J.R., Hyman, M.R., Elsner, M., Smith, C., Aslett, D.M., Lacrampe-Couloume, G., Lollar, B.S., 2009. Isotopic fractionation of methyl tert-butyl ether suggests different initial reaction mechanisms during aerobic biodegradation. *Environ. Sci. Technol.* 43, 2793-2799.

McKinney, D.C., Lin, M.D., 1996. Pump and treat ground-water remediation system optimization. *J. Water Res. Pl.-Asce* 122, 128-136.

Mcmillen, D.F., Golden, D.M., 1982. Hydrocarbon bond-dissociation energies. *Annu. Rev. Phys. Chem.* 33, 493-532.

Meckenstock, R.U., Morasch, B., Griebler, C., Richnow, H.H., 2004. Stable isotope fractionation analysis as a tool to monitor biodegradation in contaminated acquifers. *J. Contam. Hydrol.* 75, 215-255.

Melero, J.A., Sotelo, J.L., Ovejero, G., Martinez, F., Milieni, A., 2004. Catalytic wet peroxide oxidation of phenolic solutions over a $LaTi_{1-x}Cu_xO_3$ perovskite catalyst. *Appl. Catal. B-Environ.* 47, 281-294.

Müller, R.H., Rohwerder, T., Harms, H., 2007. Carbon conversion efficiency and limits of productive bacterial degradation of methyl tert-butyl ether and related compounds. *Appl. Environ. Microbiol.* 73, 1783-1791.

Müller, R.H., Rohwerder, T., Harms, H., 2008. Degradation of fuel oxygenates and their main intermediates by Aquincola tertiaricarbonis L108. *Microbiol.-Sgm* 154, 1414-1421.

Munter, R., 2001. Advanced oxidation processes–current Status and prospects. *Proc. Estonian Acad. Sci. Chem.* 50, 59-80.

Mylon, S.E., Sun, Q.A., Waite, T.D., 2010. Process optimization in use of zero valent iron nanoparticles for oxidative transformations. *Chemosphere* 81, 127-131.

Nakatsu, C.H., Hristova, K., Hanada, S., Meng, X.Y., Hanson, J.R., Scow, K.M., Kamagata, Y., 2006. Methylibium petrolelphilum gen. nov., sp nov., a novel

methyl tert-butyl ether-degrading methylotroph of the Betaproteobacteria. *Int. J. Syst. Evol. Microbiol.* 56, 983-989.

Navalon, S., Alvaro, M., Garcia, H., 2010a. Heterogeneous Fenton catalysts based on clays, silicas and zeolites. *Appl. Catal. B-Environ.* 99, 1-26.

Navalon, S., Martin, R., Alvaro, M., Garcia, H., 2010b. Gold on diamond nanoparticles as a highly efficient Fenton catalyst. *Angew. Chem. Int. Edit.* 49, 8403-8407.

Niu, H.Y., Zhang, D., Zhang, S.X., Zhang, X.L., Meng, Z.F., Cai, Y.Q., 2011. Humic acid coated Fe_3O_4 magnetic nanoparticles as highly efficient Fenton-like catalyst for complete mineralization of sulfathiazole. *J. Hazard. Mater.* 190, 559-565.

Northrop, D.B., 1981. The Expression of Isotope Effects on Enzyme-Catalyzed Reactions. *Annu. Rev. Biochem.* 50, 103-131.

NDRL/NIST Solution Kinetics Database on the WEB, http://kinetics.nist.gov/kinetics/index.jsp

Nurmi, J.T., Tratnyek, P.G., Sarathy, V., Baer, D.R., Amonette, J.E., Pecher, K., Wang, C.M., Linehan, J.C., Matson, D.W., Penn, R.L., Driessen, M.D., 2005. Characterization and properties of metallic iron nanoparticles: Spectroscopy, electrochemistry, and kinetics. *Environ. Sci. Technol.* 39, 1221-1230.

Pena, M.A., Fierro, J.L.G., 2001. Chemical structures and performance of perovskite oxides. *Chem. Rev.* 101, 1981-2017.

Pera-Titus, M., Garcia-Molina, V., Banos, M.A., Gimenez, J., Esplugas, S., 2004. Degradation of chlorophenols by means of advanced oxidation processes: a general review. *Appl. Catal. B-Environ.* 47, 219-256.

Perathoner, S., Centi, G., 2005. Wet hydrogen peroxide catalytic oxidation (WHPCO) of organic waste in agro-food and industrial streams. *Top. Catal.* 33, 207-224.

Pham, A.L.T., Lee, C., Doyle, F.M., Sedlak, D.L., 2009. A silica supported iron oxide catalyst capable of activating hydrogen peroxide at neutral pH values. *Environ. Sci. Technol.* 43, 8930-8935.

Pignatello, J.J., Liu, D., Huston, P., 1999. Evidence for an additional oxidant in the photoassisted Fenton reaction. *Environ. Sci. Technol.* 33, 1832-1839.

Pignatello, J.J., Oliveros, E., MacKay, 2006a. Advanced Oxidation Processes for Organic Contaminant Destruction Based on the Fenton Reaction and Related Chemistry. Crit. *Rev. Env. Sci. Technol.* 36, 1-84.

Progress on Sanitation and Drinking-Water, World Health Organization (WHO)/United Nations International Children's Fund (UNICEF) Joint Monitoring Programme for Water Supply and Monitoring. 2010.

Regenesis Bioremediation Products, Oxygen Release Compounds (ORC).1996.

Rey, A., Faraldos, M., Casas, J.A., Zazo, J.A., Bahamonde, A., Rodriguez, J.J., 2009. Catalytic wet peroxide oxidation of phenol over Fe/AC catalysts: Influence of iron precursor and activated carbon surface. *Appl. Catal. B-Environ.* 86, 69-77.

Rohwerder, T., Breuer, U., Benndorf, D., Lechner, U., Muller, R.H., 2006. The alkyl tert-butyl ether intermediate 2-hydroxyisobutyrate is degraded via a novel cobalamin-dependent mutase pathway. *Appl. Environ. Microbiol.* 72, 4128-4135.

Rosell, M., Barcelo, D., Rohwerder, T., Breuer, U., Gehre, M., Richnow, H.H., 2007a. Variations in C-13/C-12 and D/H enrichment factors of aerobic bacterial fuel oxygenate degradation. *Environ. Sci. Technol.* 41, 2036-2043.

Rosell, M., Finsterbusch, S., Jechalke, S., Hubschmann, T., Vogt, C., Richnow, H.H., 2010. Evaluation of the effects of low oxygen concentration on stable isotope fractionation during aerobic MTBE biodegradation. *Environ. Sci. Technol.* 44, 309-315.

Rosell, M., Gonzalez-Olmos, R., Rohwerder, T., Rusevova, K., Georgi, A., Kopinke, F.D., Richnow, H.H., 2012. Critical evaluation of the 2D-CSIA scheme for distinguishing fuel oxygenate degradation reaction mechanisms. *Environ. Sci. Technol.* 46, 4757-4766.

Rosell, M., Lacorte, S., Barcelo, D., 2007b. Occurrence and Fate of MTBE in the Aquatic Environment Over the Last Decade. In *Fuel Oxygenates;* Barceló, D., Ed.; Springer-Verlag: Berlin Heidelberg, Germany 5, Part R, 31-55.

Ross, C., Murdoch, L.C., Freedman, D.L., Siegrist, R.L., 2005. Characteristics of potassium permanganate encapsulated in polymer. *J. Environ. Eng.* 131, 1203-1211.

Rotello, V.M., 2004. Nanoparticles: Building Blocks for Nanotechnology New York.

Rusevova, K., Kopinke, F.D., Georgi, A., 2012. Nano-sized magnetic iron oxides as catalysts for heterogeneous Fenton-like reactions - influence of Fe(II)/Fe(III) ratio on catalytic performance. *J. Hazard. Mater.*, DOI: 10.1016/j.jhazmat.2012.09.068

Savage, N., Diallo, M.S., 2005. Nanomaterials and water purification: Opportunities and challenges. *J. Nanopart. Res.* 7, 331-342.

Schafer, F., Muzica, L., Schuster, J., Treuter, N., Rosell, M., Harms, H., Muller, R.H., Rohwerder, T., 2011. Formation of alkenes via degradation of tert-alkyl ethers and alcohols by aquincola tertiaricarbonis L108 and methylibium spp. *Appl. Environ. Microbiol.* 77, 5981-5987.

Scharschmidt, M., Fisher, M.A., Cleland, W.W., 1984. Variation of transition-state structure as a function of the nucleotide in reactions catalyzed by dehydrogenases .1. Liver alcohol-dehydrogenase with benzyl alcohol and yeast aldehyde dehydrogenase with benzaldehyde. *Biochemistry* 23, 5471-5478.

Scherer, M.M., Gorski, C.A., Nurmi, J.T., Tratnyek, P.G., Hofstetter, T.B., 2010. Redox behavior of magnetite: implications for contaminant reduction. *Environ. Sci. Technol.* 44, 55-60.

Schmidt, H.J., Schafer, H.J., 1979. Oxidation of hydrocarbons with benzyl(triethyl)ammonium permanganate. *Angew. Chem.-Int. Ed.* 18, 68-69.

Schmidt, R., Battaglia, V., Scow, K., Kane, S., Hristova, K.R., 2008. Involvement of a novel enzyme, MdpA, in methyl tert-butyl ether degradation in methylibium petroleiphilum PM1. *Appl. Environ. Microbiol.* 74, 6631-6638.

Schmidt, T.C., Zwank, L., Elsner, M., Berg, M., Meckenstock, R.U., Haderlein, S.B., 2004. Compound-specific stable isotope analysis of organic contaminants in natural environments: a critical review of the state of the art, prospects, and future challenges. *Anal. Bioanal. Chem.* 378, 283-300.

Schramm, V.L., 2007. Enzymatic transition state theory and transition state analogue design. *J. Biol. Chem.* 282, 28297-28300.

Seiyama, T., 1992. Total oxidation of hydrocarbons on perovskite oxides. *Catal. Rev.* 34, 281-300.

Shaabani, A., Lee, D.G., 2001. Solvent free permanganate oxidations. *Tetrahedron Lett.* 42, 5833-5836.

Shaabani, A., Mirzaei, P., Naderi, S., Lee, D.G., 2004. Green oxidations. The use of potassium permanganate supported on manganese dioxide. *Tetrahedron* 60, 11415-11420.

Shabbir, G., Qureshi, A.H., Saeed, K., 2006. Nano-crystalline $LaFeO_3$ powders synthesized by the citrate-gel method. *Mater. Lett.* 60, 3706-3709.

Siegrist, R.L., Urynowicz, M.A., West, O.R., Crimi, M.L., Lowe, K.S., 2001. Principles and Practices of in Situ Chemical Oxidation Using Permanganate. Battelle Press, Columbus, Ohio.

Sinquin, G., Petit, C., Libs, S., Hindermann, J.P., Kiennemann, A., 2001. Catalytic destruction of chlorinated C-2 compounds on a $LaMnO_{3+\delta}$ perovskite catalyst. *Appl. Catal. B-Environ.* 32, 37-47.

Smith, C.A., Hyman, M.R., 2004. Oxidation of methyl tert-butyl ether by alkane hydroxylase in dicyclopropylketone-induced and n-octane-grown Pseudomonas putida GPo1. *Appl. Environ. Microbiol.* 70, 4544-4550.

Smith, C.A., Hyman, M.R., 2010. Oxidation of gasoline oxygenates by closely related non-haem-iron alkane hydroxylases in Pseudomonas mendocina KR1 and other n-octane-utilizing Pseudomonas strains. *Environ. Microbiol. Rep.* 2, 426-432.

Soleymani, M., Moheb, A., Babakhani, D., 2011. Hydrogen peroxide decomposition over nanosized $La_{1-x}Ca_xMnO_3$ ($0 <= X <= 0.6$) perovskite oxides. *Chem. Eng. Technol.* 34, 49-55.

Soon, A.N., Hameed, B.H., 2011. Heterogeneous catalytic treatment of synthetic dyes in aqueous media using Fenton and photo-assisted Fenton process. *Desalination* 269, 1-16.

Stefan, M.I., Mack, J., Bolton, J.R., 2000. Degradation pathways during the treatment of methyl tert-butyl ether by the UV/H2O2 process. *Environ. Sci. Technol.* 34, 650-658.

Stucki, J.W., Anderson, W.L., 1981. The quantitative assay of minerals for Fe^{2+} and Fe^{3+} using 1,10-Phenanthroline:1.sources of vvariability. *Soil Sci. Soc. Am. J.* 45, 633-637.

Su, H.J., Jing, L.Q., Shi, K.Y., Yao, C.H., Fu, H.G., 2010. Synthesis of large surface area $LaFeO_3$ nanoparticles by SBA-16 template method as high active visible photocatalysts. *J. Nanopart. Res.* 12, 967-974.

Sun, S.M., Wang, W.Z., Zhang, L., Shang, M., 2009. Visible light-induced photocatalytic oxidation of phenol and aqueous ammonia in flowerlike $Bi_2Fe_4O_9$ suspensions. *J. Phys. Chem. C.* 113, 12826-12831.

Sun, Y.K., Ma, M., Zhang, Y., Gu, N., 2004. Synthesis of nanometer-size maghemite particles from magnetite. *Colloid Surf. A-Physicochem. Eng. Asp.* 245, 15-19.

Sun, Z.X., Su, F.W., Forsling, W., Samskog, P.O., 1998. Surface characteristics of magnetite in aqueous suspension. *J. Colloid. Interface Sci.* 197, 151-159.

Tanaka, H., 2005. An intelligent catalyst: the self-regenerative palladium-perovskite catalyst for automotive emissions control. *Catal. Surv. Asia* 9, 63-74.

Tang, J., Myers, M., Bosnick, K.A., Brus, L.E., 2003. Magnetite Fe_3O_4 nanocrystals: Spectroscopic observation of aqueous oxidation kinetics. *J. Phys. Chem. A* 107, 7501-7506.

The European Fuel Oxygenates Association (EFOA) Technological developments. http://www.efoa.eu/en/markets/ether-market-drivers-and-future-developments/technological-developments.aspx.

The European Fuel Oxygenates Association (EFOA) Ether Facts and Figures. http://www.efoa.eu/en/markets/ether-facts-and-figures.aspx.

Thiemer, B., Andreesen, J.R., Schrader, T., 2003. Cloning and characterization of a gene cluster involved in tetrahydrofuran degradation in Pseudonocardia sp strain K1. *Arch. Microbiol.* 179, 266-277.

Tiwari, D.K., Behari, J., Sen, P., 2008. Application of nanoparticles in waste water treatment. *World Appl. Sci. J.* 3, 417-433.

Tratnyek, P.G., Johnson, R.L., 2006. Nanotechnologies for environmental cleanup. *Nano Today* 1, 44-48.

Tully, F.P., 1988. Hydrogen-atom abstraction from alkenes by OH - ethene and 1-butene. *Chem. Phys. Lett.* 143, 510-514.

Urynowicz, M.A., 2008. In situ chemical oxidation with permanganate: Assessing the competitive interactions between target and nontarget compounds. *Soil Sediment. Contam.* 17, 53-62.

Vainberg, S., McClay, K., Masuda, H., Root, D., Condee, C., Zylstra, G.J., Steffan, R.J., 2006. Biodegradation of ether pollutants by Pseudonocardia sp strain ENV478. *Appl. Environ. Microbiol.* 72, 5218-5224.

Valdes-Solis, T., Valle-Vigon, P., Alvarez, S., Marban, G., Fuertes, A.B., 2007. Manganese ferrite nanoparticles synthesized through a nanocasting route as a highly active Fenton catalyst. *Catal. Commun.* 8, 2037-2042.

van Beilen, J.B., Funhoff, E.G., 2007. Alkane hydroxylases involved in microbial alkane degradation. *Appl. Microbiol. Biotechnol.* 74, 13-21.

van Beilen, J.B., Smits, T.H.M., Roos, F.F., Brunner, T., Balada, S.B., Rothlisberger, M., Witholt, B., 2005. Identification of an amino acid position that determines the substrate range of integral membrane alkane hydroxylases. *J. Bacteriol.* 187, 85-91.

Van Breukelen, B.M., 2007. Extending the Rayleigh equation to allow competing isotope fractionating pathways to improve quantification of biodegradation. *Environ. Sci. Technol.* 41, 4004-4010.

van Wezel, A., Puijker, L., Vink, C., Versteegh, A., de Voogt, P., 2009. Odour and flavour thresholds of gasoline additives (MTBE, ETBE and TAME) and their occurrence in Dutch drinking water collection areas. *Chemosphere* 76, 672-676.

Velleitner, N.K., Papailhou, A.L., Croue, J.P., Peyrot, J., Dore, M., 1994. Oxidation of methyl tert-butyl ether (MTBE) and ethyl tert-butyl ether (ETBE) by ozone and combined ozone hydrogen peroxide. *Ozone-Sci. Eng.* 16, 41-54.

Vikesland, P.J., Heathcock, A.M., Rebodos, R.L., Makus, K.E., 2007. Particle size and aggregation effects on magnetite reactivity toward carbon tetrachloride. *Environ. Sci. Technol.* 41, 5277-5283.

Voelker, B.M., Kwan, W.P., 2003. Rates of hydroxyl radical generation and organic compound oxidation in mineral-catalyzed Fenton-like systems. *Environ. Sci. Technol.* 37, 1150-1158.

Waldemer, R.H., Tratnyek, P.G., 2006. Kinetics of contaminant degradation by permanganate. *Environ. Sci. Technol.* 40, 1055-1061.

Wang, Y.L., Xia, Y.N., 2004. Bottom-up and top-down approaches to the synthesis of monodispersed spherical colloids of low melting-point metals. *Nano Letters* 4, 2047-2050.

Weaver, J.E., Exum, L.R., Prieto, L.M., 2010. Gasoline Composition Regulations Affecting LUST Sites. EPA/600/R-10/001; Office of Research and Development, United States Environmental Protection Agency: Washington, DC, January 20010.

Wu, J.J., Muruganandham, M., Yang, J.S., Lin, S.S., 2006. Oxidation of DMSO on goethite catalyst in the presence of H_2O_2 at neutral pH. *Catal. Commun.* 7, 901-906.

Xue, X.F., Hanna, K., Deng, N.S., 2009a. Fenton-like oxidation of Rhodamine B in the presence of two types of iron (II, III) oxide. *J. Hazard. Mater.* 166, 407-414.

Xue, X.F., Hanna, K., Despas, C., Wu, F., Deng, N.S., 2009b. Effect of chelating agent on the oxidation rate of PCP in the magnetite/H2O2 system at neutral pH. *J. Mol. Catal. A-Chem.* 311, 29-35.

Yavuz, C.T., Mayo, J.T., Yu, W.W., Prakash, A., Falkner, J.C., Yean, S., Cong, L.L., Shipley, H.J., Kan, A., Tomson, M., Natelson, D., Colvin, V.L., 2006. Low-field magnetic separation of monodisperse Fe_3O_4 nanocrystals. *Science* 314, 964-967.

Youngster, L.K.G., Rosell, M., Richnow, H.H., Haggblom, M.M., 2010. Assessment of MTBE biodegradation pathways by two-dimensional isotope analysis in mixed bacterial consortia under different redox conditions. *Appl. Microbiol. Biotechnol.* 88, 309-317.

Zach-Maor, A., Semiat, R., Shemer, H., 2011. Removal of heavy metals by immobilized magnetite nano-particles. *Desalin. Water Treat.* 31, 64-70.

Zhang N., Schindelka J., Herrmann H., Rosell M., Martín S. H., Richnow H. H. 2012. Two dimensional isotope analysis to characterize photooxidation reaction mechanism of fuel oxygenates by UV/H_2O_2 process. Book of Abstracts, *Joint European Stable Isotope Users Group Meeting*, JESIUM 2012, Leipzig.

Zhang, W.X., 2003. Nanoscale iron particles for environmental remediation: An overview. *J. Nanopart. Res.* 5, 323-332.

Zhou, H., Smith, D.W., 2001. Advanced technologies in water and wastewater treatment. *Can. J. Civil. Eng.* 28, 49-66.

Zhou, T., Li, Y.Z., Ji, J., Wong, F.S., Lu, X.H., 2008. Oxidation of 4-chlorophenol in a heterogeneous zero valent iron/H_2O_2 Fenton-like system: Kinetic, pathway and effect factors. *Sep. Purif. Technol.* 62, 551-558.

Zhuang, Y.A., Ahn, S., Luthy, R.G., 2010. Debromination of polybrominated diphenyl ethers by nanoscale zerovalent iron: Pathways, kinetics, and reactivity. *Environ. Sci. Technol.* 44, 8236-8242.

Zwank, L., Berg, M., Elsner, M., Schmidt, T.C., Schwarzenbach, R.P., Haderlein, S.B., 2005. New evaluation scheme for two-dimensional isotope analysis to decipher biodegradation processes: Application to groundwater contamination by MTBE. *Environ. Sci. Technol.* 39, 1018-1029.

Acknowledgments

First of all I would like to thank my advisor Prof. Dr. Frank-Dieter Kopinke for giving me the opportunity to work in his research group. I gratefully acknowledge his support, guidance and never-ending valuable ideas.

I would like to thank Dr. Anett Georgi, who has provided me with enormous amounts of guidance and freedom over my PhD work. She taught me to analyze my data carefully, to write well and more importantly to think deeply about my research topic.

This way I would like to thank Dr. Katrin Mackenzie, whose door was always open for my questions, and also the colleagues from the Department of Environmental Engineering, who have been friendly and helpful to me.

Special thanks to Prof. Dr. Francisco Medina Cabello, Dr. Sandra Contreras and the CATHETER group for cooperation and friendly environment during my internship.

Lastly, I thank Oscar Osegueda for his encouragement and being here for me as well as my parents for their support in all aspects of my life.

Curriculum vitae

Name: Klara Rusevova
Date of Birth: 10th October 1983
Place of Birth: Plovdiv, BG
Nationality: Czech Republic

Education

05/2009 - present	**Doctoral candidate in chemistry** Faculty of Chemistry and Mineralogy, University of Leipzig. *"Novel colloidal reagents and catalysts for oxidation of organic pollutants in water"* Supervised by Prof. Frank-Dieter Kopinke and Dr. Anett Georgi, conducted at Department of Environmental Engineering, Helmholtz Centre for Environmental Research - UFZ, Leipzig
09/2003 – 06/2008	**Master of Science in chemistry** Faculty of Environmental Technology, Institute of Chemical Technology of Prague, Czech Republic *"Laboratory scale test design for in situ chemical oxidation technique"*
09/1995 – 06/2003	**Gymnasium Prague**

Special qualification

05/2009 - present	Member of The Excellence Graduate School Leipzig School of Natural Sciences "Building with Molecules and Nano-objects" (BuildMoNa) supported by the Deutsche Forschungsgemeinschaft (DFG)
03 - 05/2011	Internship at Department of Chemical Engineering (in the group of Heterogeneous Catalysis), University Rovira i Virgili, Tarragona, Spain *"Preparation and characterization of supported nanocatalysts for oxidation approaches in water treatment"*
10/2008 - 05/2009	Internship at Department of Environmental Engineering, Helmholtz Centre for Environmental Research - UFZ, Leipzig *"Novel approaches for in situ chemical oxidation with permanganate"*
03 - 07/2007	ERASMUS program at the Faculty of Mechanical & Energy Engineering, Leipzig University of Applied Science

Scientific activities

Publications

K. Rusevova, F.-D. Kopinke, A. Georgi. Stabilization of potassium permanganate particles with manganese dioxide. *Chemosphere*, **2012**, 86, 783-788

M. Rosell, R. González-Olmos, T. Rohwerder, **K. Rusevova**, A. Georgi, F.-D. Kopinke and H. H. Richnow. Critical evaluation of the 2D-CSIA scheme for distinguishing fuel oxygenates degradation reaction mechanisms. *Environ. Sci. Technol.*, **2012**, 46 (9), 4757–4766

K. Rusevova, F.-D. Kopinke, A. Georgi. Nano-sized magnetic iron oxides as catalysts for heterogeneous Fenton-like reactions: Influence of $Fe(II)/Fe(III)$ ratio on catalytic performance. *J. Hazard. Mater.* **2012**, *accepted* (DOI: 10.1016/j.jhazmat.2012.09.068).

K. Rusevova, A. Georgi, R. Köferstein, M. Rosell, F.-D. Kopinke. $LaFeO_3$ and $BiFeO_3$ perovskites as nanocatalysts for contaminant degradation in heterogeneous Fenton-like reaction. **2012**, *submitted.*

Conference contributions

6th IWA Specialist Conference on Oxidation technologies for Water and Wastewater Treatment, Goslar, Germany, 7-9 May 2012
"Nanoscale iron-containing perovskites as efficient catalysts for wet peroxide oxidation of organic contaminants"

IWA Regional Conference on Wastewater Purification & Reuse, Heraklion (Crete), Greece, 28-30 March 2012
"Fe-based perovskites as efficient catalysts for wet peroxide oxidation of organic contaminants"

8th UFZ-PhD Conference, Leipzig, 26 May 2011
"Get rid of the wastewater: Iron-based catalysts for pollutant oxidation in water"

4th BuildMoNa Workshop, Dresden, 26-27 September 2011
"Nanoscale iron-based catalysts for the oxidation of pollutants in water"

8th International Nanotechnology Symposium – Nanofair, Dresden, Germany, 6-7 July 2010
"Iron-based nanoparticles catalysts for oxidation of pollutants in water"

41st CUSO Summer School in Chemistry: From Structure to Function in Nanomaterials, Villars Switzerland, 22-26 August 2010

Leipzig, October 2012

Novel Colloidal Catalysts and Reagents for Oxidation of
Organic Pollutants in Water

Der Fakultät für Chemie und Mineralogie der Universität Leipzig

eingereicht von

M.Sc. Klara Rusevova

Im Oktober 2012

Angefertigt im Department Technische Umweltchemie am Helmholtz-Zentrum für
Umweltforschung - UFZ in Leipzig und am Institut für Technische Chemie der
Universität Leipzig

Background and Motivation

Chemical oxidation processes have emerged as a powerful and versatile tool for
treatment of organically contaminated water streams. Oxidation processes are highly
attractive for several reasons: i) high achievable reaction rates, ii) potential to reduce
toxicity and potentially complete mineralization of treated contaminants, iii) no
concentration of waste for further treatment (e.g., as in case of membrane filtration or
sorption on activated carbon), and iv) non-selective degradation allowing the treatment
of highly recalcitrant pollutants and pollutant mixtures at once. Low selectivity towards
different targets can be an advantage or a disadvantage depending on the circumstances.
Groundwater remediation by means of *in situ* chemical oxidation (ISCO) became a
widely applied approach world-wide. The most developed technique is based on the
oxidation with potassium permanganate ($KMnO_4$). $KMnO_4$ was recognized to be an
effective oxidant for remediation of non-aqueous phase liquids (NAPL) such as
tetrachloroethene, which are used in many commercial processes.

Advanced oxidation processes (AOPs) are highly suitable when dealing with clean up of wastewaters and industrial effluents, which are often loaded with different types of recalcitrant pollutants. AOPs are based on generation of highly reactive oxygen species such as hydroxyl radicals ($\cdot$OH) which can effectively attack a wide range of organic compounds. Fenton reagent, consisting of a homogeneous solution of iron ions and hydrogen peroxide (H_2O_2), is a broadly applied means for generation of $\cdot$OH.

Although ISCO with $KMnO_4$ and Fenton oxidation are considered as efficient treatment techniques with respect to the contaminant degradation, in a large scale they face several shortcomings. Thus, the main aim of the present study is to propose and test novel strategies, where integration of colloidal reagents and catalysts plays the key role.

Practical significance of the study

The main drawbacks of ISCO with permanganate are associated to i) high consumption of the oxidant by non-target compounds present in the subsurface and ii) non-uniform distribution of permanganate in the treatment zone, which can result in zones of incomplete contaminant degradation. This problem can be reduced by designing a new delivery system based on a solid barrier for passive remediation, where the oxidant remains active for long periods. This concept is well known for the reductive treatment with zero-valent iron. However, for ISCO such a technique was not developed so far. The reason for this leak is the non-availability of long-living, less water soluble strong oxidants.

Thus, the aim of this study was to invent a novel approach for stabilization of $KMnO_4$ particles, which can be introduced into the contaminated zone in form of a suspension and remains active over a period of months to years. Furthermore, to obtain an oxidant with sufficient mobility in porous matrices and to reach captured contaminants (NAPL phase), it is highly desirable to fabricate stabilized $KMnO_4$ particles in the lower micrometer to sub-micrometer range.
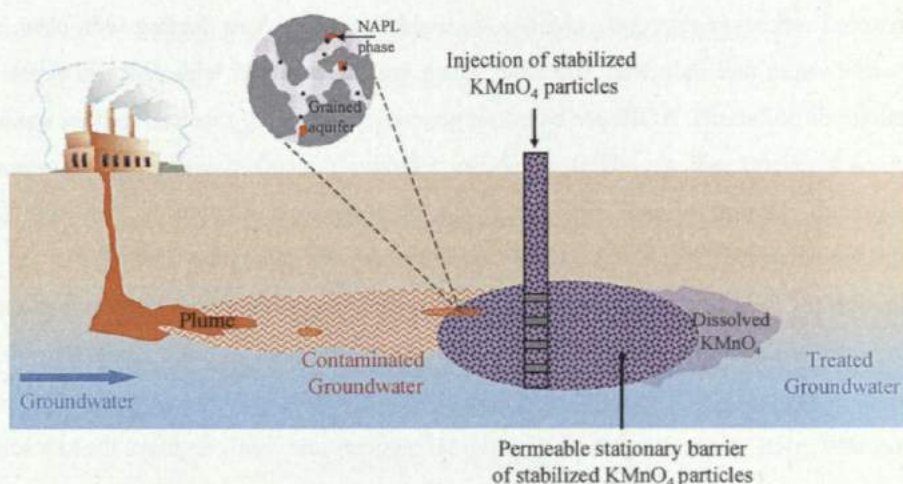
Fig. 1. Concept of application of stabilized KMnO$_4$ particles as a slow-release oxidant in a contaminated aquifer.

With respect to the homogeneous Fenton reaction, the major problems are related to the i) low working pH (about pH 3) in order to achieve high reaction rates and ii) production of precipitated wastes, mostly in form of iron sludge, which requires their subsequent removal. An alternative to the conventional Fenton reagent is based on the implementation of solid catalysts in so-called heterogeneous Fenton-like reactions. An ideal catalyst exhibits a high reactivity towards removal of various contaminants, efficient H$_2$O$_2$ utilization, stability over a broad range of working conditions (pH, temperature), and is environmentally benign. Moreover, when the catalyst size is reduced to the nanometre range, two main factors can improve the catalyst performance: i) a higher surface-to-volume ratio and ii) if non-supported nanocatalysts are used, little or no mass transfer restrictions are expected.
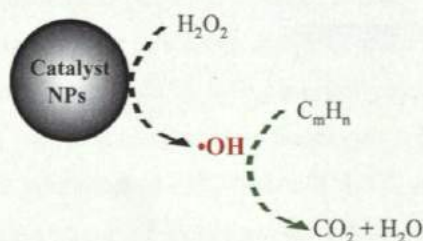

Fig. 2. A simplified scheme of the reaction pathways in heterogeneous Fenton-like reactions using non-supported Fe-containing catalyst NPs.

In a second part, this study is focused on the replacement of conventional Fenton reagent (*i.e.* dissolved iron) by iron-containing nanocatalysts in order to improve the overall performance and versatility of the Fenton process for contaminant degradation. For this purpose, various catalysts with low-environmental impact were synthesized. The obtained solids were characterized and tested in heterogeneous Fenton-like reactions.

Results of the study

1. Stabilized potassium permanganate particles as novel reagent for ISCO

A new potassium permanganate reagent with slow-release properties was designed for possible application as oxidant in a reactive barrier for efficient plume remediation. Manganese dioxide (MnO_2) was tested as a suitable coating for $KMnO_4$ particles because of its insolubility in water, adsorptive and catalytic properties and environmental compatibility. The MnO_2-coated $KMnO_4$ particles (MCP) were synthesized by i) partial reduction of solid $KMnO_4$ using the acid-catalyzed reaction with n-propanol or ii) the comproportionation of Mn(VII) and Mn(II) in n-propanol as reaction medium. The obtained particles were characterized by scanning electron microscopy and BET analysis, where the MCP revealed much higher specific surface areas (approx. $40 \ m^2 \ g^{-1}$) than the native $KMnO_4$ ($0.04 \ m^2 \ g^{-1}$).
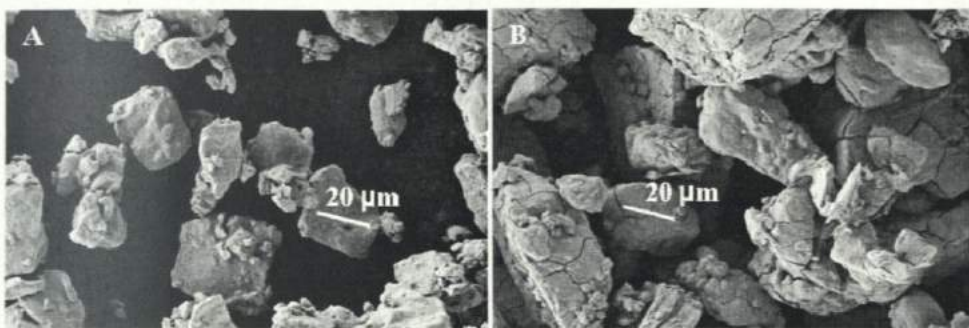

Fig. 3. Scanning electron microscopy images of native $KMnO_4$ particles (A) and coated MCP particles (B).

The longevity of MCP was tested in column experiments and showed that for MCP with a residual $KMnO_4$ fraction of 70 wt%, the duration of permanganate release under flow-through conditions was prolonged by a factor of 10 compared to native $KMnO_4$.

Although the coating process was successful, the release prolongation is considered to be quite moderate. This is probably due to the non-uniform structure of the synthesized MnO_2 coating, which contains relatively wide defects in form of cracks. Experiments on the oxidation of benzaldehyde in dry dichloromethane as solvent, which is a representative NAPL, revealed that the reaction does not take place with native $KMnO_4$, but only with MCP. It is obvious that MnO_2 plays a significant role in oxidation processes in non-aqueous media and this property can be utilized for treatment of NAPL-contaminated zones. Moreover, this study indicates that the invented MCP can be applied in other heterogeneous systems, where an oxidant in solid phase is required.

2. Iron-based nanocatalysts in heterogeneous Fenton-like system

Two different types of minerals have been elucidated as suitable nanocatalysts in the heterogeneous Fenton-like reaction: i) Magnetic Fe(II,III) oxides such as magnetite (Fe_3O_4) which contain Fe^{II} and Fe^{III} in their structure, are environmentally friendly and easy to separate due to their magnetic properties. ii) Orthoferrites with perovskite structure, in particular $LaFeO_3$ (LFO) and $BiFeO_3$ (BFO), which due to their well-defined structure and intrinsic redox properties have found an application in advanced technologies such as solid oxide fuel cells, electrode materials, chemical sensors and catalysts (mainly for gas phase reactions).

Magnetite and both perovskite catalysts were prepared by co-precipitation and by means of the sol-gel method respectively. Transition electron microscopy (TEM) images confirmed crystallite sizes in the nanometer range for magnetite and commercial Fe(II,III) oxide, whereas in case of perovskites aggregates of single nanoparticles were observed. This can be attributed to aggregation phenomena caused by the applied high temperature calcination. BET analysis revealed relatively low specific surface areas for LFO ($5.2 \, m^2 \, g^{-1}$) and BFO ($3.2 \, m^2 \, g^{-1}$) in comparison with magnetite ($95 \, m^2 g^{-1}$) or commercial Fe(II,III) oxide ($45 \, m^2 g^{-1}$).
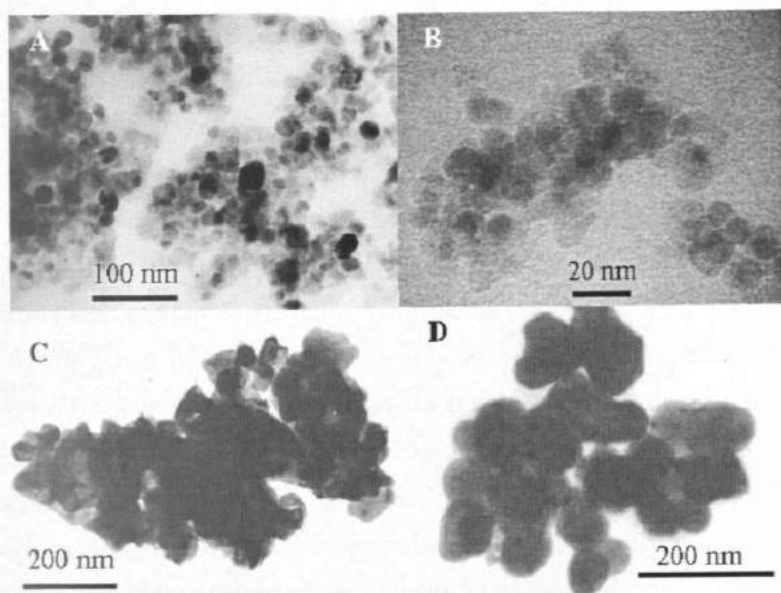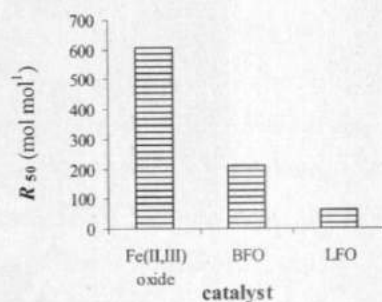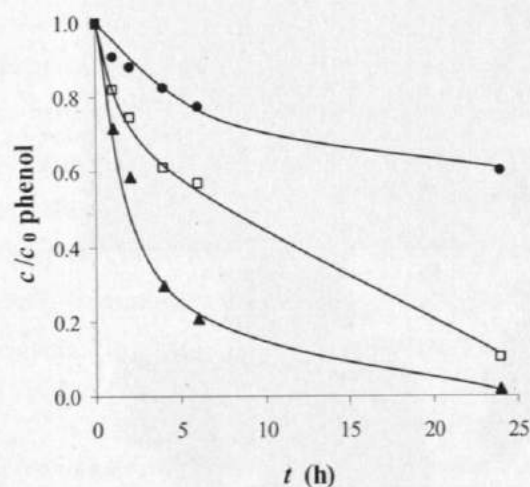
Fig. 4. TEM images of commercial Fe(II,III) oxide (A), Fe$_3$O$_4$ (B) LFO (C) and BFO (D).

The catalytic activity of the prepared materials was tested in batch experiments using phenol as a model contaminant and hydrogen peroxide as oxidant. In batch experiments carried out at room temperature and pH = 7, LFO and BFO perovskites revealed a higher catalytic activity (normalized to catalyst mass concentration) and more efficient utilization of H$_2$O$_2$ in comparison to various Fe(II,III) oxides. For instance, for the half-life of phenol values of 2.5, 5 and > 24 h were determined for BFO, LFO and commercial Fe(II,III) oxide, respectively, under identical reaction conditions ($c_{0,phenol}$ = 25 mg L^{-1}, $c_{0,H2O2}$ = 3 g L^{-1}, and c_{cat} = 1 g L^{-1}, pH = 7 ± 0.2).

R_{50} (mol mol^{-1}) corresponds to the moles of H_2O_2 needed to oxidize 1 mol of phenol until $c/c_{0, \text{phenol}} = 0.4-0.5$ is reached.

Fig. 5 Kinetics of phenol oxidation and H_2O_2 utilization in the heterogeneous Fenton-like systems with Fe(II,III) oxide (●), LFO (□) and BFO (▲); ($c_{cat} = 1$ g L^{-1}, $c_{0,H2O2} = 3$ g L^{-1}, $c_{0,\text{phenol}} = 25$ mg L^{-1}, pH = 7 ± 0.2).

It has been shown that nano-sized magnetite is susceptible to fast oxidation under Fenton conditions and is converted into maghemite (γ-Fe$_2$O$_3$), starting from the surface and continuing to the core of the particle. The presence of residual Fe(II) in the nanoparticle core appears to be of minor importance for the catalytic activity in phenol degradation by H_2O_2. However, if the Fe(II) content was raised above the stoichiometric ratio of magnetite (achieved by reduction of commercial Fe(II,III) oxide with NaBH$_4$), then only the non-productive decomposition of H_2O_2 was accelerated. Furthermore, the catalyst surface emerged as an important scavenger of reactive species, since it was observed that the reaction rates of phenol oxidation were relatively insensitive to the catalyst concentration in the range of 1-10 g L^{-1}, whereby particle agglomeration seems to play a key role. Thus, based on the obtained results, magnetite has catalytic properties for H_2O_2 activation. However, its intrinsic catalytic activity appears to be rather low, *i.e.* not adequate for practical application.

LFO and BFO were further investigated under various reaction conditions, in particular variation of catalyst and H_2O_2 concentration, reaction pH and temperature. Additionally, the stability and reusability of the catalysts were tested, which are prerequisites for further practical application. In summary, BFO revealed a better catalytic performance than LFO when reaction conditions such as catalyst concentration or temperature were varied in order to achieve high phenol degradation rates. For example, an increase in the reaction temperature from 20 °C to 60 °C improved the catalyst activity of BFO by a factor of 10, whereas LFO showed only a very slight improvement. In 4 consecutive batch runs BFO revealed a constant catalytic activity, whereby the concentration of methyl *tert*-butyl ether (MTBE) was reduced by 80% within 6 h of reaction at 40 °C. The higher activity of the BFO perovskite can be attributed to the structural and intrinsic properties of the material, where the synthesis step can play a crucial role (e.g., existing surface defects in the structure or impurities).

3. Determination of reactive species in heterogeneous Fenton-like system

It is often assumed that heterogeneous Fenton-like reactions proceed via •OH, in a similar manner as the homogeneous Fenton reaction. However, clear evidence is missing so far. In this study the reactive species involved during LFO- and BFO-catalyzed Fenton-like reactions at neutral pH conditions were investigated by analyzing the carbon and hydrogen isotope fractionation coupled to the oxidation of two model compounds, MTBE and ethyl *tert*-butyl ether (ETBE). The obtained isotope fractionation results from perovskite-catalyzed reactions have been compared to other abiotic chemical oxidation systems, in particular permanganate, homogeneous Fenton- and Fenton-like ($Fe^{3+} + H_2O_2$) oxidation. The strong similarity in the observed C- and H-fractionation indicates that the perovskite-catalyzed oxidation follows the same pathway as the homogeneous Fenton reaction, which means that it involves •OH as dominant reactive species. In addition, the C- and H-bulk enrichment factors determined for these abiotic oxidation reactions formed a reference for evaluating biodegradation pathways for fuel oxygenates applied by various bacteria strains.

Achievements and Outlook

The present thesis was focused on the innovation of two well known *chemical oxidation processes* for treatment of contaminated water streams.

A novel strategy has been proposed for *in situ* chemical oxidation which is based on an oxidant with slow-release properties obtained after modification of soluble potassium permanganate.

- Micro-sized $KMnO_4$ particles were successfully coated with MnO_2 (MCP) by partial reduction of $KMnO_4$.

- MCP is an oxidant with slow-release properties.

- In non-aqueous solvents MCP revealed an improved oxidation activity in comparison to native $KMnO_4$.

A significant contribution has been achieved in the field of advanced oxidation processes by implementation of two types of nanocatalysts for heterogeneous Fenton-like reactions.

- Nano-sized magnetic Fe(II,III) oxides with various Fe(II)/Fe(III) ratios and orthoferrites with perovskite structure - $LaFeO_3$ and $BiFeO_3$ - were prepared and tested as potential nanocatalysts in Fenton-like reactions.

- Nano-sized Fe(II,III) oxides showed relatively low catalytic activity for phenol oxidation at pH = 7 irrespective of their Fe(II)/Fe(III) ratio, whereby strong agglomeration effects can additionally hinder their catalytic performance.

- BFO revealed a better catalytic activity than LFO when reaction conditions such as catalyst concentration or temperature were varied in order to achieve high phenol degradation rates.

- BFO showed promising results relevant for practical application.

Finally, based on isotope fractionation studies hydroxyl radicals have been suggested to be the major reactive species responsible for the contaminant degradation in heterogeneous Fenton-like reactions with iron-containing perovskite nanocatalysts.

Publications

K. Rusevova, F.-D. Kopinke, A. Georgi. Stabilization of potassium permanganate particles with manganese dioxide. *Chemosphere*, **2012**, 86, 783-788

M. Rosell, R. González-Olmos, T. Rohwerder, **K. Rusevova**, A. Georgi, F.-D. Kopinke and H. H. Richnow. Critical evaluation of the 2D-CSIA scheme for distinguishing fuel oxygenates degradation reaction mechanisms. *Environ. Sci. Technol.*, **2012**, 46 (9), 4757–4766

K. Rusevova, F.-D. Kopinke, A. Georgi. Nano-sized magnetic iron oxides as catalysts for heterogeneous Fenton-like reactions: Influence of Fe(II)/Fe(III) ratio on catalytic performance. *J. Hazard. Mater.* **2012**, 241-242, 433-440.

K. Rusevova, A. Georgi, R. Köferstein, M. Rosell, F.-D. Kopinke. LaFeO$_3$ and BiFeO$_3$ perovskites as nanocatalysts for contaminant degradation in heterogeneous Fenton-like reaction, **2012** *submitted.*

Helmholtz Centre
for Environmental Research – UFZ
Permoserstraße 15 I 04318 Leipzig I Germany
Internet: www.ufz.de